1-1-2016

Development Of An Elderly Female Torso Finite Element Model For Restraint System Research And Development Applications

Anil Kalra Kalra
Wayne State University,

DEVELOPMENT OF AN ELDERLY FEMALE TORSO FINITE ELEMENT MODEL FOR RESTRAINT SYSTEM RESEARCH AND DEVELOPMENT APPLICATIONS

by

ANIL KALRA

DISSERTATION

Submitted to the Graduate School

of Wayne State University,

Detroit, Michigan

in partial fulfillment of the requirements

for the degree of

DOCTOR OF PHILOSOPHY

2017

MAJOR: MECHANICAL ENGINEERING

Approved By:

_____

Advisor Date

_____

_____

_____

_____

DEDICATION

I would like to dictate this thesis to my parents

whose blessings have made me capable enough to pursue higher studies

&

to my amazing wife, Geet, whose understanding nature for my work and affection for my family

has made it possible for me to complete this work

&

to my son Aarav, whose smiles have inspired me to move towards success in life

ACKNOWLEDGEMENTS

First and foremost, I would like to express my gratitude to my advisor: Dr. King Yang, who has given me this opportunity to complete such research work under him. His moral support, guidance and supervision throughout the research work are highly acknowledged. Further, I would also like to thank my committee members Dr. Trilochan Singh, Dr. Clifford Chou, Dr. John Cavanaugh and Dr. Albert King for their valuable support throughout the research work. I would like to express my special gratitude to Dr. Paul Begeman, who provided me the experimental data of rib bending tests. Also, I praise the enormous amount of help and teaching by Dr. Xin Jin and Dr. Feng Zhu whose mentoring skills and technical experience guided me throughout the development of finite element modeling and validation.

A special acknowledgement goes to my office mate Tal Saif, whose intense support and helps especially during late evenings motivated me to work hard to achieve my goal. Also, I would like to thank other PhD students of department: Ming Shen, Valerie Mika, Ke Feng and Runzhou Zhou, with whom the endless research related discussions, have increased the level of my knowledge pool. I also recognize the continuous support of graduate students who helped me on this project to complete it especially Prashant. Thanks to everyone at AHML lab: Tushar, Varun, Anand, Rohit, Zhaoing, Vinit, Vikrant, Haonan, Oscar, Yun, Prajwal and Dhruv. Funding to complete this project for developing CHARM-70F was provided by Toyota's Collaborative Safety Research Center (CSRC), North America.

TABLE OF CONTENTS

LIST OF TABLES

LIST OF FIGURES

CHAPTER 1. INTRODUCTION

1.1. BACKGROUND AND SIGNIFICANCE

A rapid increase in the elderly population in the United States has created a tremendous amount of pressure on automotive safety engineers to protect this vulnerable population in motor vehicle crashes. According to U.S. Census Bureau data reported by the National Highway Traffic Safety Administration (NHTSA), there is an increase of about 7-10% in the population 65 and older in the next couple of decades which in turn will result in more elderly drivers, passengers, and pedestrians involved in traffic crashes. Lyman *et al.* (2002) showed that by 2030, there will be a 155% increase in fatal crashes involving people above the age of 65. Coughlin and Reimer (2006) also pointed out that older people have the second highest fatality rate, based on deaths per 100,000 people, in automobile crashes. According to a U.S. Administration on Aging (AOA) report published in 2002, one in every 10 persons is a woman who is at least 60 years old which approximates 10% of the total driving population and these numbers are increasing in the coming decades. Moreover, Baker *et al.* (2003) reported that while the total number of elderly females involved in fatal crashes is less than that of the total number of elderly males, their percentage for involvement in such fatal crashes is higher than that of elderly males. Because of increasing population and higher involvement in car crashes of elderly females, there is a greater chance for them to face casualties and other safety challenges in car crashes. These findings suggest that elderly females are a vulnerable segment of the population that needs special attention for their safety.

Recently, NHTSA published a report (Dec. 2013) regarding the traffic safety concerns of older people. This report stated that although the total number of fatalities in road crashes has decreased nationwide, there is hardly any change in the total number of fatalities involving people of age 65 and older (65+). NHTSA also stated about the fact that older Americans are staying mobile and active longer, due to the fast-pace advancements in medical science and with the current life expectancy approaching 80 years on average. The older population has been projected to drive more miles and is expected to continue driving later in life than previous generations.

The current increase in the population of senior citizens, combined with the fact that they are relatively independent, calls for lone travel in automobiles, induces the need to address automotive safety related issues for senior citizens. The higher risk of mortality for older age occupants in car crashes suggests a need for a thorough and focused literature survey on this particular group of subjects. In order to develop a finite element (FE) model of an elderly female, a review of literature falls into two general categories: (a) the types of injury elderly women sustain in vehicle crashes, and (b) the basic information needed for the development of an age-specific FE female model.

1.2. FE MODEL DEVELOPMENT – SOLUTION TO THE PROBLEM

Safety features (such as air bags, collapsible steering column, and child booster seats) equipped in modern-day automobiles to reduce injuries during crashes are designed based on the anthropometric details of mid-size males, small females, and children of 1, 3, and 10 years old.

Thus, it would be of interest to learn how the safety features developed for those anthropometries interact to the vulnerable population of elderly females. To date, available automotive anthropomorphic test devices (ATDs), also known as crash dummies, used for testing the efficacy of safety features in car crashes are designed to represent younger males and females. For example, the Hybrid III 50th percentile adult male dummy was based on responses of 45 years old male subject, as shown by Kuppa and Eppinger (1998). Consequently, the safety of the elderly population, especially the mid-size elderly female, could still be a major concern. However, developing a new crash dummy to represent any age- or gender-specific population is very costly. Another possible remedy geared specifically towards elderly females is the use of FE models with similar anthropometric details to predict the effectiveness of safety features during automotive crashes.

A significant body of work has been reported by various research groups about the development of lumped-mass models and FE models of the human thorax and abdomen. Recently, a number of FE models have been developed, which represent various population sizes (*e.g.*, 10-year-old child, 50th percentile male, and 5th percentile female). For example, Zhao and Narwani (2005), Petitjean *et al.* (2003), Shah *et al.* (2001), and Ruan *et al.* (2003) have emerged to investigate injuries using detailed FE models of the human thorax for adult males. Some FE models were developed to represent the elderly population as reported by Tamura *et al.* (2005), Ito *et al.* (2009), and Samantha *et al.* 2015), however, they focused only on elderly male. Kimpara *et al.* (2005) developed an FE model of a small adult female, but the model geometry

and anthropomorphic details may be different from those of an average elderly female. All these models are being used for designing safety features in the automotive industry for protecting different segments of population, but little attention has been given to the development of an FE model for elderly females, which have been known as one of the most vulnerable segments of population.

Along with geometric differences, the stiffness as well as the strength of human bones and tissues differ with age and gender, which result in different biomechanical response for different people due to similar physical insult (Zhou *et al.*,1996). For example, Hamilton *et al.* (1986) estimated that the ratio of the lateral stiffness of an adult thorax to that of a child thorax is two and half times, using FE models representing a single rib of a 50-year-old adult and of a 6-year-old child. Similarly, there have been number of studies reported in literature which shows the change in bone material as well as structural properties with respect to age and gender. In other words, one cannot directly use a previously developed FE model, which represents either a younger male, younger female, or elderly males to predict the responses of this vulnerable elderly female population in automotive crashes.

The aforementioned facts raise the demand for an accurate FE model specifically developed for average older females that have accurate age-specific anthropomorphic details. There is a need to study the gender- and age-based injury criteria and possible reasons for high fatalities associated with this vulnerable population. This dissertation research focuses on the development of an FE model with appropriate anthropomorphic as well as stiffness details of the

upper torso representing an average 70-year-old female. The results produced by this research can be used as a tool to make safer cars for elderly female drivers and can help in understanding the mechanism of injuries for elderly females sustained in fatal crashes.

CHAPTER 2. EPIDEMILOGY REVIEW

2.1. INTRODUCTION

In May 2013, NHTSA published a report on injury vulnerability and effectiveness of occupant protection technologies for older occupants (Kahane 2013, May). In this report, NHTSA analyzed a total of 36 years of Fatality Analysis Reporting System (FARS) (1975-2010) data as well as other databases, such as FARS-Multiple Cause of Death (MCOD, 1987-2007) and NHTSA's Crashworthiness Data System (CDS, 1988-2010) that identify specific injuries. According to the FARS database (1975-2010), with given similar physical insults, a 70-year-old male driver is, on the average, 5.04 times as likely to die as a 21-year-old male driver. For female drivers, the corresponding cumulative increase from an age of 21 to 70 is a factor of 3.87; for male right front (RF) passengers, 6.70; and for female RF passengers, 5.67. When the fatality risk for a female driver is considered, the results show that for drivers aged 21 to 30, the fatality risk averages 25.9% higher for females than for males of the same age group; for drivers 65 to 74, 1.4% lower. For RF passengers aged 21 to 30, fatality risk averages 29.2% higher for females than for males of the same age group; for RF passengers aged 65 to 74, females remain 11.4% higher than males.

Overall, when the combined male and female cumulative fatality risk is considered, the analysis showed that a 70 years old male driver is more vulnerable than a female driver of the same age, but the difference is very small (1.4%). Additionally, a 70 years old female RF passenger has an 11% higher risk than male RF passenger of the same age. It can be concluded that elderly RF female passengers are more vulnerable that of elderly RF male passengers, but the fatality risk for both elderly female and male drivers are almost identical. The data were investigated further in the report to determine the trend of the fatality risk for females as

compared to males for different model year (MY) cars, crash scenarios, different body regions, and different occupant protection systems.

Overall, it was concluded in the report that injury response of elderly female is different from that of other occupants when involving in similar type of crashes. Elderly females were found to be a vulnerable segment of population especially for RF passengers in all cases. A detailed study is needed to further discuss the reasons for such vulnerability as the biomechanical responses of elderly female can be different from other segments of population in car crashes. Further, new safety systems can be designed to reduce the fatality risk for elderly females, only if a properly validated physical surrogate or numerical model is available to represent this vulnerable segment of population.

2.2. THORACIC INJURIES IN ELDERLY – MAGNITUDE OF THE PROBLEM

In a similar kind of study, Kent *et al.* (2005) surveyed two U.S. data sources: FARS and the National Automotive Sampling System/Crashworthiness Data System (NASS/CDS). They concluded that 47% of drivers over 64 years of age who died in a frontal crash sustained a fatal chest injury. Wang (2008) from the University of Michigan published a report based on data taken from the Crash Injury Research and Engineering Network (CIREN) and revealed that the predicted risk of AIS (Abbreviated Injury Scale) 3 and higher (AIS 3+) injuries is greater for the thorax at the age of 60 or older. Also, it was found that rib fractures were the most serious injury sustained by 40% of the patients over the age of 60 who died of chest injuries from automobile collisions.

In the early 1970s, Kroell *et al.* (1971) and Kroell *et al.* (1974) conducted a number of human cadavers frontal chest pendulum impact tests and found age as a significant factor in ribcage loading. In similar studies for lateral impact tests with human cadavers, Cavanaugh *et al.*

(1993), Eppinger *et al.* (1984), and Morgan *et al.* (1986) developed different criteria for predicting injuries to the thorax in side-impact collisions and included age as a factor. In real world crash accident studies, Stawicki *et al.* (2004) studied trauma patients aged 18 and older admitted to a trauma center in Pennsylvania from January, 1988 through December, 2000 and determined the number of rib fractures as a measure of mortality rate. They concluded that overall trauma related to rib fractures is higher in elderly patients. In a similar way, Stitzel *et al.* (2010) collected data of patients with AIS 3+ injuries and determined the age of 55 as a threshold for increased mortality from crash-induced thoracic injuries. Kent and Patrie (2005) developed a thoracic injury function based on 93 human cadaver tests and found that only 13% of chest deflection was needed for a 50% risk of rib fracture in 70-year-old subjects, whereas 35% of chest deflection was needed for subjects that were 30 years old. In another study by the same group, Kent *et al.* (2008) found that most of the patients over the age of 60 who died of chest injury in automotive blunt trauma had no injuries worse than rib fractures.

There have been a number of studies done supporting the fact that the thorax of elderly people is more prone to injuries than that of younger people in automobile crashes. In these crashes, the ribs and the sternum are the main parts of the thorax which absorb the energy of impact and result in a fracture if the said impact energy exceeds a tolerance value. The severity of thorax injuries is directly proportional to the number of rib fractures sustained. To identify the effect of age on rib fractures,Bulger *et al.* (2000) tried to define the relationship between the number of rib fractures and morbidity/mortality. They concluded that elderly patients with rib fractures occurred in blunt chest trauma had twice the mortality and thoracic morbidity rates compared to younger patients with similar injuries. In another retrospective studies, rib fracture together with increased age was associated with increased probability of death. Holcomb *et al.*

(2003) studied 171 patients with AIS 2+ trauma-related injuries of chest. They found that rib fracture increased the probability of death in people over 45 years of age. Stawicki *et al.* (2004) studied 27,855 patients with more than one rib fracture and found that overall, trauma-related mortality was higher for patients over the age of 65. In other studies, it was concluded that there was a higher number of rib fractures in elderly people, as compared to young adults (Bansal *et al.* (2011), Kemper *et al.* (2011), Hanna and Hershman (2009), Zhou *et al.* (1996)).

Age is not the only important factor with respect to injury risk; gender related differences are crucial as females, in general, are not as strong as males. In a study of accident samples in the United Kingdom (UK) population, Lenard and Welsh (2001) reported that female drivers accounted for one third of the total drivers involved in accidents and female RF passengers are more vulnerable in frontal crashes than male drivers, especially in skeletal injuries of chest.

For rear-end impact there are more soft tissue neck (whiplash) injuries in females than males. Roberts and Compton (1993) established a relationship between delta V (change in car speed) and injuries for more than 20,000 accidents and concluded that the median level of AIS 3+ injuries was found to be occurred at 38 km/h (kilometer per hour) for females and 44 km/h for males. Bose *et al.* (2011) did a multivariate regression analysis to depict effects due to different age, mass, BMI category, crash delta V, and number of crash events. In this analysis, they found that in comparable crash conditions, the odds of an effectively belted female driver to sustain AIS 2+ chest and spine injuries was 38% (95% CI is (1%, 89%)) and 67% (95% CI is (34%, 109%)) higher respectively, than those of a belted male driver, where CI stands for confidence intervals which suggest that there is a 95% probability the population parameter lies within the interval.

From all these studies mentioned above, it is clear that injury responses of elderly victims are different from that of younger crash victims. If the injuries are segregated on the basis of gender, elderly female drivers are more likely to be injured especially in the thoracic region. These studies implicitly call for the demand of a different restraint system (seat belt, airbag and pre-tensioners) or safety design for the elderly population, especially for women in frontal impacts. The magnitude of the problem worsens with advanced age in females. There is an urgent need to develop different strategies to study the injury thresholds and injury severity for this vulnerable group of the population. One such proposed strategy is the development of an FE model for an elderly female.

Also, it is important to select an appropriate age, corresponding height and weight for the target FE model which can represent the average elderly female population. Different researchers have defined different age thresholds for defining the elderly population. For example, Zhou et al. (1996) examined the experiments done in literature in order to find the effect of age on thoracic injury thresholds. The authors suggested to divide the specimens into three groups: Young group < 35 years old, middle aged group from 36 to 65, and the elderly group from 66 and up. Kent and Pentrie (2005) predicted the risk of rib fracture for younger (30 years old) vs. elderly (70 years old) to show the effect of chest deflection between two segments of population. Kahane (2013) presented a report focusing on injury vulnerabilities for older occupants and women. The author used 65-74 years old group of specimens to represent elderly population. Therefore in this study, a mean value of 70 years is chosen to be the targeted occupant age to represent the average elderly female. Further, the height and weight for an average 70 years old female are taken as 1.6 m and 73 kg, respectively, from the statistical average data reported in the

Vital and Health Statistics by CDC (Centers for Disease control and Prevention) – "Anthropometric reference Data for Children and Adults; United States, 2007-2010."

2.3. SPECIFIC AIMS

To overcome the limitations and to better understand the injury mechanism in this vulnerable population, the main objective of this research is directed efforts towards developing an FE model representing an average 70 years old female. The main focus of this study will be on developing the torso portion of the female whole body model. Four specific aims are set up for this dissertation research as listed below:

Specific Aim 1: Development of an FE model representing an average 70 years elderly female torso, consisting of the thorax, abdomen, and pelvic.

Specific Aim 2: To study the age- and gender-dependent geometric and material properties of human ribs due to bending loads.

Specific Aim 3: Validation of the component models, taken from the developed FE torso model in Specific Aim 1, against experimental data under various loading conditions on the ribs, thorax, abdomen, and upper extremities.

Specific Aim 4: Integration of the developed torso model with models developed for other body regions and validates the integrated model against data obtained from sled tests.

CHAPTER 3. ANATOMICAL AND STRUCTURAL DIFFERENCES IN FEMALE RIBCAGE

3.1. ANATOMICAL DIFFERENCES

In general, male and female bodies differ substantially, especially in the ribcage, head, and pelvic areas. It is important to consider these differences both in terms of body size and shape. Females have smaller collarbones than those of males and have narrower ribcages that are slanted inwards, contrasting straighter and broader male ribcage as shown in Figure 3-1. A female thoracic ribcage, in general, is more rounded and smaller in size than that of a male. A female pelvis is smaller than that of a male; the hips are wider than the shoulders in females as well. Males have hips that tend to be narrower than their shoulders. The female sacrum and pelvic ring is also wider than those of males. The female chest has less volume and a shorter sternum. The upper margin of the sternum for the female is located at about the level of the third vertebra; in males, it is located near the second vertebra (Grey's anatomy atlas).

Although males generally have larger skeletal elements than females, the research related to changes in rib sexual dimorphism is limited. Few studies (Ashly *et al.* (1956), Indar *et al.* (1980)) have been reported to identify the gender of an individual on the basis of sternum's relative size, shape, and relative differences in the length of the body of the sternum compared with the manubrium between males and females. The oldest technique for distinguishing the sex of the individual is called Hyrtl's law, which proposes that the manubrium is less than half the length of the body of the sternum in males, whereas it is greater than half the length of the body of the sternum in females (Steele and Bramblett (2012)). Figure 3.2 shows a detailed skeletal anatomy for a typical human thorax.

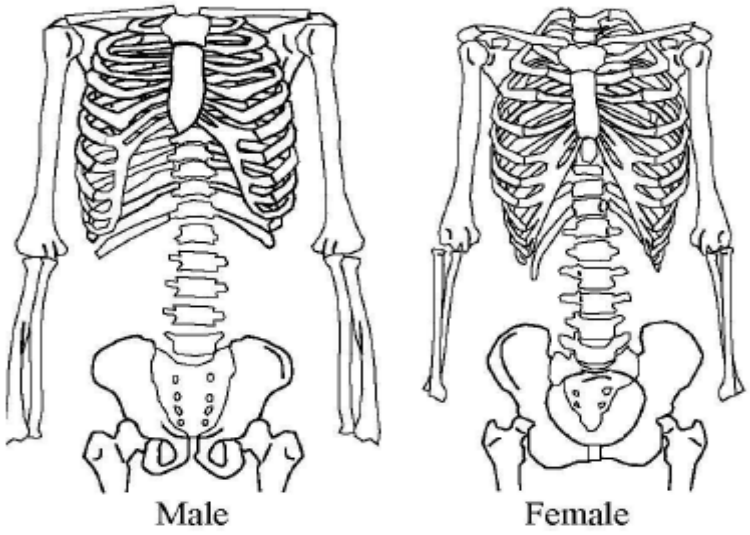

Figure 3-1 Geometric Comparison between male and female (Kimpara *et al.* 2005)

Similarly, Stewart (1979) documented that the maximum length of the scapula is the best body part for the diagnosis for gender. Based on combined sample of American blacks and whites studied by Stewart (1979), the mean value of the maximum length of scapula was 138±9.5 mm for females and 159.6±8.6 mm for males. Krogman (1962) stated that male sacrum is characterized as being longer, narrower with more even curvature, and often composed of more than five segments, whereas the female sacrum is characterized as being shorter, broader, with a tendency to a marked curvature between the second and third sacral elements, and typically composed of five segments. Other variations in term of length and diameters of bones such as in ulna, radius, femur, tibia, *etc*. have been reported in literature for diagnosis of gender.

In most recent studies, Bellemare *et al.* (2003) compared the thoracic configuration of 21 normal male and 19 normal female subjects and found that for the same height and weight, the volume of male lungs is around 10-12% greater than that of females. All lung volumes were examined at three different locations using anterior-posterior and lateral chest radiographs. Also, they concluded that females had smaller radial rib cage dimensions in relationship to height than males, a greater inclination of ribs, a comparable diaphragm dome position relative to the spine,

and a shorter diaphragm length. Female rib cages could accommodate a greater volume expansion because of a greater inclination of the ribs that would be well suited to accommodate large abdominal volume displacements during pregnancy. Wang *et al.* (2012) showed that there were differences in vertebral depth and height and also facet angles, between males and females which might be a factor worthy considering when analyzing the causes of higher risk of neck injuries in females.

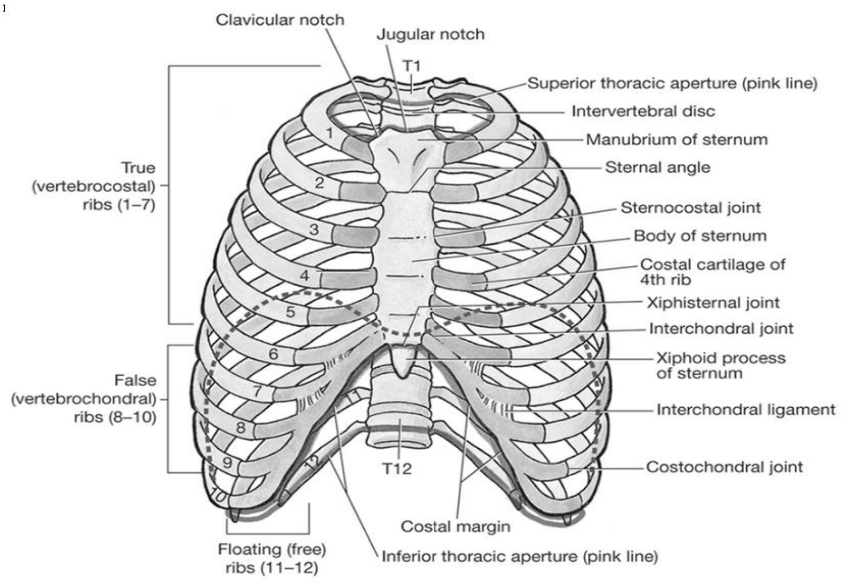

Figure 3-2 Anterior view of thoracic skeleton (Moore's Clinical Anatomy, 2nd ed.)

3.2. GEOMETRICAL DIFFERENCES IN RIBS

The chest wall protects the underlying viscera by surrounding them with bony structures like ribs, sternum, and clavicles. Rib fractures account for over 50% of the thoracic injuries from non-penetrating injuries like motor vehicle crashes. Multiple rib fractures interfere with normal costovetebral and diaphragmatic muscle excursion resulting in reduced air exchange or causing hemo- and/or pneumo-thorax. As described earlier, the shape of the ribcage differs between male and female. Additionally, the ribcage size may change with age in order to accommodate internal organs within the thoracic cavity, among other reasons. Therefore, it is of great importance to

study the geometric differences in ribs in order to extract the dimensions needed to form an average 70 years old female chest model.

According to the study of Kent *et al.* (2005) and Gayzik *et al.* (2008), the rib structure tends to become more perpendicular to the spine as age increases and the rib angle (from the superior-most posterior point of the rib, to the superior-most anterior point of the rib) gets changed with age. The rib angle depends on age, gender, weight, and BMI (Body Mass Index, defined as a person's weight in kilograms divided by the square of height in meters). In the study reported by Kent et al. (2005), 152 subjects (71 males and 81 females) from the University of Michigan Transportation Research Institute (UMTRI) database were measured to determine the rib angle, primarily at the 9th rib. Eq. 3.1 was developed using a multivariate regression model for the rib angle calculation as shown below.

$$Rib\ angle(9876)(deg.) = 35.4 + 0.0412 * age\ (years)\ + 0.572 * BMI\ \left(\frac{kg}{m^2}\right) + 1.03 * gender \quad \text{[Eq. 3.1]}$$

Where 9876 sequence was used to define the angle of the 9th rib preferentially, if the data were unavailable, then use angle of the 8th, then 7th, and then 6th rib in the calculations. Also, male = 1 and female = 0 for gender in the equation.

The gender does not seem to be a significant factor for the 9th rib angle, but a considerable change is noticed at the level of the 6th rib. For the targeted 70 years old female model, the rib angle at 9th level is found to be 54.6 degrees according to Equation 3.1.

3.3. GEOMETRIC DIFFERENCES IN THORACIC SKELETON

Along with difference in inclination of the ribs, various researchers have shown that there are differences in the overall dimensions (width, depth and height) of the skeletal rib cage with age and gender. Bellemere *et al.* (2003) studied chest radiographs of 40 subjects (21 males and

19 females,), whose descriptions are shown in Table 3-1, and measured the lungs volume, internal ribcage dimensions, diaphragm positions relative to spine and diaphragm length of these specimens.

Table 3-1 Specimen descriptions for Bellemere study

Gender	Males	Females
No. of samples	21	19
Age, Years	44.1±18.9	48.2±19.5
Weight, kg	70.7±10.9	57.3±6.1
Height, cm	171±4.9	159.9±7

It was found that females had smaller rib cage dimensions, greater rib inclinations and shorter diaphragm length. Further, the difference between male and female ribcage geometry in terms of the anterior-posterior rib cage diameter and lateral diameter were also shown.

Gayzik *et al.* (2008) studied CT scans of 63 adult males to acquire the locations of landmarks for the ribcage (106 landmarks were extracted on each side) and quantified age-related shape changes in the male thorax using Procrustes superimposition. Centroid size (CS) of the ribcage landmark dataset was taken as a basic parameter to quantify the changes on basis of individual's height, weight, and BMI. Using these landmarks, a line model can be developed for any given age, height, and weight of male specimens.

In a recent study, Shi *et al.* (2014) at UMTRI developed a statistical rib cage geometry model which accounted for variations by age, gender, stature, and BMI. In their study, rib geometries of 89 subjects of both genders with ages of 18-89 years were extracted using threshold based CT image segmentation with the help of 464 landmarks on the left side of each

subject's ribcage. The whole dataset was analyzed using series of numerical analysis which includes rigid registration, principal component analysis (PCA), and multivariate regression analysis. Additionally, the landmark coordinate locations were predicted as functions of age, stature, BMI, and sex.

In this study, data reported by Gayzik were used to develop a stick model representing the rib cage of 70 years old male. Data provided by Bellemere were then applied to scale a female stick model of the same age from the stick model of the male. More descriptions of these procedures are provided in Chapter 4.

3.4. CHAPTER CONCLUSION

All the aforementioned studies claim that the thoracic structures of a 70 years old female are not only different from that of a male of the same age but also different from that of younger females. With increasing age, changes in female thorax geometry become more prominent and needs to be considered for creating an accurate FE model that can represent an average 70 years old female.

The geometrical differences related to elderly female thorax, such as the internal anterior-posterior rib cage diameter, internal lateral diameter of rib cage, and rib angle were emphasized in the development of the FE model for a 70 years old female. FE models representing different population groups are generally developed from patient specific medical scans where the attributes of the model depend on geometric details of one individual, and how close this individual represents that population. Theoretically, an FE model representing a particular segment of the population should be based on average statistical data, but retrieving medical scans from a large number of specimens is very costly and time consuming. On the other hand,

statistical data available in literature can be used to determine the average geometric details of a particular segment of population.

Such an effort is described in the upcoming chapter of this dissertation. A statistically average geometric model was retrieved through literature representing 70 years old female. Further, morphing or scaling of the ribcage geometric model developed from CT scans were performed, as needed (explained in Chapter 4), to best match the statistically averaged geometric models. Also, FE mesh was developed from the geometric models.

CHAPTER 4. MATERIALS AND METHODS

In general, human body finite element models have been developed from 3-D rendering of surfaces retrieved from medical scans of cadavers or volunteers (Yang *et al*. (2006)). Since they are based on one individual selected to match a specific gender and size of the population, such as a 50^{th} percentile male, they are considered as patient specific models. In the current section, an average 70 years old female geometric model was first developed based on data published by Gayzik *et al*. (2009) and Bellemere *et al*. (2003) in which medical scans of two groups of volunteers rather than an individual subject were acquired. Because the geometric model lacks the 3-D details of the human body, a patient specific model similar to a 3-D FE model of a 70 years old average size female was created and then scaled to match the average representative geometry for this group. Complete details of the incorporated procedures to create this model are described in this chapter.

4.1. DEVELOPMENT OF STATISTICALLY ACCURATE TORSO LINE MODEL

In this section, results from Gayzik *et al*. (2009) and Bellemere *et al*. (2003) were used to develop a line model of the rib cage for an average 70 years old female. The development of a line model, or so called stick model, is completed in these steps:

4.1.1. Development of a rib cage line model to represent a 70 years old male

Gayzik *et al*. (2008) described the outer geometry of ribcages based on 106 landmarks on the thoraxes taken from CT scans of 63 adult males. Further, a relationship was established between the landmark locations and age, based on quadratic regression as shown in Equation 4.1.

$$x(n) = \beta_0(n) + \beta_1(n) \times (age) + \beta_2(n) \times (age)^2 \qquad \text{[Eq. 4.1]}$$

In this equation, x(n) represents the coordinate in the x-axis of the nth landmark, age is in years, and β_0, β_1, and β_2 are the coefficients of the quadratic equation.

The same equation with different coefficients can be written for y(n) and z(n), which represent the y and z coordinates of the nth landmark, respectively. All coefficients were reported for each landmark location and were provided as supplementary material along with publication. The Gayzik study reported the coefficients for both the right and left sides of ribcage. In the current study, only the 53 landmarks on the left side were chosen to develop the line model of the left ribcage, because the ribcage is assumed to be symmetrical. Using these equations and associated coefficients, the landmark coordinates (x,y,z) for all 53 landmarks on the left side were calculated for a 70 years old male subject. Further, these landmark coordinates were imported into Hypermesh 10.0 (Altair, Troy, MI) as individual nodes to represent all 53 locations for the left side of the ribcage. Straight lines were used to connect the adjacent nodes to form a line model representing the left side of the ribs. This line model was then reflected about the mid-sagittal plane on to the right side to form a complete ribcage geometric stick model named as S-M70 as shown in Figure 4-1.

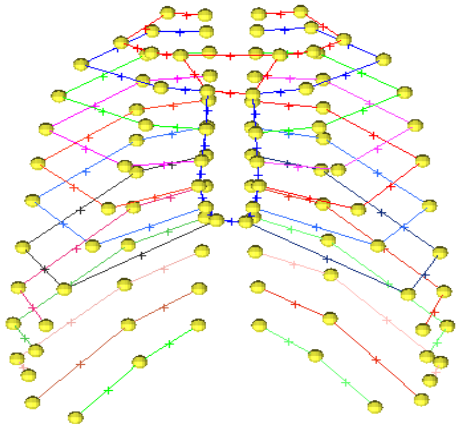

Figure 4-1 A frontal view of the S-M70 line model representing a 70 years old male ribcage (Developed from 53 landmarks on the left side and then reflected to form the complete ribcage)

4.1.2. Scaling the 70 years old male line model to develop a female line model

Bellemere *et al.* (2003) measured the anterior-posterior ribcage diameter, lateral ribcage diameter, and 6th rib angle for 21 normal male and 19 normal female subjects from chest radiographs. In this second step, the male to female ratios in various thoracic dimensions were calculated based on data listed in Table 4-1. Only the ratios determined from the maximum values were selected to scale the aforementioned male ribcage line model (S-M70) to form the 70 years old female stick model named as S-F70 using Hypermesh 10.0 as shown in Figure 4-2. The ratios determined from the minimum values were not included because the ratio generated from these values was found to be irrelevant to show the difference between male and female rib angles.

Table 4-1 The ratios between male/female ribcage dimensions calculated from Bellemare data

Bellemare *et al*. (2003)		Male	Female	Ratio(Male/Female)
Anterior-posterior rib cage diameter (cms), a	Max	9.51	8.75	1.09
	Min	7.71	7.35	1.05
lateral rib cage diameter (cms), d	Max	14.92	14.3	1.04
	Min	13.4	13.06	1.03
6th Rib angle (degrees), h	Max	60.04	51.38	1.17
	Min	43.52	42.94	1.01

4.1.3. Rib angle measurement study for S-F70 model

According to Bellemere *et al.* (2003), the 6th rib angle ranged from 44 to 55 degrees for elderly females and according to Kent *et al.* (2005a), the approximate 9th rib angle is 54 degrees for 70 years old females as that calculated previously in Chapter 3. A 2-D plane measurement of

rib angle on the lateral view of the S-F70 model is done using Image-Pro Plus 6.0 software (Rockville, MD) as shown in Figure 4-3. The measured angles at the 6th rib (AN6 = 54.5º) and at the 9th rib (AN9=53º) are consistent with the literature findings and lie within the range reported, even though the range reported by the Bellemere study is quite wide, and the data may be biased for mid age people of similar stature, height, and BMI. Based on these findings, the rib angles used in the current study are considered a reasonable representation of an average 70 years old female.

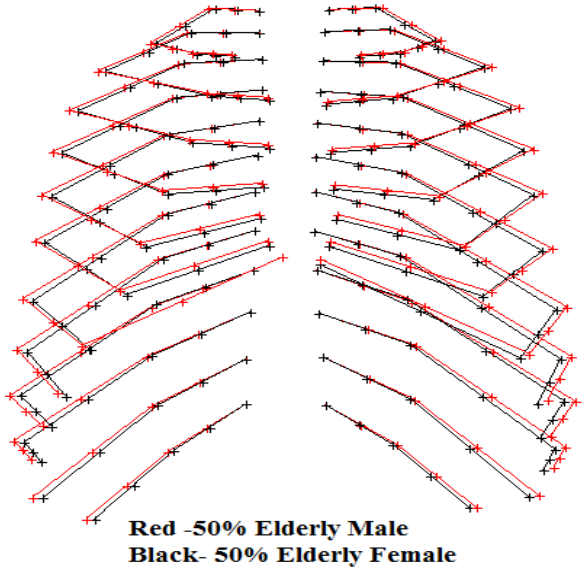

Figure 4-2 Comparison of S-M70 stick model (developed using data of Gayzik *et al.* 2008) to S-F70 stick model (using the scaling factors calculated from data reported by Bellemere *et al.* 2003). The lines representing the sternum were hidden to better highlight the differences between male and female of the same stature.

It should be noted that the height and weight of the developed S-F70 model is unknown since the Gayzik study did not include these factors for calculating the age dependent landmarks of thoracic skeletons. Also, a stick model did not include the 3-D rib structure needed to develop an FE model. Therefore, the S-F70 stick model can be used for comparing the overall geometric

details, such as the thoracic width, height, and rib angles, but 3-D medical scans are still needed to develop the FE mesh for an average 70 years old female. Such an effort has been made and is described in the next section.

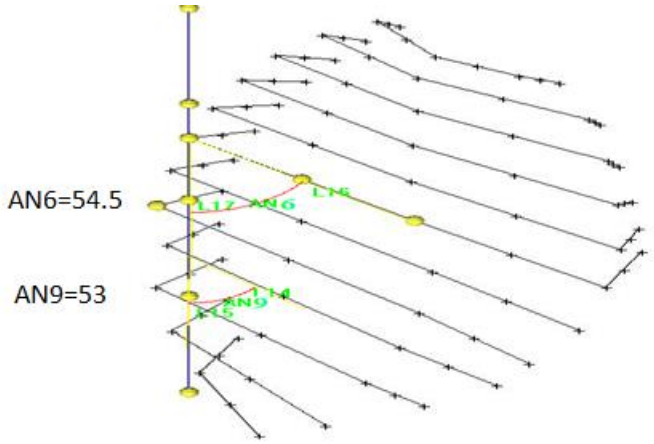

Figure 4-3 Rib angle measured on the 6th rib (54.5º) and 9th rib (53º) of the 70 years old female stick model

4.2. METHODS FOR MESH DEVELOPMENT

Researchers in the Advanced Human Modeling Laboratory of the Bioengineering Center at Wayne State University continue to develop numerical models to analyze the effects of car crashes on human body. Previous FE models have been developed through the use of modeling software such as Mimics (Materialise, Leuven, Belgium), Hypermesh (Altair engineering Inc., Troy, MI, USA), and LS-DYNA (LSTC, Livermore, CA, USA). The schematic diagram for the development of a human model is shown in Figure 4-4. The same approach was applied in this research for the development of an FE model representing a 70 years old female. In addition, the current study also employed statistical data (as shown in Section 4.1) to ensure that the eventual FE model represent an average 70 years old female. The upcoming sections of this chapter will follow the steps explained in the schematic diagram to create an FE mesh of an average 70 years old female thorax.

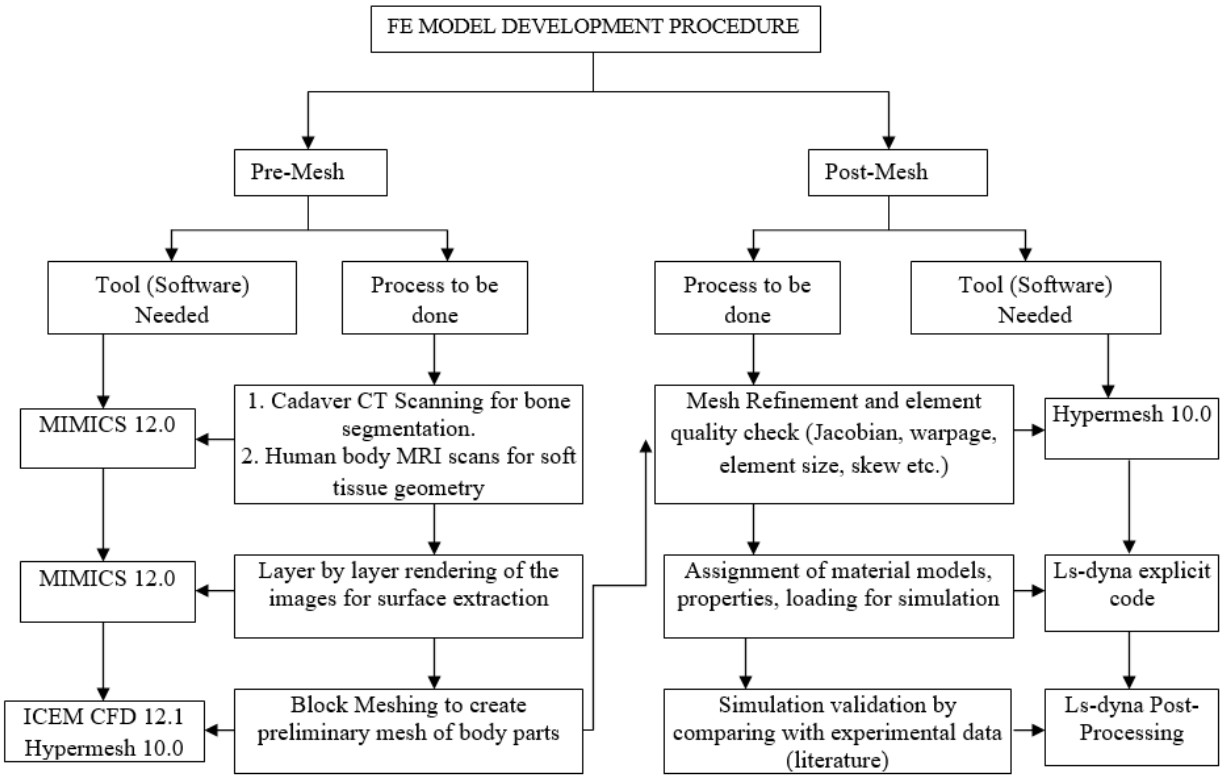

Figure 4-4 A schematic diagram for the development of an FE human model

4.2.1. CAD surface extraction for 3-D skeletal geometry

As previously described, an average 70 years old female has an anthropometric measurements of 1.6 m in height and 73 kg in weight, based on statistical results from Centers for Disease Control and Prevention (CDC). But, it is not an easy task to find a cadaver which matches exactly the same anthropomorphic details as described through CDC data. Therefore, the closest match - a female cadaver (WSU No. 938, 73 years old) with a height of 1.6 m and a weight of 62 kg was selected to extract thoracic skeleton geometry from computed tomography (CT) scan images with the approval of the Institutional Review Board/Human Investigation Committee of Wayne State University (WSU). The cadaver was scanned at the Oakwood Hospital Radiology Department in Taylor, MI. The scan resolution was set as 1.0 X 1.0 X 5.0 mm for the whole body while some of the regional parts, like the head and thorax, were scanned

at 1.0 X 1.0 X 1.0 mm resolution so that accurate details for these regions can be captured individually. After collecting the medical images, the 3-D rendering of the scanned slices was done using Mimics 12.0 and the computer aided design (CAD) surfaces of the ribs, clavicles, and scapulae were retrieved. The surface directly extracted from the CT scans of the ribs was not smoothed, so the 3-matic software within Mimics was used to smoothen the surfaces of ribs as shown in Figure 4-5. This 3-D geometric model is named – WSU_F160-62 model. Later on, the smoothened surface will be scaled based on the statistical model S-F70 developed through data in literature, which represents the average 70 years old female overall geometry. Along with the ribs, CAD surfaces of other bones like scapula, sternum, clavicle, pelvic, sacrum, and vertebras were also retrieved through these scans.

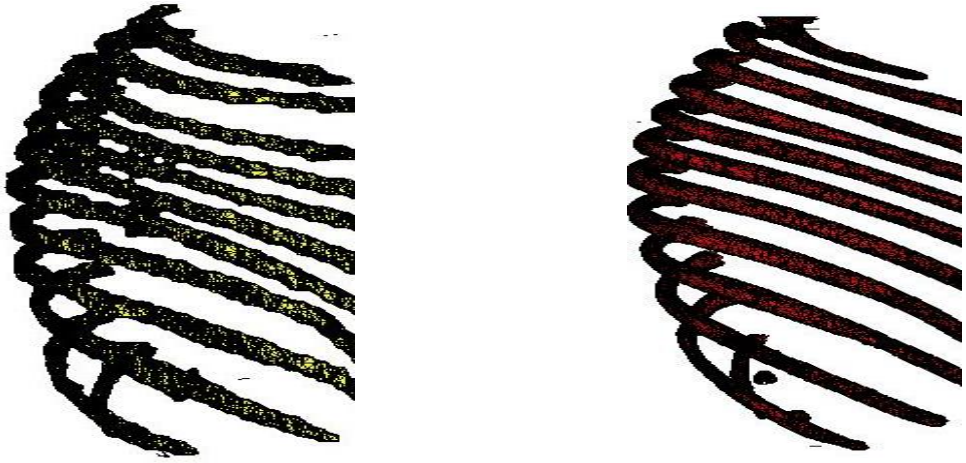

(a) b)

Figure 4-5 A lateral view of the extracted ribcage geometry: (a). Original surfaces extracted from CT scan images, and (b) Smoothened surfaces of WSU_F162-60 using 3-matic software available in Mimics

4.2.2. Scaling the patient specific mesh to statistically average geometric model

The CAD surfaces developed so far were based on CT scan images of one cadaver, which can be characterized as a patient-specific model. Although the cadaver was carefully chosen to closely match the overall anthropometric details for an average 70 years old female, some specific attributes of the model might not represent an average person within that particular segment of the population. This argument, in general, is valid because biological variations exist even among persons of the same age, height, weight, and gender. Therefore, it is important to compare the geometry retrieved from CT scans of the 73 years old female cadaver to the statistical average geometric model representing an average 70 years old female.

Therefore, the rib cage of the WSU_F160-62 geometric model was compared with that of the S-F70 stick model shown in Figure 4-6. Results indicated that the WSU_F160-62 model was approximately 5% smaller in depth and 10% smaller in width than the S-F70 stick ribcage model (Figure 4-6). Therefore, the ribcage of the WSU_F160-62 model was scaled to 1.05 times in anterior-posterior direction and 1.1 times in lateral direction to match the statistical averaged dimensions. The angle of the ribs were not adjusted since there was minor difference in terms of angles between the two models. The need to expand the WSU_F160-62 is understandable, because an average 70 years old female weighs 73 kg while the WSU_F160-62 represents a 73 years old, 62 kg female. Please note that the center of scaling was located at the mid sternum as predicted through the stick model.

4.2.3. CAD surface extraction for soft tissues

Because normal CT scans cannot provide soft tissue geometries, the CT scan images of the cadaver used for extracting skeletal geometry cannot be used to retrieve soft tissue CAD models. Therefore, a 65-year-old female contrast CT scanned data were retrieved from an online

database available at www.cancerarchieve.net. These data were used to extract the geometry of the heart, lungs, liver, kidneys, pancreas, spleen, gall bladder, aorta, vena-cava, and the rest of the abdominal tissues. A similar set of procedures were followed as explained earlier in Section 4.2 to get the CAD surface data of soft tissues by 3-D rendering of images. Figure 4-7 shows snapshots of several internal organs and blood vessels taken from extracted soft tissue CAD data.

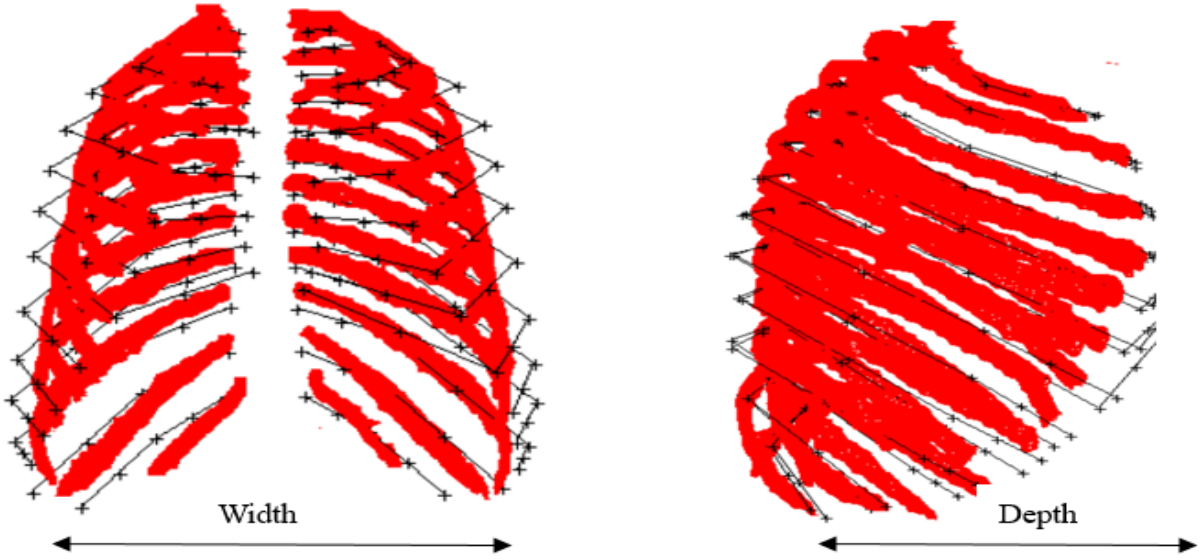

Frontal view Lateral view

Figure 4-6 Comparison between the smoothened WSU_F160-62 model (red) with the previously developed S-F70 stick model representing a 70 years old female (black)

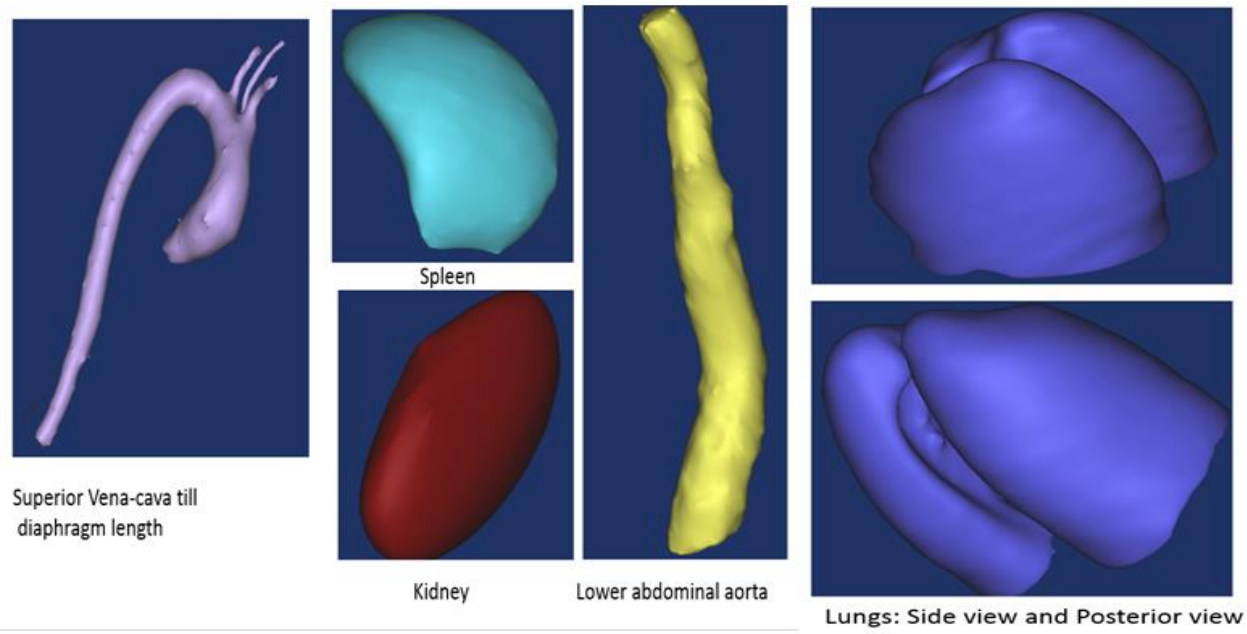

Figure 4-7 CAD surafce extraction for different soft tissues

Aside from internal organs and blood vessels, the external contours for the body shape was retrieved from the University of Michigan Transportation Research Institute (UMTRI) database of the Toyota CSRC (Collaborative Safety Research Center) project through personal communication as shown in Figure 4-8. This database is based on surface scanning of 200 men and women at both driving and standing statures. Among these volunteer subjects, more than 2/3 of the samples were from age 60 and older. Detailed procedures for scanning the volunteers were listed in Reed *et al.* (2013). The volunteers were scanned in their normal driving postures and in standing position in a reconfigurable laboratory mock setup. The landmarks were identified for key representative bones in the human body such as sternum ends, shoulder acronym position and other bone positions. The retrieved outer surface data representing an average 70 years old female for the standing as well as for the driving postures are shown in Figure 4-8.

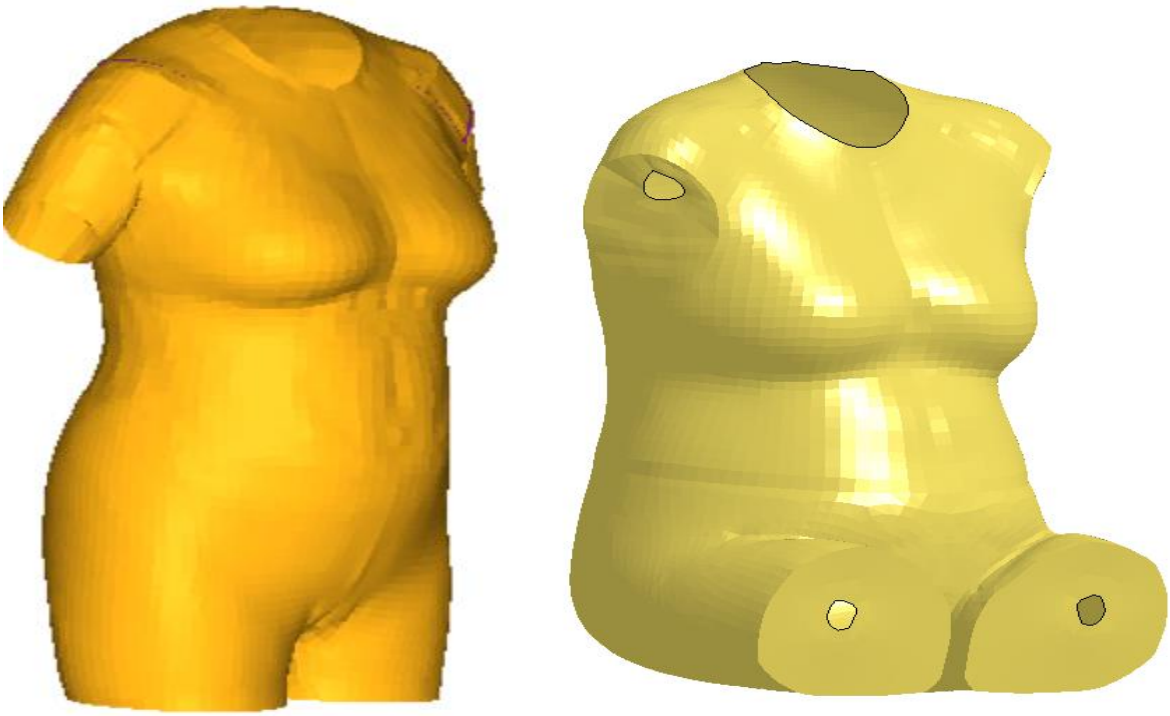

(a) (b)

Figure 4-8 Outside surface retrieved from UMTRI data for an average 70 years old female (a). Standing posture (b). Driving Posture

4.2.4. Finite element meshing

After the detailed geometric model of the ribcage is determined, the step-by-step procedures used to develop the torso FE model of an average 70 years old female follow the same processes as shown in Figure 4-4, which explains the hierarchy of the procedures that were followed during the FE model development for the thoracic region. This section of the dissertation focuses on developing a high quality mesh for the model.

After the geometrical rendering of the surface, the preliminary mesh for the different body regions was generated by the block meshing technique with the help of Ansys ICEM developed by Dessaults Systems, Paris, France. Figure 4-9 displays the step-by-step generation of the 3-D mesh from the rendered surface of the scapula bone.

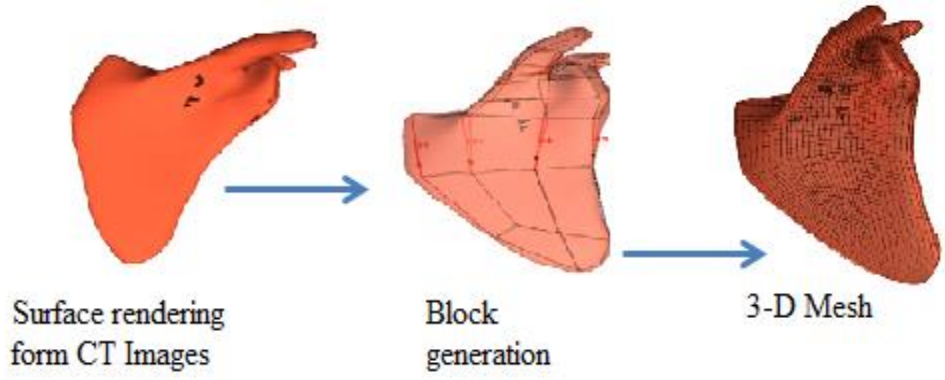

Figure 4-9 Step-by-step generation of a preliminary mesh

Once the preliminary mesh was generated, it was refined on the basis of certain element quality check parameters with the help of Hypermesh 10.0. The necessary quality check was performed while modifying the attributes of the mesh parameters, such as Jacobian value < 0.4, warpage < 50, aspect ratio < 5, skew angle < 60º, average element size around 3 mm. *etc*.

Most of the bony structure was modeled as hexahedral mesh for trabecular bone and shell elements were used to represent cortical bone. Also, some cavities in the thoracic and abdomen region were built using tetrahedral elements. The ligaments at different anatomical locations were modeled using 1-D elements which can take only tensile loads.

The finalized mesh for skeletal bones was integrated in the outer body surface provided by UMTRI. The landmarks for the joint locations and key identifiable points at different regions of the body, like scapula, elbow, shoulder, pubic symphonies, *etc*., were provided by the group for positioning the skeletal structures in the outer body surface. Based on these landmarks, appropriate meshed components of the skeletal bones such as the sternum, thoracic spine, lumbar spine, and other bones were integrated with the outer surface. An example of positioning of ribs, sternum and thoracic spine along with the given landmarks is shown in Figure 4-10. For both postures, similar positioning of the skeletal components was done according to landmark

locations, although some minor adjustments were also made based on valid anatomical configurations.

Once the skeletal components were integrated with the outer surface, the soft tissue components were also integrated inside the skeletal parts according to valid anatomical configurations. The gaps inside the soft tissues were filled with 3-D tetrahedral elements. The example for tetrahedral elements filling the gap between thoacic soft tissue parts, like the heart, lungs, aorta, and superior vena cava is shown in Figure 4-11. The tetrahedral elements were made in such a way that it provided a nodal connection between different body parts. Similar filling of nodal connected tetrahedral solid elements were done in the abdominal cavity to fill the gap between the liver, gall bladder, spleen, kidneys, and other injury relevant parts. The lower abodmen was meshed with a single volume representing the overall structure for the smaller intestine, larger intestine, transverse colons, asending colons, jejunum rectum, and other injury relevant parts in this region as shown in Figure 4-12. Methods related to the detailed meshing of these lower abdominal parts was beyond the scope of this disseratation.

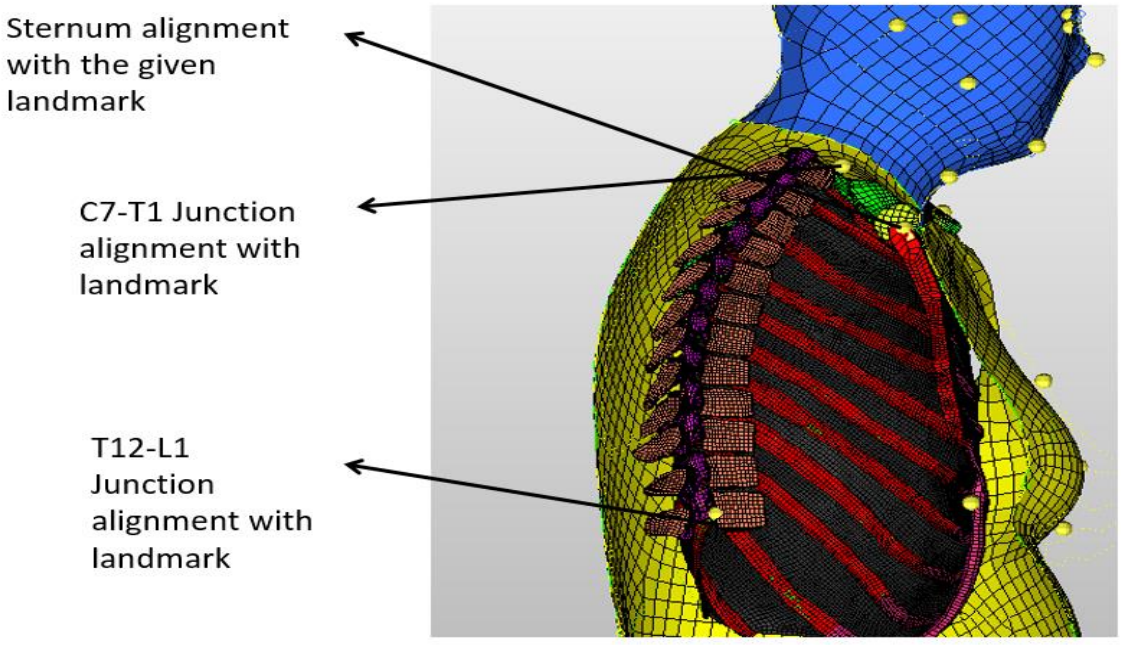

Figure 4-10 Example of integrating of bony structure into outer body surface in accordance with landmarks provided by UMTRI

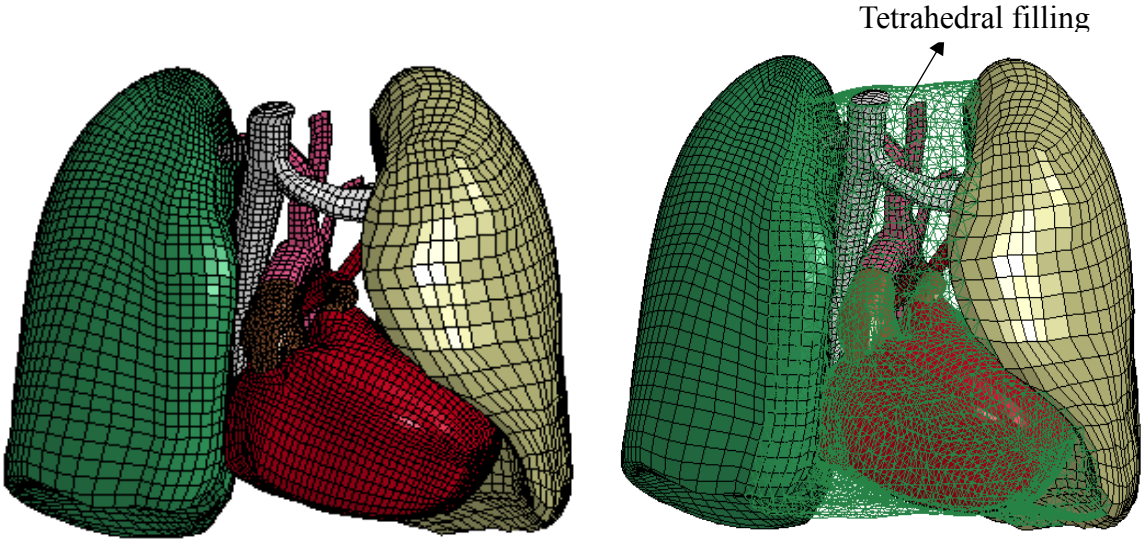

Figure 4-11 Snapshot showing the heart, lungs, aorta, superior vena cava without tetrahedral solid mesh filling between the gaps (Left), and with filled tetrahedral solid elements (Right)

The final mesh for the torso skeleton along with different injury relevant soft tissues positioned at their respective places is shown in Figure 4-13. The model consisted of around 600,000 solid elements, 200,000 shell elements, and 300 1-D elements.

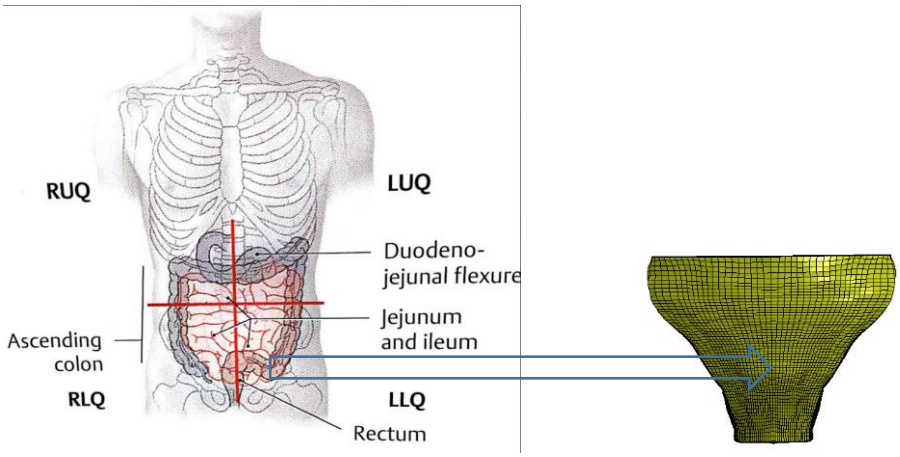

Figure 4-12 Snapshot showing a single volume representation of other lower abdominal parts

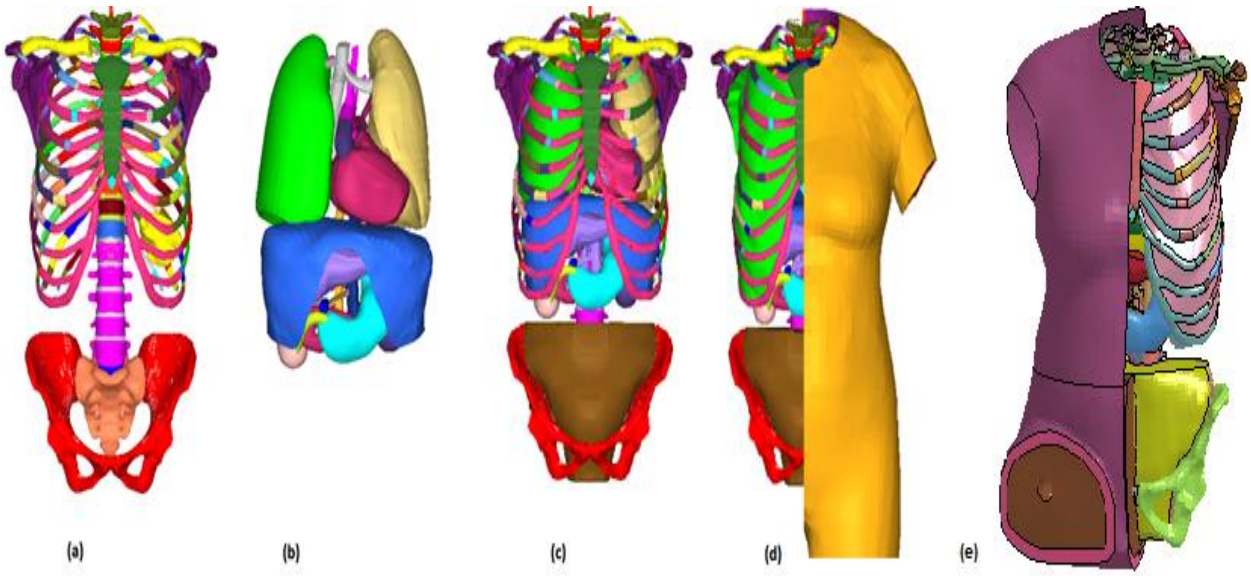

Figure 4-13 Snapshot showing the mesh (solid mode) for (a) skeletal components, (b) soft tissue components, (c) assembly for skeletal and soft tissue components, (d) integration of the mesh with outer standing surface from UMTRI, and (e) integration of the mesh with outer sitting surface from UMTRI

4.3. CHAPTER CONCLUSION

This section of the dissertation demonstrated the development of S-M70 and S-F70 stick models and how they were used to scale a 73 years old female geometric model (WSU_162-60) to represent the torso region of an average 70 years old female torso. Further, a high quality FE mesh of skeletal as well as soft tissue components was generated with the help of block meshing technique. The outer body surface for an average 70 years old female was retrieved from UMTRI and the skeletal components were integrated inside this surface with the help of landmark provided by UMTRI. The injury relevant soft tissue components, such as the heart, lungs, liver, kidneys, stomach, pancreas, aorta, vena cava, and other soft tissues presented in thoracic and upper abdominal cavity were positioned inside the skeletal mesh according to valid anatomical configurations. The lower abdominal cavity was modeled with single volume.

CHAPTER 5. AGE AND GENDER RELATED CHANGES IN BIOMECHANICAL RESPONSES OF HUMAN RIBS

Once the mesh is developed, the next task is to define suitable material properties in the model. Yang *et al.* (2006) summarized the material properties of developed FE models, but those were majorly focused on younger populations. The current model requires inclusion of age and gender dependent material properties, especially for the ribs because they are the prime load bearing element for frontal impact and there is a high risk on injury for elderly female (Kent *et al*. (2005)). Further analyses are focused on defining the age and gender related effects in the structural properties of human ribs and the estimation of suitable material model for 70 years old female ribs. Because the majority of the data have been published in the Stapp Car Crash Journal, many sections in this chapter are directly taken from Kalra et al. (2015) with re-assigned table and figure numbers. Also, Equations 5-6a, 5-7a and 5-8a not published in the 2015 Stapp paper were included in this chapter.

5.1. INTRODUCTION

Rib fracture is one of the most common and serious injuries sustained by people, and in particular women and the elderly, in motor vehicle crashes as discussed in previous sections. The higher risk of serious injury and death due to rib fractures demands a dedicated study to identify the effects of the biomechanical responses of ribs with age and gender. The research conducted so far cannot be collectively analyzed, on a single platform to track changes in biomechanical responses of ribs based on gender and age, due to differences in the loading conditions. Current study addresses a strong need for analysis of biomechanical properties associated with rib injuries likely to be sustained in crashes by different age- and gender-based populations.

Rib fracture risks that are related to gender and age can be estimated from structural- and material-biomechanical properties. Structural properties are macroscopic, and are related to size, such as length, diameter, and cross-sectional area. Material properties are microscopic, and are related to distributions of materials (*e.g.*, collagen, mineral content, connectivity of trabecular bone).

In many studies, stiffness, mean and maximum bending forces, and mean and maximum deflections are considered to be indicators of structural responses of the rib. For instance, Granik and Stein (1973), Yoganandan and Pintar (1998), Stitzel *et al.* (2003), Sandoz *et al.* (2007) and Kemper *et al.* (2007) performed 3-point bending tests on rib segments to quantify structural responses in terms of maximum force and deflection. They linked these measurements to material behaviors by calculating corresponding elastic moduli, using an approach entitled beam theory approximation. Other researchers, like Schultz *et al.* (1974), Charpail *et al.* (2005), Li *et al.* (2010), Kindig *et al.* (2011), did whole-rib bending tests to determine the maximum values of force and deflections. These values are considered stiffness responses of the isolated whole ribs. In most of the studies involving structural properties, the sample size was insufficient to determine the age- or gender-related changes in structural responses of the ribs.

Material properties characterize material responses by normalizing effects due to size differences. In other words, the study of material properties requires stress-strain responses instead of force-deflection characteristics in typical tensile tests. Because the size of the structure is predetermined in a finite element (FE) model, material property becomes a crucial component for calculating the structure response. Kemper *et al.* (2005) performed 117 tests using cortical-bone coupons from the ribs of six cadaver specimens (three males and three females) aged 18 to 67 years, and showed that the cortical bone in ribs becomes more brittle with increasing age.

Also, it was found that there were significant differences in mechanical properties between rib samples taken from males versus females. Females had a higher elastic modulus than males ($p < 0.01$), while males had a higher ultimate strain ($p < 0.01$). However, the sample size was limited in this study. Other researchers, like Kemper *et al.* (2007) and Subit *et al.* (2013), also performed tensile coupon tests, but again the sample sizes were too small to depict the differences in material properties based on age and gender.

Table 5-1 summarizes most of the tests available in the literature for rib samples under different loading conditions. Other types of studies have been reported in scientific literature regarding structural responses of ribs. Two common approaches using bending tests to link structural to material properties are (a) beam theory approximation and (b) FE modeling reverse engineering. The first approach is implemented through testing a short segment of rib, which can be approximated as a straight beam. The second approach requires further geometric details, such as cortical thickness. Since the approach using beam theory approximation is appropriate for relatively small, straight bone sections, Granik and Stein (1973) and Yoganandan and Pintar (1998) used this approach to calculate elastic moduli of ribs. Li *et al.* (2010) conducted dynamic whole-rib tests on three rib specimens, and material properties of the ribs were optimized using the second approach. A reverse engineering technique in conjunction with FE models, with geometric details captured through medical scans, was used to identify the properties.

Several researchers have attempted to associate differences in structural properties with age and gender. Kimpara *et al.* (2003) studied rib responses in side impact crashes ($N = 30$), conducted at Wayne State University (WSU), to show that responses to males were different from responses to females. Using linear regression analysis, age was not found to be a contributing factor, probably due to the small sample size. Tomasch *et al.* (2010) did three-point

bending tests on rib samples of five cadaveric specimens and used linear scaling laws to establish force-deflection curves based on age and gender, but the sample size was limited, and no statistical significance was found. In a recent study, Schafman (2015) performed whole rib bending tests on a large number of samples [184 specimens, 23 females and 70 males, aged 4 to 99 years (mean 50±25)] to identify structural differences based on age and gender. It was found that maximum force changed significantly with age and gender. Additionally, maximum percentage of deflection changed significantly with age, but not with gender, whereas linear structural stiffness changed significantly with gender, but not with age. The value of energy absorption at fracture varied significantly with age, but not with gender.

Although Schafman (2015) used a large sample size to examine the age and gender related structural differences in ribs, the whole-rib specimens used in the study did not fit the beam theory approximation, and therefore the data provided cannot be used in calculations of material properties. Additionally, the FE modeling reverse engineering approach cannot be used due to a lack of geometric details, such as cortical thickness and cross-sectional measurements, for each rib tested. The current study satisfied a similar purpose, but along with structural differences, geometric properties such as average cortical thickness, were also studied. Findings from the current study can be used to link structural and material properties. The results will provide data for implementations in FE studies, which will allow for further study of age- and gender-related differences in mechanical properties.

All aforementioned studies satisfied a similar purpose, but they could not be collectively analyzed, due to differences in loading conditions, sample preparation, sample sizes, and variations in strain rates used by the different research groups. There were large variations in biomechanical responses reported in the literature, as shown in Table 5-1. Overall, the elastic

modulus values ranged from 1.9 to 18 GPa, due to differences in loading conditions and specimens used. This large range of values makes it difficult to decide what value of elastic modulus should be used in an FE model to best replicate the behavior of human ribs in impact studies. In order to better quantify age- and gender-related changes that may link to biomechanical responses of the ribs, the current study included a larger sample size and consistent loading conditions.

5.2. METHODS AND MATERIALS

Data from 278 samples, taken from 82 cadaver specimens, were analyzed to quantify the age-, gender-, height-, and weight related changes in biomechanical properties of the ribs. All of these cadavers were used in different impact tests, at WSU Bioengineering Center, without significant loading to the chest. During autopsy, a total of four rib sections (from the sixth and seventh levels and from both sides of the body) were removed from each test subject. Each sample was approximately 150 mm long and was taken from between the axillary and medio-clavicular lines, as shown in Figure 5-1.

The rib samples were kept moist at all times during cutting, which was done with a diamond saw. To prevent overheating of the bones, a saline solution was sprayed onto the location where the cut was being made. After retrieval, the samples were wrapped in gauze that had been soaked in a 0.9% saline solution, and were stored at -20°C until the time of testing. A previous study had shown that the freezing process did not significantly alter the biomechanical properties of bone (Van Haaren *et al.* 2008). The samples were thawed to room temperature 24 hours prior to mechanical testing.

Table 5-1 Summary of rib tests available in Literature (Where E-Elastic modulus, σult= Ultimate Stress, Ɛult= ultimate strain, Fmax=Maximum load, dmax=maximum deflection, UR=upper rib, LR=lower rib, kmax= maximum stiffness, kmean = mean stiffness)

Author	Loading Type	No of specimens	Rib Level	Distance between supports(mm)	Overall rib specimen length(mm)	Loading rate(mm/sec)	Biomechanical responses
Granik and Stein (1973)	3-point bending	n/a, 15 cadavers	6 and 7	101.6	152.4	0.042	E=11.5 GPa, σ_{ult}=0.160 GPa, d_{max}=4 mm
Schultz et al. (1974)	Whole rib bending	n/a, 5 M	2,4,6,8,9,10	-	-	Incremental loading with 2.45N	F_{max}=7.35 N, UR d_{max}=30 mm, LR d_{max}=60 mm
Yoganandan and Pintar (1998)	3-point bending	120 specimens 30 cadavers	7	100	150	0.042	E=2.3 GPa, d_{max}=3 mm, F_{max}=158 N
			8				E=1.9 GPa, d_{max}=3.2 mm, F_{max}=137 N
Stitzel et al. (2003)	3-point bending (coupon)	80 specimens 2M,2F	1-12,Avg Anterior	20	29	356	E=7.5 GPa, σ_{ult}=0.116 GPa, ε_{ult}=0.032
			1-12,Avg lateral				E=11.8 GPa, σ_{ult}=0.153 GPa, ε_{ult}=0.153
			1-12,Avg Posterior				E=10.7 GPa, σ_{ult}=0.127 GPa, ε_{ult}=0.025
Kemper et al. (2005)	Tensile coupon test	117 specimens 3M,3F	1-12, anterior and lateral	-	-	0.5strain/sec	E=14 GPa, σ_{ult}=0.12 GPa, ε_{ult}=0.027
Kemper et al. (2007)	Tensile coupon test	46 specimens, 6M	4-7, anterior and lateral	-	-	0.5strain/sec	E=13.3-15.1 Gpa, σult=0.11-0.14 GPa, Ɛult=0.023-0.027
	3-point bending	48 specimens, 6M		82.55	101.6	0.7strain/sec	M_{max}=3.02-9.76 Nm, k_{max}=57.99-225.71 N/mm
Sandoz et al. (2007)	3-point bending	31 specimens 3F, 9M	4-9,	100	-	250	F_{max}=230 N, d_{max}= 5 mm
						100	F_{max}=210 N, d_{max}=4.9 mm
						0.033	F_{max}=150 N, d_{max}=4.75
Charpeil et al. (2005)	Whole rib bending	30 specimens 3M, 2F	4-9,	-	-	-	F_{mean} =87 N, d_{mean}=41 mm, k_{mean}=2340 N/m
Li et al. (2010)	Whole rib bending	3 specimens, 3M	2,4,10	-	-	2	F_{max}=41.2 - 57.1 N
						500-1000	F_{max}=87.4 - 123.4 N
Tomash et al. (2010)	3-point rib bending	140 specimens, 2F, 1M	-	-	-	0.166 and 8.33	F_{max}=90 - 120 N
Kindig et al. (2011)	Whole rib bending	27 specimens 2F, 1M	2-10,	-	-	2	F_{max}=19.5-177.3 N
Subit et al. (2013)	Tensile coupon test	10 specimens, 3 cadavers	6-7,	-	-	0.01-0.02	E=11.4-18.5 GPa, σ_{ult}=0.08-0.143 GPa, ε_{ult}=0.007-0.015%
						24	σ_{ult}=0.094-0.155 GPa,
Schafman (2015)	Whole rib bending	184 specimens 23F, 70M	-	-	-	1000-2000	F_{max} =25-300 N, d_{max}= 7.5-70%, k_{max}= 0.5-20 N/mm

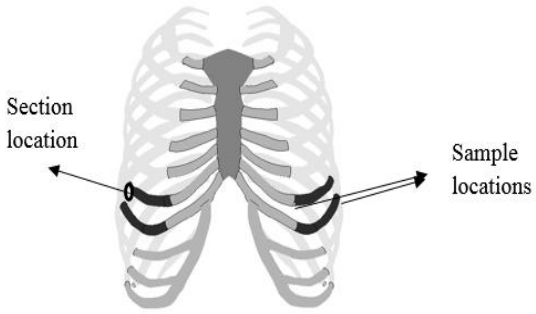

Figure 5-1 Locations of rib specimens

After thawing, each dissected rib sample was positioned on a fixture designed for 3-point testing. In order to allow the ram to load the specimen at a flat segment, slight adjustments were made in the axial direction. Anatomically, the rib is classified as a flat bone. Hence, there were no stability issues when loading the specimen in a 3-point bending scheme.

5.2.1 Bending Test

A special fixture was fabricated to provide static 3-point bending of ribs at a rate of 0.169 mm/sec. The fixture had a span of 100 mm and a semi-circular load applicator with a diameter of 10 mm, as shown in Figure 5-2. Using the ramp function of an INSTRON machine, the samples were loaded until failure.

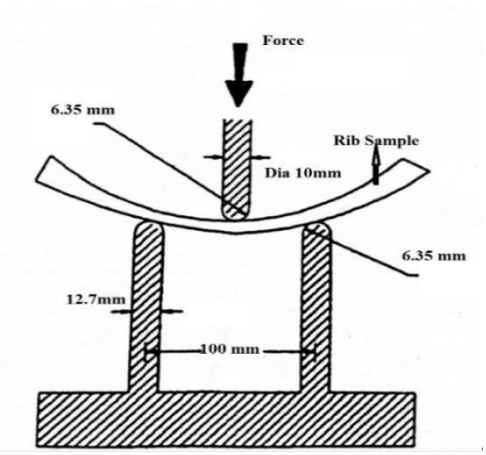

Figure 5-2 Setup for 3-point bending tests on ribs

Force data were collected using a load cell with a 250 lb (1,112 N) capacity. This load cell was one of the original load cells made by Robert A. Denton while he was employed at Wayne State University, and therefore, there is no model number. However, this load cell was calibrated against the built-in load cell in the INSTRON 1321 test system. All data were collected using a Tektronix TestLab data acquisition system set to a sampling rate of 200 Hz. The data were filtered with a low-pass Butterworth filter set to retain frequencies under 100 Hz. This low frequency was used because of the nature of low-speed testing. The force-deflection curve was plotted for each rib test, and the maximum bending moment (MBM), the maximum bending angle, the maximum rib displacement (d_{max}), and the slope of the bending moment-angle curve (SMT) were calculated for each individual test. The maximum bending moment was calculated by multiplying the maximum bending force by half of the fixture span (50 mm). Because only a small deflection angle is required to fracture the rib, the maximum bending angle (Figure 5-3) was calculated using the small angle approximation, as shown in Eq. 5-1:

$$tan\,\theta = 2d/L \qquad \text{Eq. [5-1]}$$

where θ is the bending angle, d is the deflection measured using the INSTRON LVDT, and L is the span.

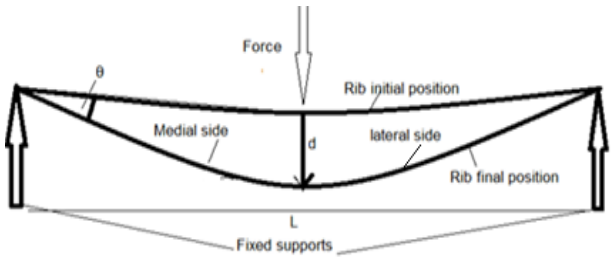

Figure 5-3 Schematic diagram showing the relevant parameters used to calculate the maximum bending angle

The medial side (towards cartilage end) of the fractured rib was saved and used to calculate the cortical thickness of each sample, and the lateral side (towards vertebrae end) was preserved for mineral content analysis. The body mass index (BMI) was calculated by dividing

the weight (in kg) by the square of the height (in m) for each cadaver specimen for which weight and height were known.

After the bending tests, medial fragments were cut from the sides opposite the fractures in order to minimize the irregularities of the fractures and produce clean transverse cross sections. For scaling purposes, each cross section was photographed with a ruler showing millimeters, as shown in Figure 5-4. A point near the geometric center of the cross-section, selected by finding the intersection of two lines located at half the distance between the inferior and superior edges and half the distance between the anterior and posterior edges, was used to draw radial lines over the entire rib before digitization of the inner and outer boundary points. The x-y coordinates of these points were used to calculate the thickness at each section.

Data points were captured using a sonic digitizer, and cortical thicknesses were calculated at various points and then averaged over the entire cortical surface, as shown in Figure 5-5 and Eq. 5-2. For mineral analysis of the bones, 2 cm rib fragments were weighed, dried in an oven at 130ºC for two hours, and then reweighed. The dry weights were obtained, and all the fragments were burned in an oven for eight hours at 700ºC, at which time the ash weights were obtained. The percentage of ash was calculated from ash weight and dry weight (Eq. 5-3).

5.2.2 Characterization of rib response

The force-deflection and corresponding moment-angle curves obtained for each of the samples were further analyzed to quantify the behaviors of the rib samples. Each curve was segmented into three main segments, 0 to point A, A to B, and B to D, as shown in Figure 5-6. Point A represents the point at which the curve departs from linearity, which can be seen by comparison with the superimposed line beginning at the origin. This linear response from 0 to A represents the elastic region. Point B represents the fracture initiation point, and the

corresponding point C on the deflection axis represents the maximum deflection at which the rib fails. Segment B-D represents the post fracture behavior of the rib. The moment and force corresponding to the yield point between A and B could be fully characterized in most of the tests, and they ranged from 15 to 20% lower than the maximum value. The slope of the force-deflection (SFD) and moment-angle (SMT) shown in Figure 5-6 are defined using Eqs. 5-4a and 5-4b.

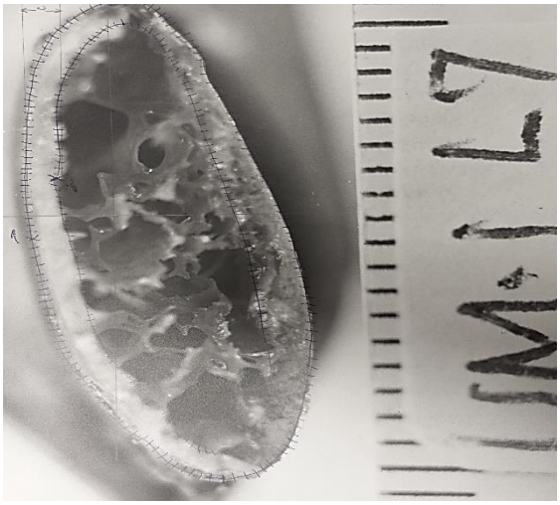

Figure 5-4 Photograph of a rib cross-section

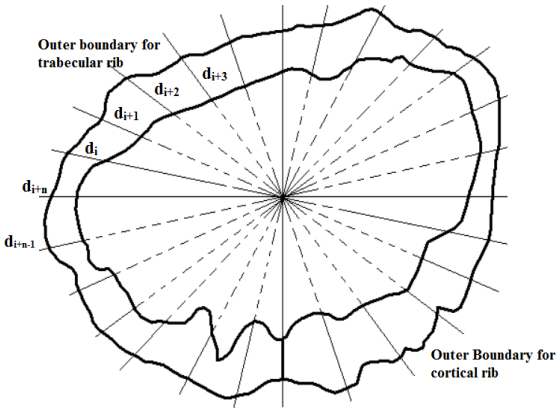

Figure 5-5 Method to calculate average cortical thickness (Cross-section taken from sample 330 R6)

Average cortical thickness: Percentage ash content:

$$d_{avg} = \sum_{n=0}^{n} \frac{d_{i+n}}{n} \quad \text{Eq. [5-2]}$$

$$\%\ ash = \frac{Ash\ Weight}{Dry\ Weight}\ X\ 100 \quad \text{Eq. [5-3]}$$

$$SFD = \frac{F_A}{d_A} \quad \text{Eq. [5-4a]}$$

$$SMT = \frac{M_{max}}{\theta_{max}} \quad \text{Eq. [5-4b]}$$

The maximum bending moment (MBM) is defined as the moment at which the rib fractures occur, and is illustrated at point B (Figure 5-6, left). The maximum rib deflection (d_{max}) is denoted as point C (Figure 5-6, left), and the maximum bending angle (θ_{max}) is depicted as point C (Figure 5-6, right). θ_{max} is calculated using Eq. 1.

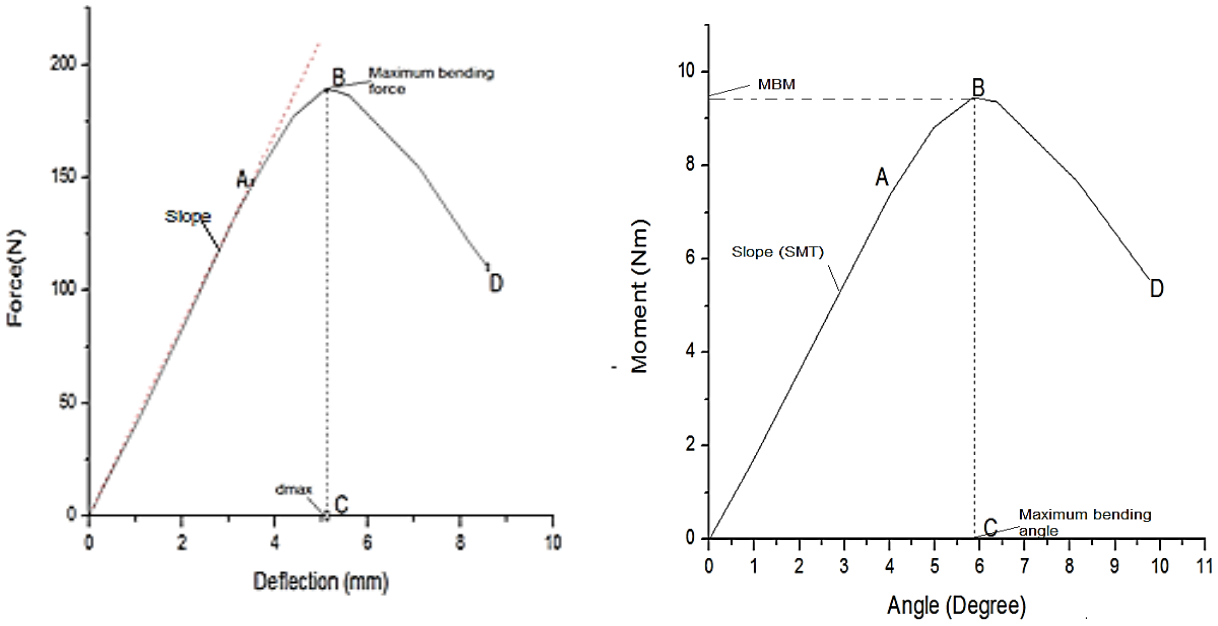

Figure 5-6 Bending test curve characterization of rib samples (Left): raw force-deflection diagram, (Right): calculated moment-angle diagram

5.3. RESULTS AND STASTICAL ANALYSIS

Differences in biomechanical responses, such as MBM, SMT, d_{max}, and cortical thickness, based on gender, age, BMI, height, weight and ash content percentage for each sample were analyzed using SPSS Statistics, version 22.0 (IBM, USA). Gender, age, height and weight represent physical characteristics, and they were directly retrieved from anthropomorphic details of cadavers. Representations of these physical characteristics were used as independent

variables. Another physical characteristic represented in this study was rib cortical thickness, which was measured directly from cross-sectional images. All biomechanical test responses and all cortical thickness measurements were considered dependent variables. The rationale for including cortical thickness in this list is that bone-remodeling processes are governed by biological factors such as age, gender, height and weight, as well as physical activities not quantifiable in cadaveric study.

In general, Student's t-tests were performed to identify differences between male and female groups. The method of Generalized Estimating Equations (GEE) was used to determine whether age, gender, height and weight were significant predictors of biomechanical responses and the average cortical thickness. Since a cadaver contributed more than one sample, statistical dependency would be presented in the dataset, *i.e.* the observations are correlated. To account this dependency, GEE was used instead of multiple regressions. Standard multiple regression assumes independent observations. The covariance matrix and the working correlation matrix was chosen as a robust estimator type and exchangeable type respectively, during GEE analysis. A p value of less than 0.05 was considered statistically significant.

5.3.1 Variations with age and gender – Student's T-test results

Ninety-four rib samples from 29 female-cadaver specimens, having a mean age of 58.83±11.5 years, and 184 samples from 53 male specimens, having a mean age of 57.75±11.83 years, were included in the analysis. Based on a t-test result, there were no significant differences in age between the samples collected for the gender tests ($p = 0.429$). Additionally, no significant differences were found between biomechanical data obtained from the 6th and 7th ribs nor from right and left ribs. Consequently, all test data were analyzed without separation of the location (6th and 7th) and side (left and right).

Also, t-test was conducted to compare the biomechanical responses (MBM, SMT, and maximum bending angle), average cortical thicknesses, percentage of ash content, BMI, height and weight between males and females. Descriptive statistical results along with t-test significance values between genders are shown in Table 5-2. The average cortical-bone thickness in males was 0.15 mm larger than that in females (p = 0.001*), the mean MBM was also found to be 2.52 Nm larger in males than that in females (p = 0.000*). Note that a "*" indicates statistical significance throughout the paper.

Table 5-2 Descriptive statistical results of the complete data set

Variable	Gender	Number of cadavers	Mean	Std. Deviation	*p* value
Age	Female	29	58.83	11.5	0.429
	Male	53	57.75	11.83	
Average cortical thickness (mm)	Female	29	0.95	0.25	0.001*
	Male	53	1.09	0.35	
MBM (Nm)	Female	29	8.16	3.2	0.000*
	Male	53	10.68	5.78	
Maximum bending angle (degree)	Female	29	5.19	2.2	0.086
	Male	53	4.78	1.66	
SMT (Nm/deg)	Female	29	2.07	0.96	0.000*
	Male	53	2.92	1.8	
BMI (kg/m^2)	Female	18	22.3	3.58	0.07
	Male	38	23.4	4.36	
Ash percentage	Female	24	40.63	8.23	0.004*
	Male	23	37.3	7.22	
Height (cm)	Female	18	160.26	7.29	0.000*
	Male	38	171	9.23	
Weight (kg)	Female	18	57.62	11.19	0.000*
	Male	38	68.46	14.06	

The maximum bending angle did not change significantly between males and females (p = 0.085), but the mean SMT was found to be significantly lower in females than in males (p =

0.000*). Height and weight were found to be significantly different, but BMI did not change significantly between males and females. Although the population attributes, in terms of the mean age and mean BMI, did not vary between males and females, the rib biomechanical responses in terms of MBM, SMT, and average cortical thickness were different between the genders.

5.3.2 Calculations for Generalized Estimating Equations (GEE)

Initially, the effects of the predictors (age, gender, percentage of ash content, height and weight) on the average cortical thickness, MBM, maximum bending angle, and SMT were analyzed. In all GEE analyses, percentage of ash content was found to be non-significant predictor with $p > 0.05$, therefore separate analyses were run by including predictors age, sex, height and weight for all biomechanical responses and the average cortical thickness value. Moreover, one aim of the current study was to predict the biomechanical responses with known anthropomorphic details of the specimens in terms of gender, age, height and weight. It would be difficult to include the percentage of ash content as a predictor variable as extra effort would be needed to burn the sample of ribs to get the percentage of ash content for that individual.

Table 5-3 summarizes the results of parameter estimates from GEE analysis for the average cortical thickness. All predictors had a p value greater than 0.05 and the lowest p value (0.084) was attributed to gender. The estimated model for cortical thickness was derived as:

Average cortical thickness (mm) = 1.526 - 0.003×age (years) + 0.133×gender - 0.004×height (cm) + 0.004×weight (kg) (0- female, 1- male) Eq. [5-5]

The results of the GEE analysis for the dependent variable, MBM, are shown in (Table 5-4), where age ($p = 0.024$*) and gender ($p = 0.025$*) were found to be the significant predictors for estimating MBM. The estimated model for MBM was derived as:

MBM (Nm) = 27.389 - 0.152×age (years) + 2.634 ×gender - 0.082×height (cm) + 0.053×weight (kg) (0- female, 1- male) Eq. [5-6]

Table 5-3 GEE estimations results for Average cortical thickness

	Average cortical thickness (mm)		
Predictor	Coefficient	Wald Chi-Square	p
Intercept	1.526	-	-
Age	-0.003	1.339	0.247
Gender	0.133	2.987	0.084
Height	-0.004	0.819	0.365
Weight	0.004	1.577	0.209

Table 5-4 GEE estimations results for maximum bending moment

	MBM (Nm)		
Predictor	Coefficient	Wald Chi-Square	p
Intercept	27.389	-	-
Age	-0.152	5.130	0.024*
Gender	2.634	5.039	0.025*
Height	-0.082	2.081	0.149
Weight	0.053	1.290	0.256

Similar results for Maximum bending force (MBF) can also be listed as:

MBF (N) = 547.770 – 3.045×age (years) + 52.674 ×gender – 1.634 ×height (cm) + 1.065×weight (kg) (0- female, 1- male) Eq. [5-6a]

Table 5-5 summarizes the results of parameter estimates from GEE analysis for the maximum bending angle. All predictors had a p value of greater than 0.05. The estimated model for the maximum bending angle was derived as:

Maximum bending angle (degree) = 7.809 + 0.017×age (years) - 0.124×gender - 0.025×height (cm) + 0.007×weight (kg) (0- female, 1- male) Eq. [5-7]

Table 5-5 GEE estimations results for maximum bending angle

	Maximum bending angle (degree)		
Predictor	Coefficient	Wald Chi-Square	p
Intercept	7.809	-	-
Age	0.017	0.996	0.318
Gender	-0.124	0.053	0.819
Height	-0.025	1.342	0.247
Weight	0.007	0.178	0.673

Similar results for maximum deflection (d_{max}) can be listed as:

d_{max} (mm) = 7.204 + 0.016×age (years) - 0.115×gender - 0.025×height (cm) + 0.007×weight (kg) (0- female, 1- male) Eq. [5-7a]

GEE analysis shows that the value of SMT correlated to age (p = 0.023*) and gender (p = 0.013*) (Table 5-6). The estimated model for the dependent variable, SMT was derived as:

SMT (Nm/deg) = 5.492 - 0.038×age (years) + 0.726×gender - 0.014×height (cm) + 0.018×weight (kg) (0-female, 1- male) Eq. [5-8]

Similar results for the value of SFD (slope of force deflection) diagram can be listed as:

SFD (N/mm) = 122.715 - 0.861×age (years) + 16.862×gender - 0.295×height (cm) + 0.399×weight (kg) (0-female, 1- male) Eq. [5-8a]

Table 5-6 GEE estimations results for slope of moment bending angle curve

	SMT (Nm/deg)		
Predictor	Coefficient	Wald Chi-Square	p
Intercept	5.492	-	-
Age	-0.038	5.190	0.023*
Gender	0.726	6.214	0.013*
Height	-0.014	1.010	0.315
Weight	0.018	1.916	0.166

Detailed results of the GEE analyses for each variable were shown in Appendix A.

5.4. DISCUSSION

There were no significant differences found in the current study in biomechanical responses between ribs at levels 6 and 7 or between the left and right sides. Similar results were reported by Yoganandan *et al.* (1998) and Schultz *et al.* (1974) for the adjacent rib levels. Granik and Stein (1973), Yoganandan and Pintar (1998) and Sandoz *et al.* (2007) performed 3-point bending on rib samples using fixtures with spans of 100 and 101.6 mm. These are comparable to

the fixtures used in the current study. As shown in Table 5-7, data obtained from the current study are consistent with published data from the aforementioned studies.

Table 5-7 Comparison of the maximum forces and deflections of similar experimental setups

Test	Age (Years)	Span (mm)	Loading rate (mm/sec)	Specimens	Mean maximum bending force (N)	Mean maximum deflection (mm)
Granik and Stein (1973)	NA	101.6	0.042	10	NA	4.064
Yoganandan and Pintar (1998)	63.6±10.5	100	0.042	11F, 19M	158	3
Sandoz *et al.* (2007)	63±7	100	0.03	3F, 9M	150	4.7
			100		210	4.85
			250		240	5.1
Current Study (2015)	59.17±12.46	100	0.169	29F	163	4.54
	57.36±12.41			53M	213	4.2

Because a larger sample size was used in the current study, the effects of gender and age became statistically significant on the maximum bending moment and angle. As expected, males had larger average cortical-bone thickness, MBM, and SMT, (Table 5-2). Between males and females, there were no statistically significant differences in the maximum bending angle and BMI, despite the fact that females had a higher average maximum bending angle than males. Lastly, the percentage of ash content was significantly higher in females compared to males. Biologically, age and gender could affect biomechanical responses of the rib. Geometrically, the cross-sectional area, and hence the cortical-bone thickness, could affect the fracture moment.

Figure 5-7 shows the difference between the cortical thicknesses of samples taken from a younger male and an elderly female specimen from the current study. Although these pictures demonstrated significant differences between ribs of a young male versus an elderly female, no statistical significant predictor was found in GEE analysis for cortical thickness. Although non-significant, gender was found to be the most efficient predictor ($p = 0.084$) in estimating the cortical thickness value (Table 5-3). Eq. [5-5] shows that of the same age, height and weight, the cortical thickness of female is 0.133 mm less than that of male. Similarly, Student t-test results also showed that females had lower value of average cortical thickness than males ($p = 0.001$*) as shown in Table 5-2.

However, the difference shown for female might be attributed to the fact that females, on average, are lighter in weight and shorter in height than males. Because the cortical thickness must be correlated with height and weight in some fashion, linear regressions were performed on the average cortical thickness for each cadaver against height and weight. No significance ($p = 0.369$) with an R^2 of 0.0147 was found for height. Similarly, there was no significance found for weight ($p = 0.102$ and $R^2 = 0.047$). Eq. [5-5] shows that age has a negative effect on the average cortical thickness, but the magnitude is very small (0.003 mm per year).

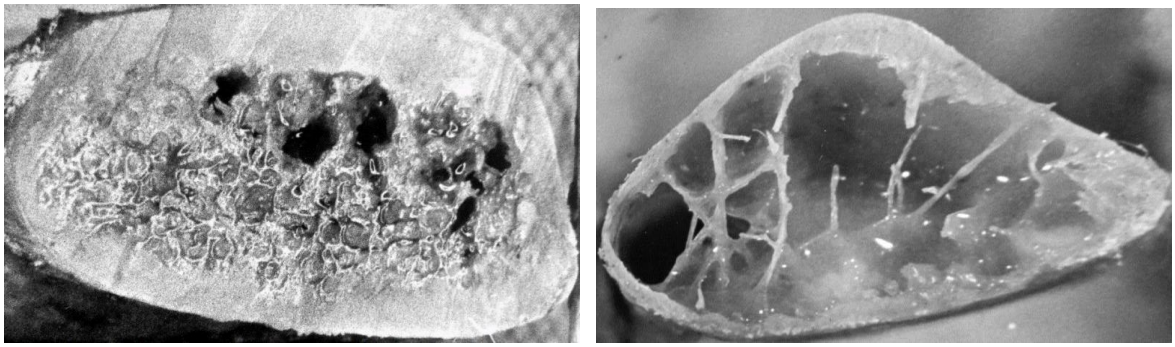

Figure 5-7 Photograph showing difference between cortical thicknesses of a younger male (312, (Left) L7 and an elderly female specimen (682, L6 (Right)

Bone loss could be attributed to a number of genetic, hormonal, and biochemical factors that are not directly related to biomechanics. There are three major age-related processes that lead to bone loss (Chen *et al.* 2013). The first and most important one is trabecular bone loss. The second process is related to bone loss within cortical bone due to increased porosity. Both processes could not be reflected in the cortical bone thickness measurement. Lastly, the effect of endocortical resorption process would be reflected in the thinning of cortical bone reported in the current study.

Age and gender were found to be significant predictors for both MBM and SMT, which along with cortical thickness value, are important parameters in defining the stiffness response to accurately validate the response of FE models. Also, there are fewer number of samples for age less than 35 years and fewer number of female samples (n = 29) than males (n = 53). The difference might be more critical for both age and gender especially for cortical thickness value, if additional data related to lower age group and female specimens could be added to the analysis.

Intuitively, a thicker rib can withstand a higher bending load. A linear regression analysis was performed to determine the effects of average cortical thickness on average MBM and

average SMT values for each cadaver without consideration of gender, as shown in Figure 5-8. It was found that there was significant change in the value of MBM ($p = 0.004^*$) with increasing cortical thickness. The ribs with the thinner cortical bone failed at lower moments, as compared to ribs with thicker cortical bone. The slope of the bending curve (SMT) did not vary significantly with changing cortical thickness.

Further, change in average value of percentage of ash content for each cadaver with age was also studied as shown in Figure 5-9. It was found that the average value of percentage of ash content varied significantly with age ($p = 0.027^*$). This finding is consistent with that reported by Currey (1969) who concluded that mineral content of bone (also known as ash content) increased with age. Similarly, studies of bone mineral density (BMD) also demonstrated an increase in mineral content with age (Cerroni *et al.*, 2000). Using beam theory, Granik and Stein (1973), Yoganandan and Pintar (1998), and Sandoz *et al.* (2007) calculated Young's modulus of rib to be 11.5, 2.3, and 11.37 GPa respectively in rib bending tests. Although the maximum bending force and maximum displacement produced by these studies were similar in range to the current study (Table 5-1), the large variation in the Young's modulus called for additional investigations. In beam theory approximation, the value of elastic modulus depends upon the maximum load, span length, maximum deflection, and moment of inertia of the cross-section, as shown in Eqs. [5-9a, 5-9b]. Because the measured maximum force and deflection are of similar values in all studies, the only difference can be attributed to different moments of inertia assumed in different studies.

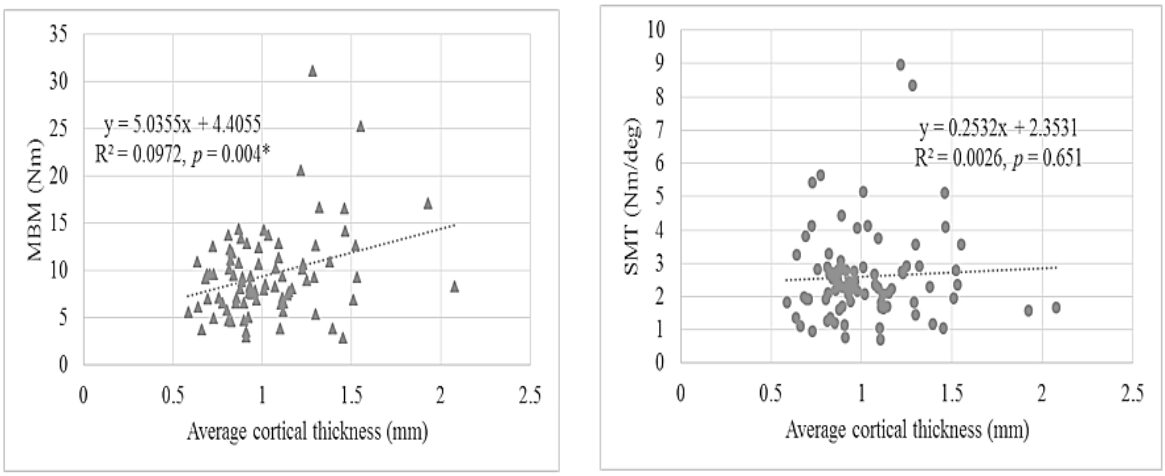

Figure 5-8 Change of average MBM (Left) and average SMT (Right) with average cortical thickness

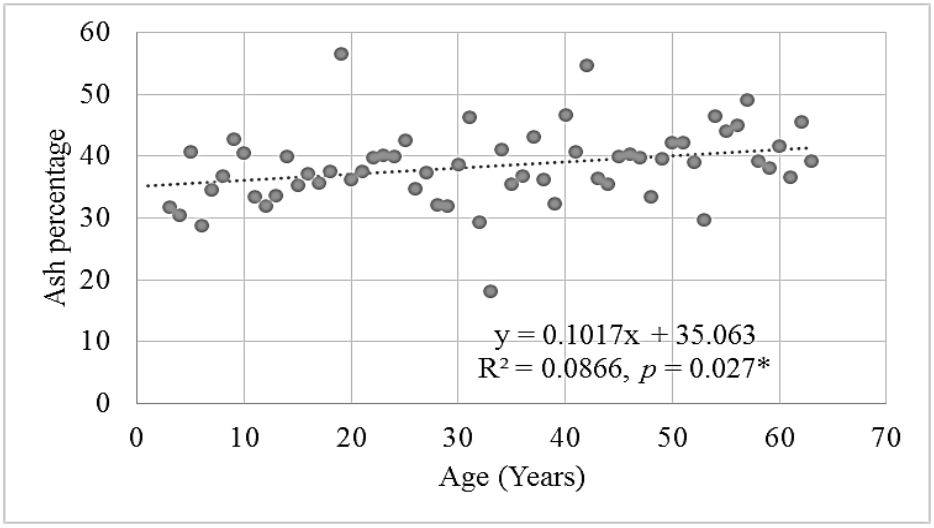

Figure 5-9 Change of average value of percentage of ash content with age

$$E = \Delta P L^3 / (48 \Delta d I) \quad \text{Eq. [5-9a]}$$

$$\sigma = P_{max} L\, c/(4I) \quad \text{Eq. [5-9b]}$$

where ΔP = Change in loads, L= Length of span, Δd =Change in deflections at loading point, I= Moment of inertia of cross-section, σ = Breaking stress, P_{max}= Breaking load, and c=Distance from neutral axis

The use of major and minor diameters to calculate cross-sectional areas of a rib provides only approximations, which may not be needed under the scheme of finite element modeling. Earlier researchers used assumed major and minor diameters to calculate sectional properties, and therefore, even though the maximum forces to fractures were similar among studies, as shown in Tables 5-1 and 5-4, the Young's modulus varied substantially. In FE modeling, the sectional bending moment of inertia is directly calculated from thickness and the mesh derived from bone contours in medical images, and therefore cross-sectional areas are not needed. This direct approach provides more accurate results than calculations based on assumed or approximated major and minor diameters from different locations of the rib. Researchers (Stitzel *et al.* 2003, Polanco-Loria *et al.*, 2012; Zhu *et al.*, 2012; Guan *et al.*, 2011, Li *et al.* 2010) had calculated the Young's modulus accurately using reverse engineering methods. In future studies, subject-specific models with average cortical thickness values from the current study could be optimized for material parameters until the moment-angle characteristics, predicted by the model, match those defined in the rib tests.

Data generated from the current study can only be used in models that represent ribs that have constant cortical thicknesses. Mohr *et al.* (2007) reported that the cortical thickness of rib is location dependent, not constant. In a Global Human Modeling Consortium study, Li *et al.* (2010) found different cortical thicknesses from analyzing fine resolution images taken from CT scans. However, these limited datasets were insufficient to generalize into a model that represents an average human population. Additionally, distinction of the boundary between cortical and trabecular bone is not clear. A high-resolution, enlarged photo of a cross-sectional view of a rib (Figure 5-7) clearly demonstrates the inability to adequately distinguish the boundary between these two bone types. Thus, the finest CT scan available could not provide

sufficient information for accurate determination of cortical thicknesses around the entire rib cage. Future efforts may be devoted to determining location-dependent cortical thicknesses to more accurately model responses associated with the rib cage.

Risk of rib fracture is not only related to age and gender, but also to biological factors such as osteon orientations in cortical bone and the amount and connectivity of trabecular bone. Cormier (1998) found that microstructures, like osteon in bone, were different for people of different ages and genders. While microstructures can be characterized, the invasive approach required to achieve such a task is not practical for live subjects. Secondly, physical activities and associated bone remodeling are known to affect both microscopic and macroscopic characteristics of the rib. In other words, the microscopic and macroscopic characteristics of bone are constantly changing, and they affect other overall biomechanical responses of bone. It is not practical to model this dynamic process using the finite element method. Lastly, a finite element model that includes explicit modeling of osteons and other microstructures would be too costly to run and may violate the continuum mechanics assumption. It may be advantageous in future studies to include information from microstructure investigations, to better predict the risk of rib fracture.

During the current studies, the bending tests were performed at a quasi-static strain rate, which may not fall in the loading range suspected in motor-vehicle crashes for thoracic injuries. Therefore, it was of great relevance to include the strain-rate effects in the constitutive material model for ribs. Sandoz *et al.* (2007) performed similar bending tests on 100-mm lengths of rib samples at the loading rates of 0.03, 100, and 250 mm/sec. Therefore, their results can be collectively analyzed with the current study due to similar boundary conditions. Future efforts

should be devoted to include strain-rate effects to identify a proper rate-dependent constitutive material model to represent the human ribs.

5.5. CHAPTER CONCLUSION

The study presented results based on 278 isolated bending tests, taken from 82 cadavers, to quantify the differences between the biomechanical responses of ribs based on age, gender, height, and weight. Significant differences were found based on age and gender for the maximum bending moment, the slope of the moment-angle curve, and the average cortical thickness of the ribs based on Student t-test results. The generalized estimated equations were derived for predicting biomechanical responses and cortical thicknesses of ribs in humans with known age, gender, height, and weight. Further, suggestions are made to include a reverse engineering approach to calculate material-model parameters for rib samples with strain-rate effects by using the findings of the current research.

CHAPTER 6. OPTIMIZATION OF MATERIAL MODEL PARAMETERS FOR 70 YEARS OLD FEMALE

6.1. OVERVIEW

The findings in Chapter 5 suggested the use of FE based reverse engineering approach to formulate the material model for 70 years old female ribs. Therefore, age- and gender-dependent computational modeling of the rib specimens was done in this chapter to interpret the experimental results with the help of FE modeling. The human long bones are strongest in compression, less strong in tension, and are weakest in shear stress, and they usually break by shear stresses or under tension, but not under compression, as the ultimate tensile stress for the bones is less than that of ultimate compressive stress (Herman (2008)). In the case of bending, there is higher tensile stress on one side and higher compression on the other. So, fracture usually occurs on the tension side. The same trend was observed in the rib-bending test of the specimens used in the current study. Therefore, selecting the most suitable material model, together with the associate parameter values, are quite important to better replicate the experimentally observed behavior of the rib specimens.

Although a linear elastic beam theory has been widely used in the literature (Stein and Granik 1973; Yoganandan and Pintar, 1998) to interpret the values of elastic modulus and ultimate stress of the bones during bending tests, the same theory was not used in the current research, due to limitations associated with this approach. The elastic beam theory demands an initially straight beam made of a single homogenous material, which is hard to find for rib specimens, due to the natural curvature of the ribs. Furthermore, as the name suggests, an elastic beam theory does not consider plasticity. Therefore, use of linear beam equations can overestimate the calculated mechanical parameters, like the ultimate strain and stress for the cortical portion of the ribs. On the other hand, use of FE modeling to estimate the properties of

the complete rib, with both cortical and trabecular bone, can be beneficial over the traditional technique.

In Chapter 5, generalized estimated equations (GEEs) were derived for predicting biomechanical responses and cortical thicknesses of ribs in humans with known age, gender, height, and weight. Based on Eqs. 5.6a, 5.7a, and 5.8a, a female with an age of 70 years, a height of 160 cms, and a weight of 73 kg has the following peak biomechanical response parameters:

SFD = 44.372 N/mm, d_{max} = 4.8 mm, MBF = 150.9 N, cortical thickness = 0.94 mm

where SFD stands for slope of force-deflection diagram, d_{max}= maximum deflection at point of fracture, MBF = maximum bending force. With these values, the corresponding force deflection curve can be estimated as shown in Figure 6-1.

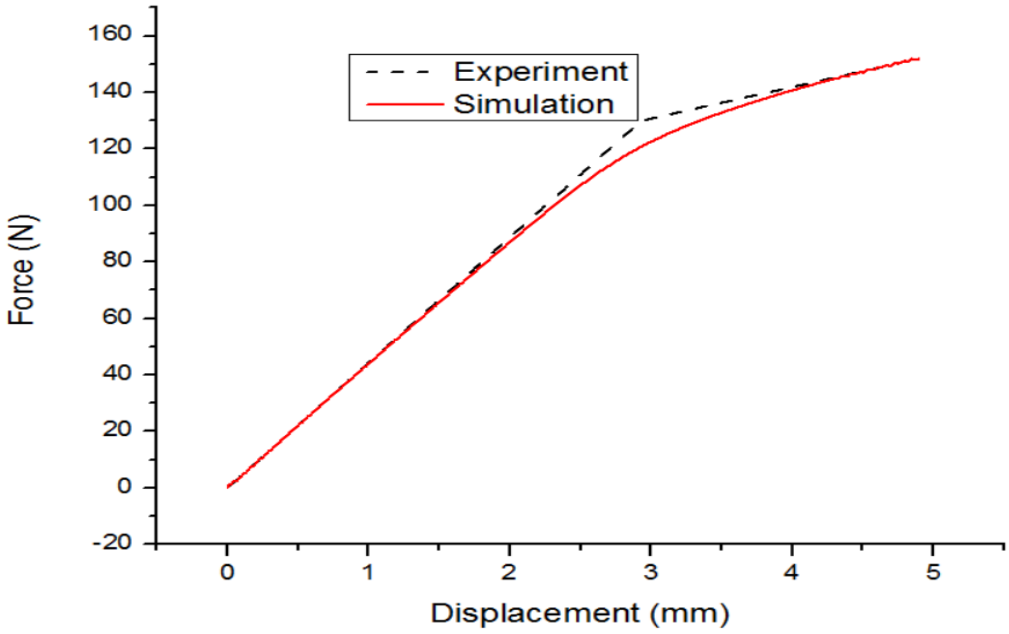

Figure 6-1 Comparison between the force-displacement curves at quasi-static loading between simulation and that calculated from GEE for a 70 years old female with a height of 160 cm and a weight of 73 kg.

This curve will be used for the purpose of optimizing the material model parameters for rib segments during reverse engineering processes to be explained in upcoming sections. Aside from optimizing the rib material constants with the SFD, d_{max}, and MBF obtained from a static loading condition, the material model parameters were also optimized for higher loading rate responses available in literature for similar experimental conditions, but using the same cortical thickness.

6.2. NUMERICAL SIMULATION SETUP FOR MATERIAL MODEL CALIBRATION

A series of numerical simulations were used to develop the material model for representing the average 70 years old female ribs. A rib section with a length of 130 mm was taken from the 6th rib of the mesh of the elderly female thorax model described in Chapter 4, the same way as that done for the rib bending test described in Chapter 5. To simulate the experimental setup for bending the ribs defined earlier in Chapter 5, meshes of a cylindrical impactor and two cylindrical supports were added as shown in Figure 6-2. All simulations were conducted using a non-linear commercial FE analysis package, LS-DYNA 971_R7.1.1 (LSTC Livermore, CA).

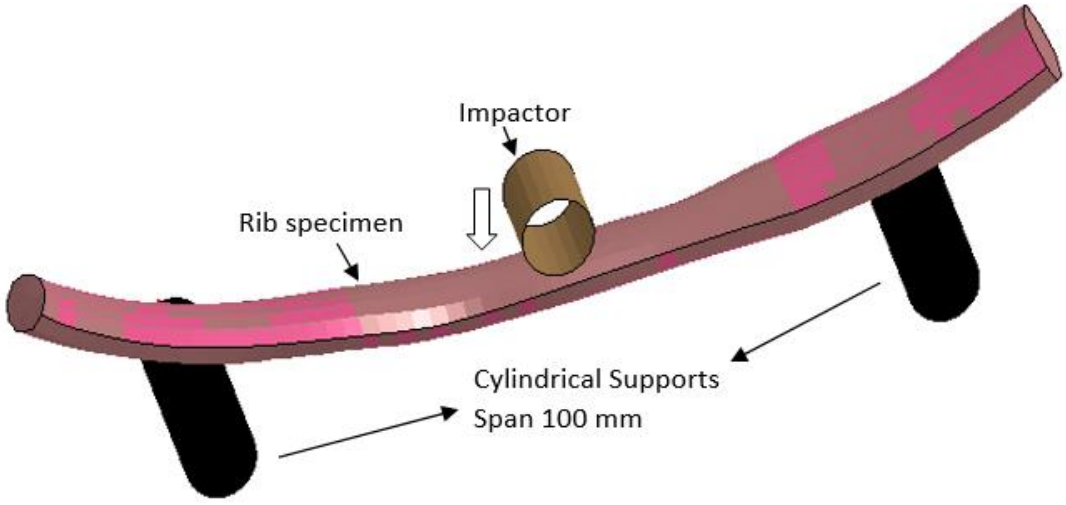

Figure 6-2 Simulation setup for rib bending test

A piecewise, linear, elastic-plastic material model (MAT_024) was incorporated to represent the behaviors of trabecular as well as cortical bones during bending of the ribs. The trabecular bone was modeled with solid elements and the cortical bone was modeled with shell elements with a thickness of 0.94 mm. The density of rib cortical material as well as the Poisson's ratio was assigned as 1.8×10^{-6} kg/mm^3 and 0.3, respectively. The material model parameters (elastic modulus, yield stress, tangent modulus, and failure plastic strain) were optimized till the best match was found. A least square method (the square of the difference between the experimental value and simulation value divide by the original experimental value at each point) was used as an objective function to document the difference between the simulation and experimental results. The failure plastic strain was determined for the first element that got deleted during the simulation and the simulation is terminated after that. The range for elastic modulus values (lowest value = 1.9 GPa, highest value = 15.1 GPa), yield stress values (lowest value = 0.05 GPa, highest value = 0.15 GPa, and tangent modulus values (lowest value = 0.5 GPa, highest value = 5.5 GPa) were chosen for design of computer experiments (DOCE) for conducting simulations with increment of 1 GPa, 0.01 GPa, and 0.1 GPa, respectively. The range for elastic modulus values were taken from literature data from rib testing presented in Table 5-1, while the yield stress and tangent modulus were estimated. Initially the increment of 1 GPa for the elastic modulus was chosen, but as the objective function was calculated to be approaching zero, the increment for elastic modulus was reduced to 0.1 GPa, while the increment for yield stress and tangent modulus were still assumed as 0.01 GPa and 0.1 GPa. A flow chart explaining the optimization process is shown in Figure 6-3. Through the optimization processes, the resulting linear elastic responses as well as the yielding and fracture points matched well against the targeted responses of the ribs during the bending test experiments, as shown in Figure 6-1.

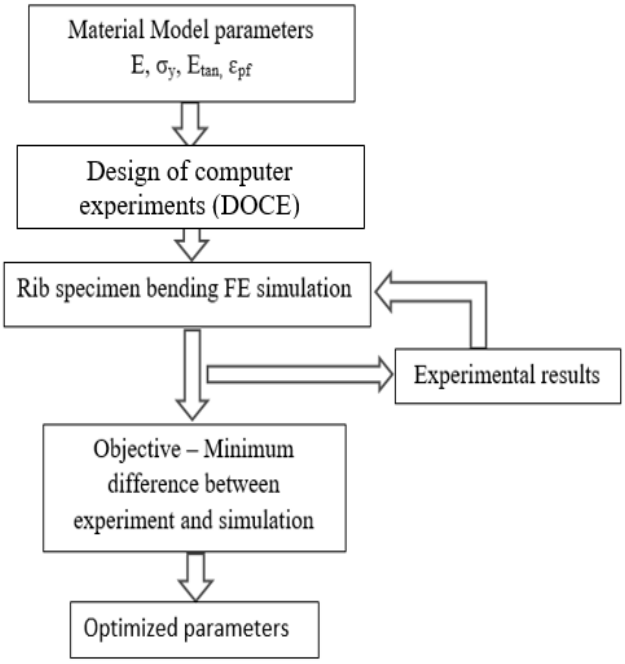

Figure 6-3 Flow chart for optimization of material model parameters

where E= Elastic modulus, σ_y = Yield Stress, E_{tan} = Tangent Modulus, ε_{pf}= Plastic strain at failure

The optimized material parameters based on the piecewise, linear, elastic-plastic material model for the rib are shown in Table 6-1.

Table 6-1 Material properties optimized for an average 70 years old female subjected to quasi-static loading based on piecewise, linear, elastic-plastic model

Type of bone	Element formulation	Elastic Modulus (GPa)	Yield stress (GPa)	Tangent Modulus (GPa)	Plastic failure strain
Cortical	Belytschko-Tsay Shell with a thickness 0.94 mm	7.3	0.054	1.35	0.014
Trabecular	Constant stress solid element	0.04	0.002	1.0	-

6.3. EFFECT OF LOADING RATE ON MATERIAL MODEL CALIBERATION

Most cortical bones were simulated with the help of elastic or an elastic plastic constitutive material model (Yang *et al.* (2006)) using different explicit codes like LS-DYNA, ABAQUS, PAMCRASH, *etc*. The different parameters required by these material models, such as the elastic modulus, yield stress, tangent modulus, or fracture strains depend on the loading rate at which the bone is loaded (Shazlye *et al.* 2005). But, the bending tests on ribs were performed at a quasi-static strain rate in the current research, which does not represent the loading range suspected in motor vehicle crashes in which thoracic injuries occurred. Therefore, it was of great relevance to incorporate the material properties for ribs at an appropriate loading rate. Sandoz *et al.*, (2007) performed 3-point bending tests on 100 mm lengths of rib specimens at the loading rates of 0.03, 100, and 250 mm/sec. In their study, the mean age of specimens used was 63±7 years, which is considered comparable with the age for the elderly specimens considered in the current study. They found that the maximum force increased with increasing speed, but there was no significant change in the maximum deflection observed at different strain rates. The results are consistent with the current study for quasi-static loading for the same span of rib bending tests, as shown in Table 6-2. It is important to note that the results at quasi-static loading rate of 0.03 mm/sec (Sandoz *et al.*, 2007) and 0.169 mm/sec (current study) have minor differences (percentage discrepancies of less than 10% for the maximum bending force and maximum deflection) in mechanical responses for females. The major differences in average maximum bending forces come from the higher loading rates of 100 and 250 mm/sec. Comparisons between the results of the current study and the previous study (Sandoz *et al.* 2007) are shown in Table 6-2.

Table 6-2 Force and deflection responses comparison with literature

Test	Age (Years)	Span (mm)	Loading rate (mm/sec)	Gender	Mean value of maximum bending force (N)	Mean value of maximum deflection (mm)
Current Study	>60	100	Quasi-static	29 Female	147	4.45
				53 Male	179	4.2
				all	163	4.32
Sandoz *et al.*, (2007)	63±7	100	Quasi-static	3F, 9M	150	4.7
			100		210	4.85
			250		240	5.1

It was found that there were no significant costal level effects in the ribs tested at different speeds (Kruskal-Wallis test at p=0.05). Additionally, the elastic stiffness for the material response was not visualized during the testing at higher speeds. (From personal communication with Dr. Xavier Trosseille, from LAB PSA Peugeot Citroen Renault, France).

But, the overall peak forces and deflections were different for different speeds showing post yield change in the bone stiffness. The same effect of loading rate was included for this study due to similar age and biomechanical responses at quasi-static loading between the two studies. Trabecular bone was excluded for loading rate effects, as there was hardly any research that discusses the loading rate dependency in the trabecular bone due to lower stiffness of trabecular bone as compared to that of cortical bone. Therefore, it is worth assuming that the effect of loading rate in trabecular bone will not be as significant as that for cortical bone.

Force-deflection curves were plotted in Figure 6-4 corresponding to each loading rate (quasi-static, 100 mm/sec, and 250 mm/sec, respectively) according to the peak force, average

slope, and deflection values defined by Sandoz *et al.* (2007). Further simulations were run to optimize the stress strain response for rib specimen by varying the material model parameters as that described in Section 6.2 for different loading velocity data. The resulting material properties are shown in Table 6-3.

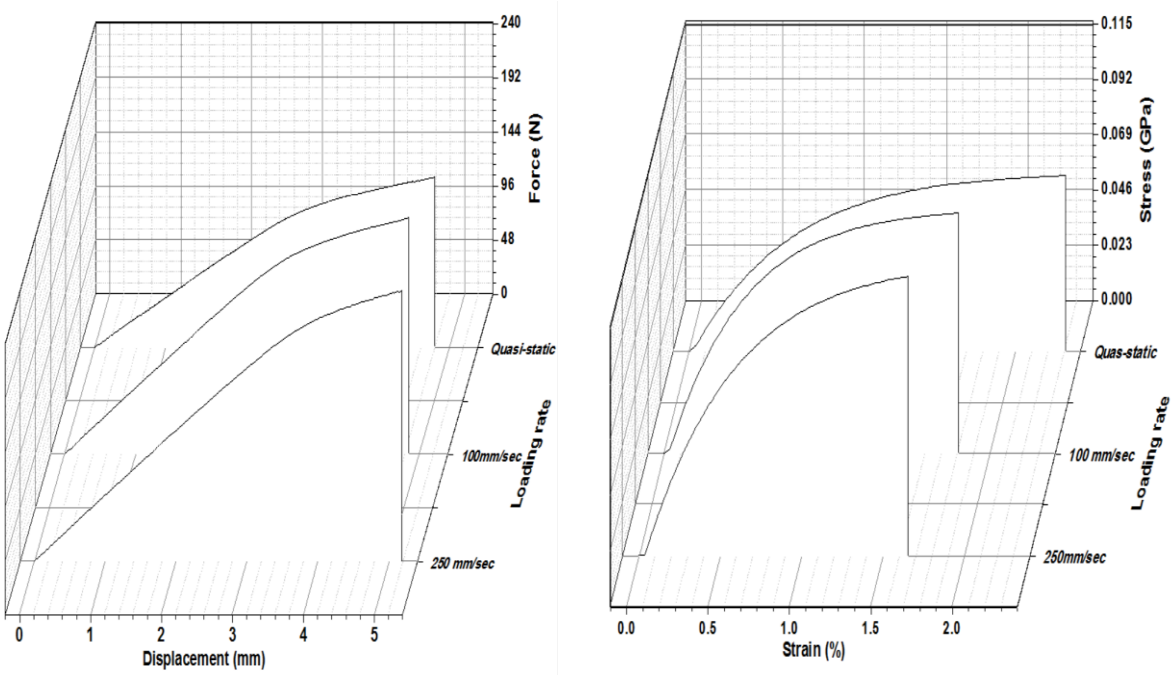

Figure 6-4 Force-deflection (Left) and Stress-strain (Right) curves at different loading rates as reported by Sandoz *et al*. (2007)

Table 6-3 Material parameters for 70 years old female rib model at different speeds

Loading rate (mm/sec)	Expected Strain rate (per sec)	Mass density (Kg/mm^3)	Elastic Modulus (GPa)	Poisson ratio	Yield stress (GPa)	Tangent Modulus (GPa)	Ultimate stress (GPa)	Plastic failure strain
Quasi-static	0.001	1.80E-06	7.3	0.3	0.054	1.35	0.072	0.014
100 mm/sec	0.4		9.8		0.08		0.098	
250 mm/sec	0.6		9.8		0.097		0.115	

6.4. CHAPTER DISCUSSION

Theoretically, strain rate dependent stress-strain behaviors can be implemented with the help of Mat_019 (MAT_STRAIN_RATE_DEPENDENT_PLASTICITY), if the corresponding strain rate values are known. However, the strain rate retrieved through computer simulations is too noisy, and data listed in Table 6-3 were based on loading speed, not the actual strain rate. Therefore, it is not possible to include strain rate effects in the material model for now. For the 70 years old model, the material properties obtained at the 250 mm/s loading speed were used. This selection was based on the fact that it is the fastest loading speed reported in the literature, which is probably closer to the loading rate experienced by ribs in typical automotive impacts compared to all other experimental data.

Further, the material properties derived for the 70 years old female in the current study were compared with the relevant material properties selected for female and elderly males by different research groups for validation of whole-body impact responses. Table 6-4 summarizes the material properties of relevant thorax FE models developed by different groups, including the elderly male FE models by Ito *et al.* (2009) and Tamura *et al.* (2005), 5^{th}percentile models of females at younger ages by Kimpara *et al.* (2005), and properties derived by Kemper *et al.* (2005) with coupon testing.

Kimpara *et al.* (2005) used the properties derived by the elastic beam equation for bending tests for females at a quasi-static rate of 0.169 mm/sec and found the Young's modulus to be 9.86 GPa and the yield stress 66.7 MPa. Compared to the current study, where the Young's modulus was found to be 7.3 GPa and the yield stress 54 MPa, there was an underestimation of the Young's modulus and yield stress in the current study. The differences might have been due

to different cortical thickness value (age effect) used as Kimpara's model, which was developed to represent younger population.

Tamura *et al.* (2005) developed a model that represents an elderly male thorax. The properties of ribs were taken from those given by Stitzel *et al.* (2003), which were based on data taken from bending tests performed at 356 mm/s and then fitted to elastic beam equations. The model also considered region-specific properties found by the Stitzel *et al*. during their tests. Three different sets of parameters were derived for the anterior, lateral, and posterior portions of the ribs. Anterior specimens in the Stitzel *et al.* study were comparable with the current tests, as the samples were taken from similar locations. The differences in the elastic modulus and the yield stress between their study and the current one could be related to the dissimilarities in the age and strain rate.

However, differences in age and strain rate are insufficient to explain the large difference in the tangent modulus (3.79 GPa from the Stitzel study versus 1.35 GPa from this study). It is believed that the elastic beam theory augmented with a correction factor for the ultimate stress used by Stitzel *et al*. might have caused a higher value for the tangent modulus they found.

Another elderly-male (75 years old) FE model was developed by Osamo *et al.* (2009). The properties used were scaled down from 55 year old (Kemper *et al*. (2005)) to elderly (75 years old) by a scaling law developed by Dokko (2009) to account for age effects, but the yield stress (54 MPa from the Osamo study versus 97 MPa from the current one) and ultimate stress (68.3 MPa from the Osamo study versus 115 MPa from the current one) were lower as compared to the current study. The difference might be due to a different value to cortical thickness used in the Osamo model. Further, the mechanical properties for the ribs has been scaled as per scaling law derived for femur cortical bone (Dokko (2009)) for Osamo model, but the rate of change in

material property for femur and ribs can be different. While in the current study the mechanical properties as well as value of average cortical thickness for anterior rib sections were derived from experiments done on 278 samples taken from 82 cadavers, which is more relevant to represent the property of ribs at elderly.

Samantha *et al.* (2015) morphed the GHBMC 50th percentile male model to 65 years old (65 YO) and also scaled down the properties of ribs according to tests done by Kemper *et al.* (2005) and Kemper *et al.* (2007). The value of the yield stress was found to be lower than that of the current study while the value of elastic modulus is higher in 65 YO male model as compared to the current study. Since Kemper *et al.* mentioned a strain rate of 0.5 sec^{-1} in the studies while the current study is performed at 100 mm/sec and 250 mm/sec, therefore a direct comparison of both studies could not be done. Further, 65 YO GHBMC male model used patient specific variable cortical thickness value at each node while the 70 years old female model in the current study used a uniform cortical thickness value based on studies of 82 cadavers, and mechanical properties developed were based on the average cortical thickness value.

Furthermore the stress-strain curves derived from the current study were compared with those retrieved for the two elderly female specimens (61 and 64 years old) reported by Kemper *et al.* (2005) at similar levels of ribs (Table 6-4). The mechanical properties especially the elastic modulus value (14.8 GPa) in Kemper study was found to be different than the current one (9.8 GPa). The possible reasons of discrepancies might be due to the different strain rate in both studies, the limited number of specimens in the Kemper study, or the fact that the material model derived by Kemper *et al.*, (2005) was based on stress-strain curves of ribs obtained experimentally, while the current material model parameters are fit for material model in computational code.

Lastly, it was shown in the current study that the stress-strain curve of ribs is affected by the loading speed. The value of elastic modulus and other parameters are different for quasi-static testing and higher loading speeds (100 mm/sec and 250 mm/sec). There was no change in the elastic modulus at higher loading speeds of 100 mm/sec and 250 mm/sec, since the corresponding strain rate values may not differ by much. The corresponding change in the elastic modulus is more evident when the strain rate is differ by a factor of at least 10, as being noticed in cortical bone testing of other bones (McElhaney (1966); Burstein *et al.* (1976); Katsamanis and Raftopoulos (1990); Öhman *et al.* (2011) and Sanborn *et al.* (2014)).

6.5. CHAPTER CONCLUSION

The reverse engineering method was used to calibrate the material model parameters to fit the responses with the help of FE simulations. Further, data of rib bending tests using elderly cadavers with similar boundary conditions but different loading speeds were collected from the literature. Different parameters of elastic-plastic material models were calibrated to best match the force-deflection characteristics of the rib specimens for quasi-static and dynamic loading rates. The material-model parameters such as the elastic modulus, yield stress, tangent modulus, and plastic-failure strain were calculated for the 70 years old female model and cortical thickness value of 0.94 mm was assigned for representative shell elements based on statistical measurements for an average 70 years old female.

The developed material properties as well as the cortical thickness values were compared with other relevant finite element models representing female and elderly specimens. The major advantage of the current study over other studies was that the cortical thickness value was assigned based on statistical measurements derived from data obtained using 82 cadavers. An average value of cortical thickness was calculated for representing the thickness at the anterior

portion of rib specimens and corresponding to this cortical thickness, the material model parameters were developed. While in other models, either this thickness value was assigned based on estimation (Kimpara's model) or by scaling the adult cortical thickness (Osamo's model). Also, the material properties and the relevant cortical thickness values were based on different datasets of experiments which accumulate errors related to different input attributes in the final outcome, while the current study used the value of cortical thickness and material properties from single set of experiments. Although Samantha *et al*. (2015) used the nodal dependent cortical thickness values (0.32-1.96 mm) for 65 YO male model, but the values were scaled values from adult GHBMC model (which was originally developed based on subject specific values). So, the model represents the subject specific model, rather than an average statistic representation for that specific population.

The current study provides the average cortical thickness value for anterior sections of rib since the measurements of cortical thickness were based on rib specimens taken from the anterior portion of the ribs, but actually the value of cortical thickness can be changed through the rib length (Abrams *et al.* (2003), Li *et al.* (2009)). Further efforts have been made in the next chapter to implement the regional differences in cortical thickness value from the data available in literature for the whole rib specimens. These differences will be implemented as different sectional values of cortical thickness in the whole rib of 70 years old female model, further supported by whole rib structural response validation. It should be emphasized that although the rib cortical thickness can be different throughout the length, but the material properties will be consistent irrespective of these geometric variations.

Table 6-4 Overview of mechanical properties of relevant FE models

Author	Model	Yield stress(MPa)		Yield strain	Young Modulus(GPa)	Tangent Modulus(GPa)	Ultimate Strain	Ultimate stress(MPa)	Thickness (mm)	Comment
Kimpara *et al.*, (2005)	5th percentile female	66.7		-	9.86	-	-		0.7	Bending Test
Tamura *et al.*, (2005)	Elderly male	Anterior	121.6	0.0145	8.394	3.792	0.02	-	-	Based on Sitzel et al. 2003 results
		Lateral	135.3	0.0111	12.211	4.61	0.02			
		Posterior	112.9	0.0103	10.998	6.332	0.02			
Osamo *et al.* (2009)	Elderly male	54		0.00699	-	-	0.0212	68.3	0.86	Scaling laws
Samantha *et al.* (2015)	65 YO male	88		0.0077	11.5	-	0.0203	117	0.32-1.96	Kemper et al. 2005, 2007
Current study	70 YO female	Quasi-static	54	-	7.3	1.35	0.014 (plastic strain)	72	0.94	Loading rate dependent bending tests
		100mm/sec	80		9.8			98		
		250mm/sec	97		9.8			115		
Kemper *et al.* (2005)	Eldlery female (61 and 64 years) - experimental data	101.9		0.0089	14.8	-	0.0227	129.3	-	Rib Coupon Test

CHAPTER 7. CORTICAL THICKNESS VARIATION AND OVERALL STIFFNESS OF A WHOLE RIB

7.1. INTRODUCTION

The identification of the material properties suitable for the 70 years old female ribs as well as the corresponding cortical thickness value were presented in Chapter 6. One of the major limitations for the earlier study was that the average cortical thickness value was measured at an anterolateral position of the rib section as shown in Figure 5.5. But, several researchers (Abrams *et al.* (2003), Li *et al.* (2009)) have shown that the average value of cortical bone thickness varies along the length of the rib from anterior to posterior. Mayeur *et al.* (2011) compared the cortical bone thickness of ribs between the GHBMC model and European THOMO project in which the micro-CT scans of the ribs were analyzed. The medical scans taken for the GHBMC model were obtained from a 25 years old living male subject, while in the THOMO project four male cadavers representing 50^{th} percentile class were used to draw the cortical thickness distribution map. Results from both studies showed varying cortical bone thickness distributions along the length of ribs.

The overall stiffness of the whole rib can be affected due to this varying thickness along the rib length or its material properties. Stitzel *et al.* (2003) conducted three-point bending tests on small specimens of 20 mm size taken from ribcage at different locations (anterior, lateral, and posterior). Using a reverse engineering approach in FE simulations while assuming rib has uniform thickness along the length of rib, they reported different material properties for rib specimens at different locations, as shown in Table 7.1.

The structural responses, in terms of the peak response and deflection during the 3-point bending test, were different for rib specimens dissected from different locations. Again, the structural responses depend on the cortical bone thickness as well as material properties of the

rib. Since the cortical bone thickness was assumed to be 0.7 mm for all rib shell elements in the Stitzel *et al*. study, different material properties were found for the three different locations in the Stitzel *et al*. study. Since it is more reasonable to assume that material properties for the rib cortical bone should be the same, the different structural response must come from varying cortical bone thicknesses along the length of the rib. Therefore, it is worthy the efforts to revalidate the response of entire rib after assigning different cortical thickness values at different sections.

Table 7-1 Material properties for rib specimens at different locations (Stitzel *et al.* (2003))

Author	Loading Type	Rib specimen location	Biomechanical responses
Stitzel *et al.* (2003)	3-point bending (coupon)	Anterior	E=7.5 GPa, σ_{ult}=0.116 GPa, ε_{ult}=0.032
		Lateral	E=11.8 GPa, σ_{ult}=0.153 GPa, ε_{ult}=0.153
		Posterior	E=10.7 GPa, σ_{ult}=0.127 GPa, ε_{ult}=0.025

In a recent SAE International conference, Weaver *et al.* (2015) showed an overall map of cortical thickness variation for the entire ribcage of the GHBMC 50th percentile male model and the 65 years old version of the model. Similar morphometric analysis for variations in size and shape of the ribs as functions of age and gender has been presented by the same group (Weaver *et al.* (2014)), based on CT scans of 339 subjects. Lynch. (2015) mentioned in her master's thesis regarding the analysis of the same dataset for age and sex dependent variations in rib cortical bone thickness, but detailed analysis of cortical bone thickness variation with age and gender has not been published in open source literature yet. Therefore, the overall change in cortical thickness for the entire ribcage related to 70 years old female was retrieved from the Wake Forest

group through personal communication. Further, the overall distribution of the cortical thickness was assigned in the 70 years old female model. The overall force deflection data of single whole rib was compared with tests done by Schafman *et al.* (2015) for the whole rib bending results for the similar age and gender.

7.2. DISTRIBUTION OF CORTICAL THICKNESS IN 70 YEARS OLD FEMALE MODEL

Through personal communication with Dr. Weaver from Wake Forest University, it was concluded that the average cortical thickness for 70 years old female should be around 0.83 mm and distributions of cortical thicknesses can be assigned using the scaling factors shown in Table 7-2.

Table 7-2 Scaling factors for cortical bone thickness distribution for the entire rib length (Personal communication with Dr. Weaver)

Posterior	Posteo-lateral	lateral	Anterolateral	Anterior
100%	126.83%	134.15%	102.44%	74.39%

Since the effects of subject's weight and height were not included in the Weaver study, it was suspected that the average cortical thickness value for 70 years old with 160 cm height and 73 kg weight may be slightly higher than that derived from Weaver study. This is because the anthropometric details of the current model represent the average elderly female who is moderately obese. Therefore, the previously calculated average cortical thickness at the anterolateral position (0.94 mm) based on GEE described in Chapter 5 was believed to be more reasonable than that reported in Weaver study. By assigning the anterolateral thickness to be 0.94 mm, the thickness values for other rib regions at the posterior, posteo-lateral, lateral, and anterior were calculated using the same scaling factor as shown in Table 7-3.

Table 7-3 Distribution of cortical thickness, in mm, for the entire ribcage at different sections of the ribcage for the 70 years old female

Location	Posterior	Posteolateral	lateral	Anterolateral	Anterior
Scaling factor	100%	126.83%	134.15%	102.44%	74.39%
Calculated cortical thickness (mm)	0.91	1.15	1.21	0.94	0.68

These cortical thickness values were assigned in the current model (Figure 7-1). Further, the average nodal thickness at the junction of adjacent sections was assigned at each junctional node so that the stress concentration due to sudden change in the cortical thickness can be avoided.

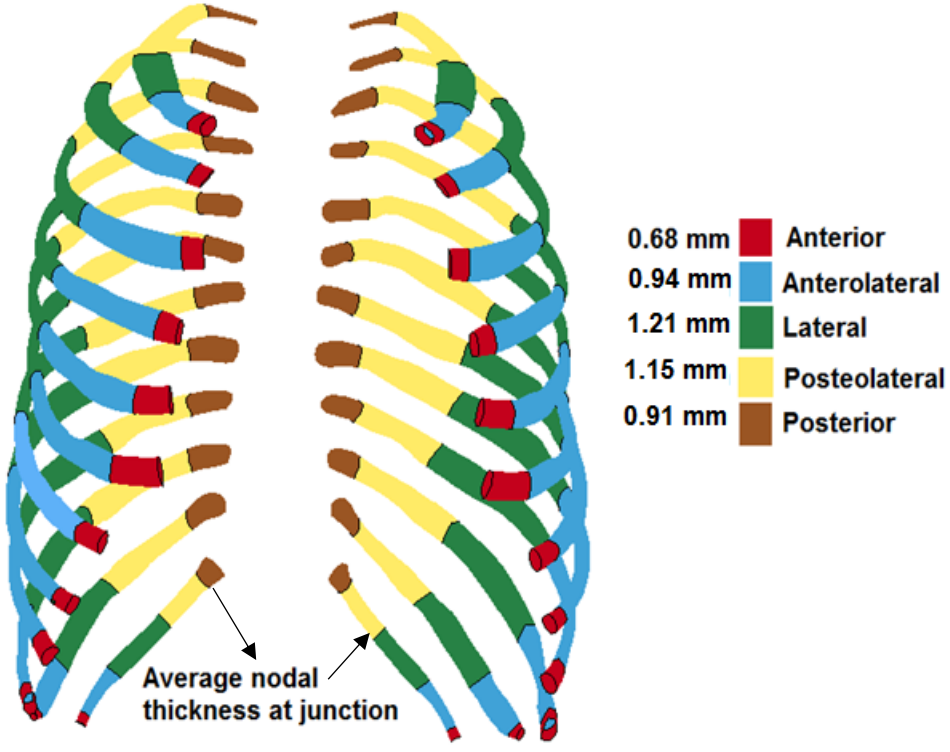

Figure 7-1 Cortical thickness distributions in the 70 years old female ribcage

7.3. VALIDATION OF STIFFNESS OF WHOLE RIB

7.3.1. Experimental Setup

Agnew *et al.* (2013, 2015) conducted dynamic bending tests on whole rib specimens. Schafman (2015) summarized these bending tests in her Master thesis. A total of 184 ribs taken from 93 cadavers (70 males, 23 females: aged 4 to 99) were loaded in a fixture which simulates the dynamic frontal impact to the thorax. The vertebral end of the ribs were potted into 4 X 4 X 3 cm^3 blocks and were allowed to rotate freely at a pivot joint in the loading direction. The pivot joint of the vertebral end of the rib fixture was fixed in all three axes and the coastal end of the rib was loaded at a velocity of 1-2 m/s along the x-direction as shown in Figure 7-2. A 54.4 kg pendulum was impacted at the coastal end of the setup. The force at the fixed end of the fixture was recorded using a load cell and the displacement of the sternal end was measured with the help of a linear displacement string potentiometer.

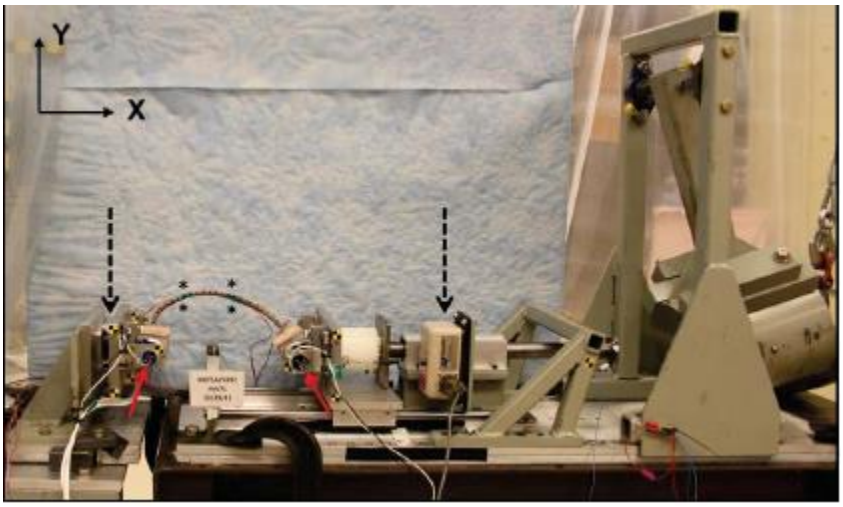

Figure 7-2 Experimental setup for testing whole rib under bending (Photo taken from Agnew *et al.* (2013))

Schafman (2015) presented a detailed analysis for change in the structural responses such as the peak force (Fmax), percent displacement in x (Dx-anterior-posterior) and y (Dy-lateral direction) directions, stiffness (K-measured from 20%-80% of force-deflection curve), and

energy absorption at failure (Utotal) with age and gender using a multi-level statistical model. It was found that rib levels as well as the speed of impactor ranged from 1-2 m/s don't affect the structural responses.

In Schafman study (2015), multiple samples were taken from the same cadaver (complete experimental dataset was listed in her thesis). To account for these repeated measurements, GEE, instead of a multiple regression model, was used to analyze these data. The covariance matrix and the working correlation matrix was chosen as a robust estimator type and exchangeable type, respectively, during GEE analysis of Schafman data. Again, a p value of less than 0.05 was considered statistically significant. Although height and weight of the cadaveric specimens were not listed in the dataset, the overall heights along the lateral direction as well as span along the horizontal direction of the individual rib specimens were listed. It is then assumed that these data can be used as surrogates for representing height and weight for the cadaveric specimens recorded in Schafman data. The effects of different predictors (age, gender, height, and span) on the Fmax, Dx, Dy, K and Utotal in Schafman data were analyzed to identify the average response of any given age, gender, height, and span of specimens.

7.3.2. Analysis of experimental results reported by Schafman

Table 7-4 summarizes the results of parameters estimated from GEE analysis of Schafman data for the peak force (Fmax). All predictors had a p value of less than 0.05, except the height (p = 0.832). The estimated model for Fmax was derived as:

Fmax (N) = -0.272 – 1.052×age (years) + 21.948×gender + 0.755×span (mm) + 0.077×height (mm)

(0- female, 1- male) Eq. [7-7.a]

Table 7-4 GEE estimation results for the peak Force (N)

	Fmax (N)		
Predictor	Coefficient	Wald Chi-Square	p
Intercept	-0.272	-	-
Age	-1.052	29.385	0.000*
Gender	21.948	5.827	0.016*
Span	0.755	14.601	0.000*
Height	0.077	0.045	0.832

Table 7-5 summarizes the results of parameters estimated from GEE analysis of Schafman data for the horizontal deflection, Dx (mm). Predictors age and height had a p value of less than 0.05 while predictors gender and span has p value of larger than 0.05. The estimated model for horizontal deflection was derived as:

Dx (mm) = 26.443 – 0.255×age (years) -4.343×gender - 0.020×span (mm) + 0.266×height (mm)

(0- female, 1- male) Eq. [7-7.b]

Table 7-5 GEE estimation results for the horizontal deflection (mm)

	Dx (mm)		
Predictor	Coefficient	Wald Chi-Square	p
Intercept	26.443	-	-
Age	-0.255	37.533	0.000*
Gender	-4.343	2.986	0.084
Span	-0.02	0.359	0.549
Height	0.266	11.132	0.001*

Table 7-6 summarizes the results of parameters estimated from GEE analysis of Schafman data for the vertical deflection Dy. All predictors had a p value of less than 0.05, except gender (p = 0.266). The estimated model for Dy was derived as:

Dy (mm) = 28.899 - 0.135×age (years) -2.082×gender + 0.171×span (mm) – 0.484×height (mm)

(0- female, 1- male) Eq. [7-7.c]

Table 7-6 GEE estimation results for the vertical deflection

	Dy (mm)		
Predictor	Coefficient	Wald Chi-Square	p
Intercept	28.899	-	-
Age	-0.135	16.362	0.000*
Gender	-2.082	1.239	0.266
Span	0.171	57.317	0.000*
Height	-0.484	59.568	0.000*

Table 7-7 summarizes the results of parameters estimated from GEE analysis of Schafman data for the stiffness, K (N/mm). All predictors had a p value of less than 0.05, except span (p = 0.133). The estimated model for stiffness was derived as:

K (N/mm) = 5.267 – 0.023×age (years) + 1.496×gender + 0.011×span (mm) - 0.052×height (mm)

(0- female, 1- male) Eq. [7-7.d]

Table 7-7 GEE estimations results for stiffness (N/mm)

	K (N/mm)		
Predictor	Coefficient	Wald Chi-Square	p
Intercept	5.267	-	-
Age	-0.023	8.575	0.003*
Gender	1.496	8.674	0.003*
Span	0.011	2.257	0.133
Height	-0.052	6.793	0.009*

Table 7-8 summarizes the results of parameters estimated from GEE analysis of Schafman data for the total energy, Utotal (J). All predictors had a p value less than 0.05, except gender (p = 0.318) and height (p=0.054). The estimated model for total energy was derived as:

Utotal (J) = -2.077 – 0.082×age (years) + 0.445×gender + 0.035×span (mm) + 0.047×height (mm)

(0- female, 1- male) Eq. [7-7.e]

Table 7-8 GEE estimations results for total energy (J)

	Utotal (J)		
Predictor	Coefficient	Wald Chi-Square	p
Intercept	-2.152	-	-
Age	-0.074	42.701	0.000*
Gender	0.419	0.998	0.318
Span	0.038	14.933	0.000*
Height	0.029	3.726	0.054

For validating the numerical model of the whole rib of an average 70 years old female, it was important to compare the model-predicted average response for the same age and sex obtained from the experiments. Therefore, the structural response during the experiment in terms of Fmax, Dx, Dy, K and Utotal for a 70 years old female was calculated for a rib specimen from Eq. (7-7.a-e) and the model predicted responses were compared further with these responses as shown in upcoming sections.

7.3.3. Numerical simulation

The whole rib from the 70 years old female model at 6th level was used for simulating the stiffness comparison reported by Schafman (2015). Since the rib level did not affect the experimental results, so the rib at any level can be chosen for FE model result comparison. The

FE mesh was assigned different cortical thickness in different regions throughout the length as shown in Figure 7-3. Also, the ribs were impacted at constant velocity of 1 m/s. The simulation setup (Figure 7-3) was set up according to that used for experiment. The corresponding height and span of the simulated 6th rib were measured as 85 mm and 188 mm, respectively, following the same protocol used in experiment These values will be used in structural response calculated based on GEE analysis of Schafman (2015) data Eqs. (7-7.a-e).

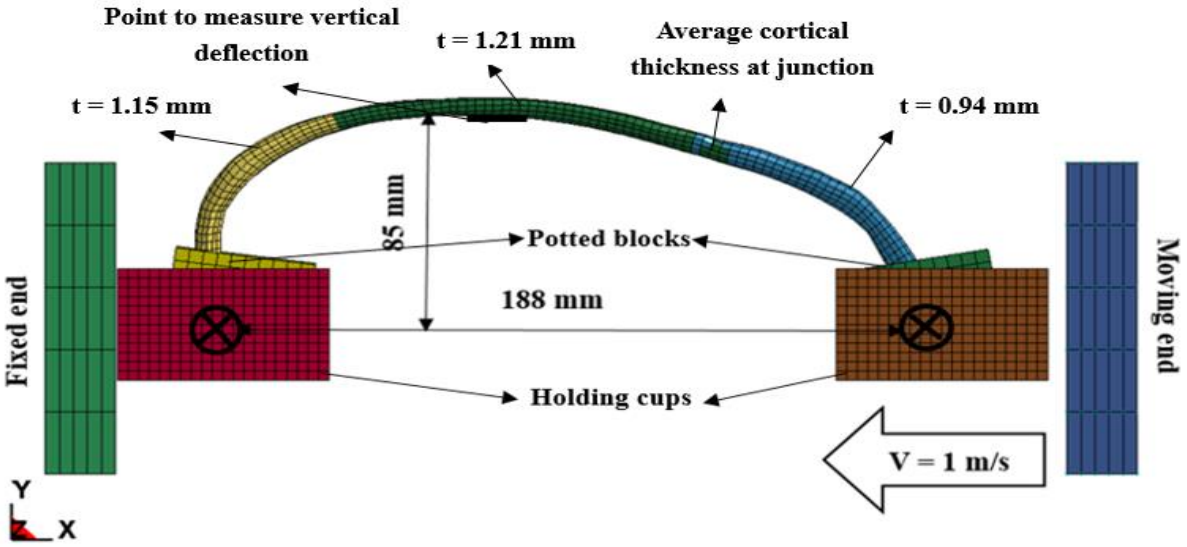

Figure 7-3 Simulation setup for whole rib bending test

At the fixed end, the pivot point was restricted from any translations and rotations about X- and Y-axis. In other words, only rotation about the Z-axis is allowed. At the moving end, the pivot point has no translations along the Y- and Z-axes and no rotations about the X- and Y-axes while allowing it to translate in the X-axis and rotate about the Z-axis. The reaction force at the posterior end was retrieved through contact force and the displacement in the horizontal and vertical directions were measured from the model by extracting relative nodal displacements. Figure 7-4(a) showed the force-deflection curve from simulation (Filtered at CFC 180) while the

sample force-deflection curve from the experiment is shown in Figure 7-4 (b). Figure 7-4 (c) shows the vertical deflection time history.

7.3.4. Predicted simulation vs experimental structural response

The structural responses during the experiment, in terms of Fmax, Dx, Dy, K and Utotal, for the 70 years old female with a rib height of 188 mm and span length of 85 mm can be calculated from Eqs (7-7.a-e) respectively. The corresponding structural response values were also retrieved from the numerical simulations in terms of peak responses. The energy required for fracture was calculated from the area under the curve. A brief comparison between the experimental and simulation results was shown in Table 7-9. The percentage discrepancies between the experimental and simulation responses are less than ±10%, except the peak vertical deflection. The model over predicted the deflection in the vertical direction by 46%. The possible reason might be due to the length of rib potted into the blocks. It was found during the simulations that the deflection results are very sensitive to the potted length of rib. In current simulations, the end nodes of ribs till the whole depth of the block were constrained to the potting blocks.

With the value of failure plastic strain threshold assumed to be 0.014 for element deletion as predicted in an earlier section, the rib fractured primarily at two locations in the numerical model as shown in Figure 7-5 (left). Similar fractured locations were observed by Agnew *et al*. (2013) during the experiment in which two simultaneous rib fractures occurred (Figure 7.5 (right)). Schafman (2015) presented a detailed analysis for the rib fracture location in her thesis and it was shown that the highest frequency of rib fractures were in anterior sections as 55.7% followed by lateral sections as 34%, as shown in Table 7-10.

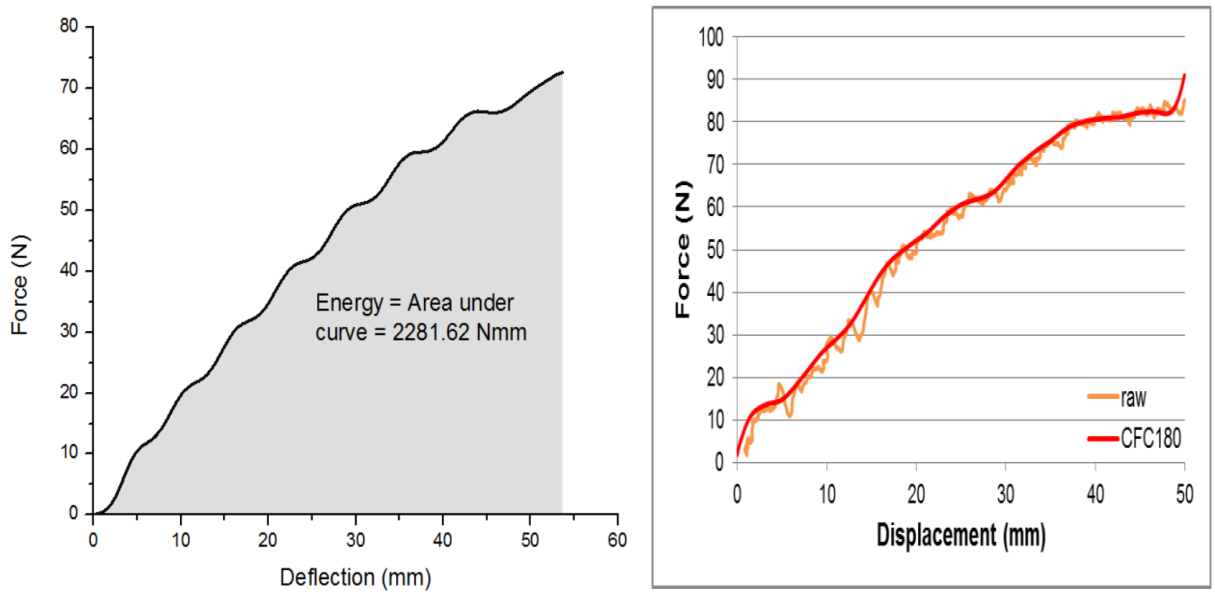

(a) (b)

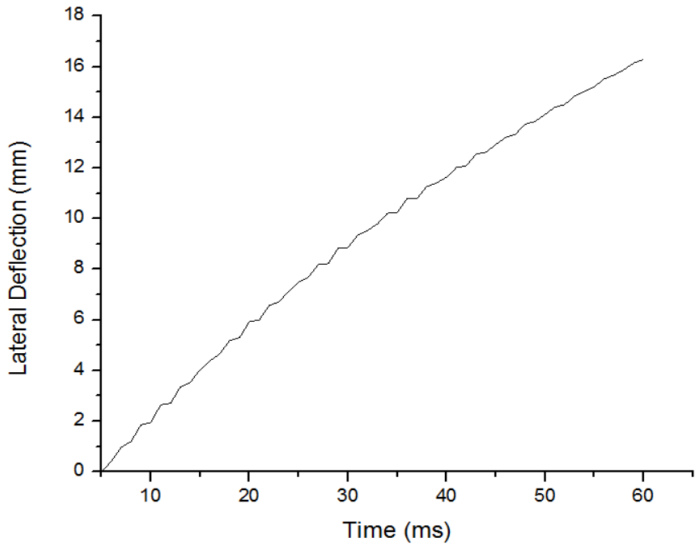

(c)

Figure 7-4 (a) Simulated force vs. horizontal direction displacement, (b) Typical force vs. horizontal displacement obtained experimentally, and (c) The model predicted vertical displacement time history

Table 7-9 Experimental vs simulation results for whole rib testing

Structural response	Experimental values from GEEs	Numerical model predicted response	% Discrepancies
Peak Force (N)	74.18	73.05	1.52
Peak horizontal deflection (mm)	26.113	28.45	-8.95
Peak vertical deflection (mm)	12.87	18.8	-46.08
Stiffness (N/mm)	1.28	1.4	-9.37
Energy to fracture (J)	2.27	2.28	-0.44

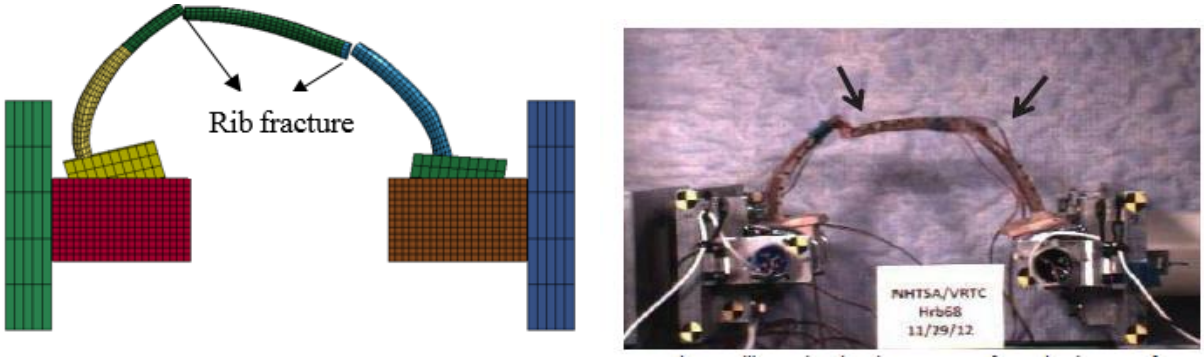

Figure 7-5 Simulation predicted rib fracture (left) and a snapshot (right) showing two simultaneous rib fractures during an experiment (Photo taken from Agnew *et al.* (2013).

Table 7-10 Rib fracture locations during experiments (Schafman (2015))

Location	Frequency (%)
Anterior	55.7
Lateral	36
Posterior	8.4

It should be noted that the anterior, lateral, and posterior sections are different in terms of location in Schafman (2015) than current rib sections.

7.4. DISCUSSION

The cortical thicknesses as well as material properties are the key parameters which defines the structural response for a cortical bone. Although one can change either value to achieve the overall stiffness during 3-point loading of cortical rib specimens, it is hypothesized that the fracture or failure parameters as well as fractures locations may not be easily simulated through these manipulations. For example, a rib with a thinner cortical bone is expected to fail at a lower load whereas the same rib with a higher cortical bone thickness with the same material properties would withstand higher loads before failure. But, a rib with varying cortical thickness, which represents actual geometric characteristics, may fracture at different loads and locations. In the current study, the rib was modeled with varying cortical bone thicknesses for different sections based on statistical data and predicted similar response in terms of the peak structural responses as well as fracture locations. But, it is worth to see the effect of constant cortical thickness on the structural response prediction capabilities. Therefore, a series of parametric studies were conducted with different constant cortical bone thickness values as per each section to determine the change in structural response as well as fracture locations based on the same material properties. Table 7-11 shows the simulation matrix for the parametric study in detail.

The results of parametric study showed that the overall stiffness calculated from the force-deflection curve, peak force, peak deflection, as well as the energy increases with increasing cortical thickness for rib bones during such type of loading as shown in Figure 7-6. The case with constant cortical thickness of 1.2 mm and 1.15 mm throughout the rib provided similar stiffness response as provided by the variable cortical thickness case for different sections, but the difference in the peak deflection is 4 mm (7.4%) for both cases and the energy value is 0.14 J and 0.23 J (10.52%) less than the latter case respectively.

Table 7-11 Simulation matrix for the whole rib bending test parametric study

Simulation run serial number	Cortical bone thickness at different sections (mm)					Material model parameters
	Anterior	Antero lateral	Lateral	Posteo lateral	Lateral	Elastic plastic material model parameters
1 (Model)	0.68	0.94	1.21	1.15	0.92	Elastic modulus = 9.8 GPa
2	0.68 constant thickness					Poisson's ration = 0.3
3	0.94 constant thickness					Yield Stress = 97 MPa
4	1.21 constant thickness					Tangent Modulus = 1.35 GPa
5	1.15 constant thickness					Failure Strain = 0.014
6	0.92 constant thickness					

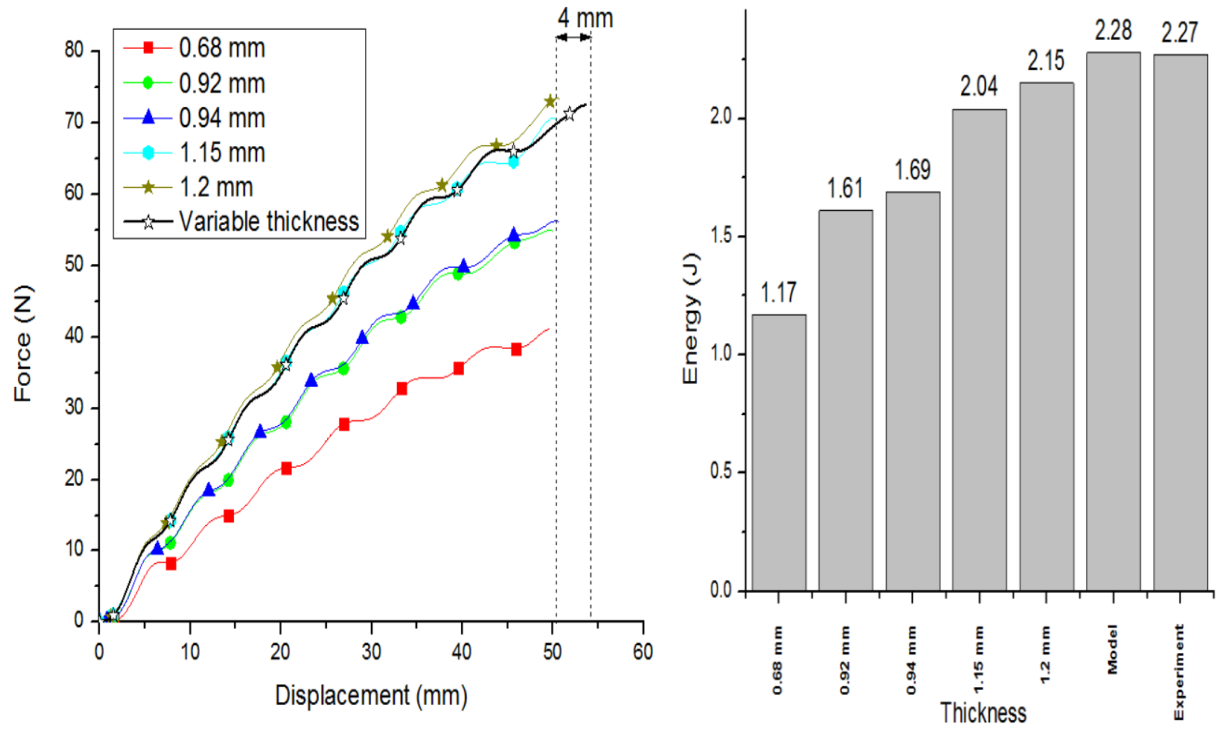

Figure 7-6 Force-deflection curves (Left) and energy values (Right) for different cortical thickness cases

Quantitative analyses of the results of parametric studies are shown in Table 7-12. It can be interpreted from these results that the majority of the stiffness for the whole rib comes from

lateral section of ribs due to the nature of bending loading. Therefore, the overall response can be simulated with the help of constant cortical thickness at the lateral section. The percentage discrepancies for the cases with similar cortical thickness at the lateral sections (Run 5 and Run 6) are less than 10% from experiment as shown in Table 7-12.

Along with the peak force, deflection and energy values, fracture locations also play a major role in validating the overall structural response of the whole rib bone. Figure 7-7 shows the model predicted fracture locations for each parametric run case. It should be noted that the fracture locations were identified when the very first element reached the plastic strain failure threshold during the simulation. The results showed that the fracture location occurred primarily at the lateral region for cases with a constant cortical thickness value.

Table 7-12 Percentage discrepancies for structural responses for parametric study cases

Simulation run	Peak Force (N)	Discrepancies from experiment	Peak horizontal deflection (mm)	Discrepancies from experiment	Energy to fracture (J)	Discrepancies from experiment
Experimental value		74.18 N		26.11 mm		2.27 J
1 (Model)	73.05	1.52%	28.45	-8.96%	2.28	-0.44%
2 (0.68 mm)	41.1	44.59%	26.37	-0.98%	1.17	48.46%
3 (0.94 mm)	54.89	26.00%	26.58	-1.80%	1.61	29.07%
4 (1.21 mm)	56.2	24.24%	26.94	-3.16%	1.69	25.55%
5 (1.15 mm)	70.53	4.92%	26.75	-2.45%	2.04	10.13%
6 (1.2 mm)	73.41	1.04%	26.98	-3.35%	2.15	5.29%

On the other hand, fracture locations were different for the case with variable cortical thickness in different sections of the rib. The latter case represented more accurately the fracture

behavior of ribs as seen in experiments, where a higher percentage of rib fractures occurred at anterior and lateral regions.

Li *et al.* (2010) showed the influence of mesh density, cortical thickness, and material properties on human rib fracture prediction. It was concluded that an FE model with varying cortical bone thickness at each node more accurately predicts the force-deformation behavior than a constant thickness model. Also, the model-predicted fracture location changed depending on the way the cortical bone thicknesses are represented. Similar conclusions were made in this study when regional cortical thickness was assigned based on statistical data, instead of subject specific cortical thickness assignment at each node as done by Li *et al.* (2010). Overall, the rib with variable cortical thickness was able to match the structural responses as well as the fracture locations better than the cases with constant cortical thickness value.

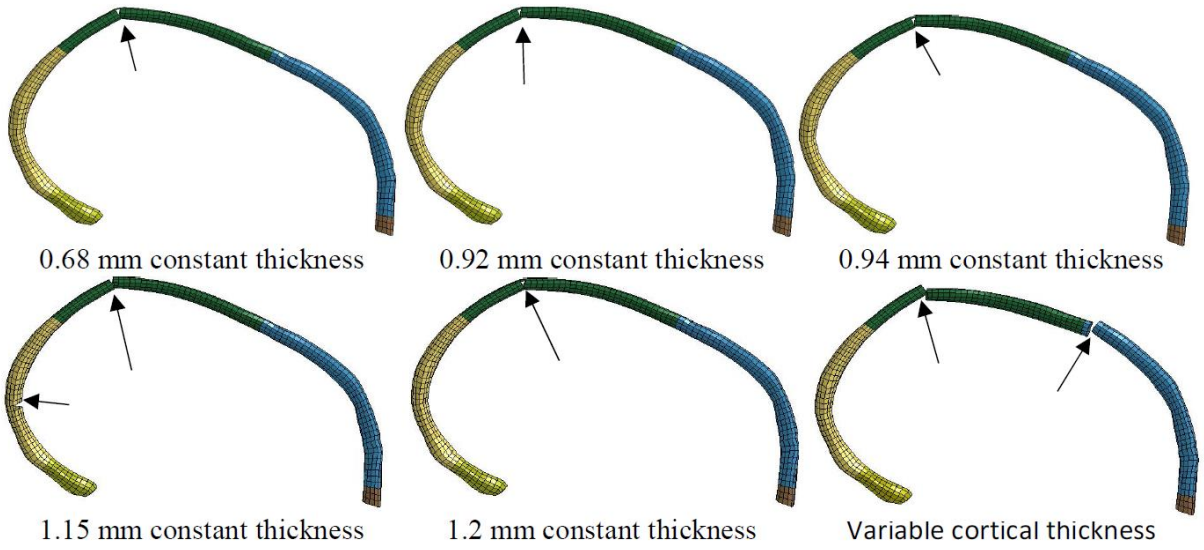

Figure 7-7 Model predicted fracture locations in parametric cases

Moreover, the cortical thickness variation may also be different even in people of the same age, gender, height, and weight. Therefore, a subject specific model with nodal thickness assigned based on detailed scans of the individual specimen may not be a good representation for

the whole population within that segment. A region specific cortical thickness variations based on average statistical data can be a better alternative to represent such a segment of population. Such an effort has been made in this study for representing the overall rib structural response for the 70 years old female with statistically average data for cortical bone thickness in different regions of ribs.

It is well known that the cortical bone thickness can vary in a local region for the bone as shown in Figure 5-4. But in this study, the overall cortical thickness was taken as an average value for a particular section, namely the anterior, anterolateral, lateral, posteolateral, or posterior location. Therefore, the local thickness of the rib specimens can be over or under estimated. Some of the typical measurements of cortical bone in earlier studies were even in the range of 0.3 mm (Appendix A). Although the overall stiffness response and approximate location of the fracture can be well predicted for a bending scenario as experienced in frontal impact, the structural response of the ribs in other loading scenarios can be different. This is one of the limitations of the current study. On the other side, the model with varying regional cortical thicknesses will be able to represent the overall population rather than a subject specific model when the local cortical thickness details can be included. Another limitation of the current study is the difference between structural response as well as fracture locations according to rib level. Different ribs at different rib levels from 1-12 may have different cortical thickness variations, but the supportive data to provide such variations for all ribcage are not currently available yet.

CHAPTER 8. VALIDATION OF THE 70 YEARS OLD FEMALE THORAX MODEL

8.1. INTRODUCTION

Numerous cadaveric studies have been conducted to study the injury tolerance of human thorax based on sled and component level tests. By collecting elderly female cadaver test data under different test conditions, corridors will be generated for validating model predictions. In general, the overall stiffness of the thorax depends on different underlying stiffness of the soft tissues as well as the bony structure. A lumped mass model (Lobdell *et al.* (1973)) can be used to define the overall stiffness characteristic of a thorax as shown in Figure 8-1.

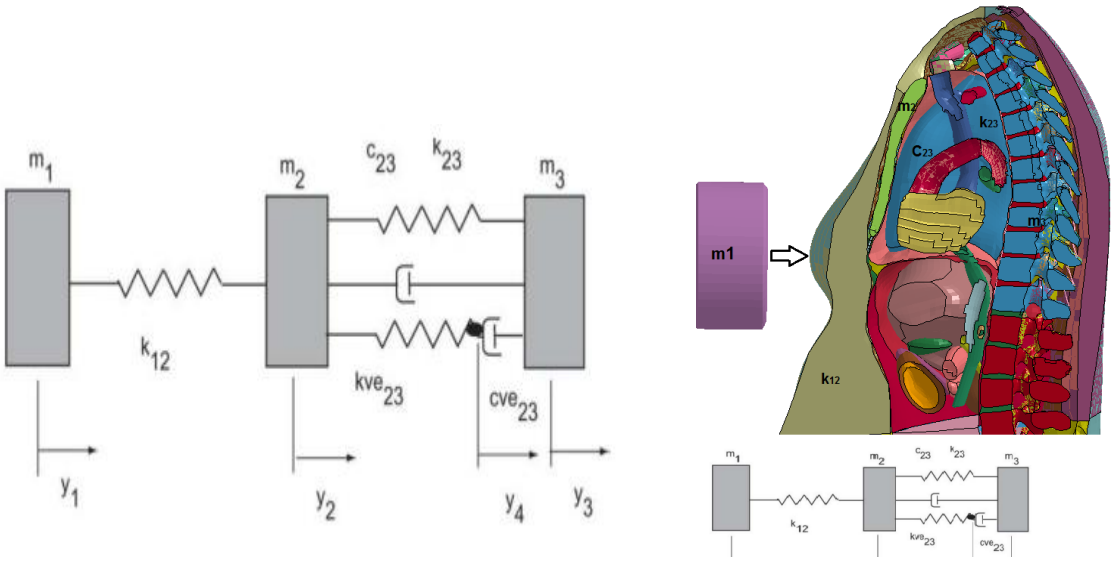

Figure 8-1 One dimensional model of human thorax (Reproduced from Prasad *et al.* (2005) (Left) and equivalent representation of FE model (Right)

The model consisted of rigid bodies with different masses m_1, m_2, and m_3 connected by springs and dampers. Mass m_1 represented the impactor mass and m_2 and m_3 represented the effective masses of the sternum and thoracic vertebrae, respectively. Spring k_{12} represented the skin and flesh between the impactor and sternum. The connection between sternum and thoracic vertebrae as well as soft tissues like heart, lungs, *etc*. was represented by the spring and damper

system. The bony structure defines the major stiffness response which is highly age and gender dependent as shown in previous chapters of this dissertation. But, along with bony structure, viscous effects provided by soft tissues in the thoracic cavity play a major role in its load bearing capability of the thorax. Verriest (1985) studied the thoracic injury criteria and found that the resistance to compression offered by the ribcage alone was lower than the resistance to the intact thorax. Therefore, it is worth to include the age and gender dependent behavior of these soft tissues in models. However, there are not much data available showing the differences in the mechanical properties of soft tissues such as the lungs, heart, *etc.* as functions of age and gender. Noted that costal cartilage has been observed to show a significant decrease in strength with age this affects the overall resistance of the rib cage because the costal cartilage provides a link between sternum and ribs. Figure 8-2 shows the ratio of mechanical properties of some of the soft tissues along with costal cartilage reported by Yamada (1970). It is clearly shown that soft tissue strength reduced due to aging especially for hyaline costal cartilage which contributes the significant reduction in the overall resistance of the ribcage. Also, aortic ruptures were one of major causes for fatality in car crashes. Different mechanisms have been proposed for the aortic ruptures like stretching of the arterial vessels in longitudinal directions, hydraulic pressurization of the thoracic aorta during crash, *etc*. (Hardy *et al*. 2006). Yamada (1970) showed that there is a decrease of 29-32% in ultimate tensile strength of the human arterial tissues in elderly age group as shown in Figure 8-3.

Since studies are limited to reprimand the material models for soft tissue with age and gender effect, the material properties available in literature were used in the current model as shown in Table 8-1, which were directly taken from the GHBMC model. However, the thresholds for soft tissue injury prediction were based on those used by Shigeta *et al.* (2009) as

prescribed in the THUMS 4.0 version. Although there are age related properties reported, there are no age related threshold changes reported for soft tissues in literature. Therefore, the values used by Shigeta, which are based on test data available, were adapted in this study as the threshold values for soft tissue injury predictions in the 70 years old female model.

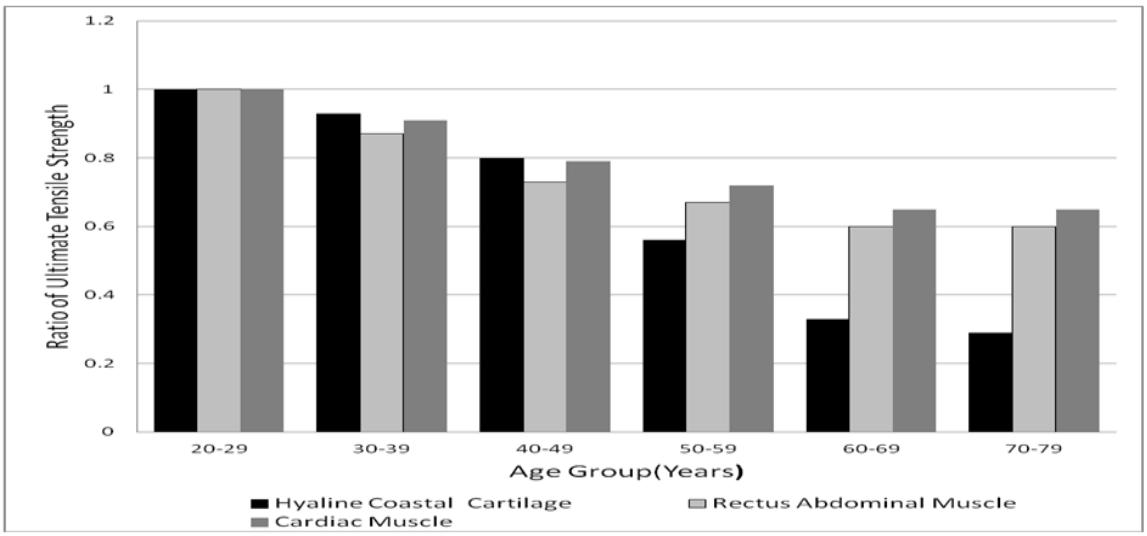

Figure 8-2 Ratio of ultimate tensile strength of soft tissues in different age groups (Zhou *et al.* 1996 and reproduced from Yamada 1970)

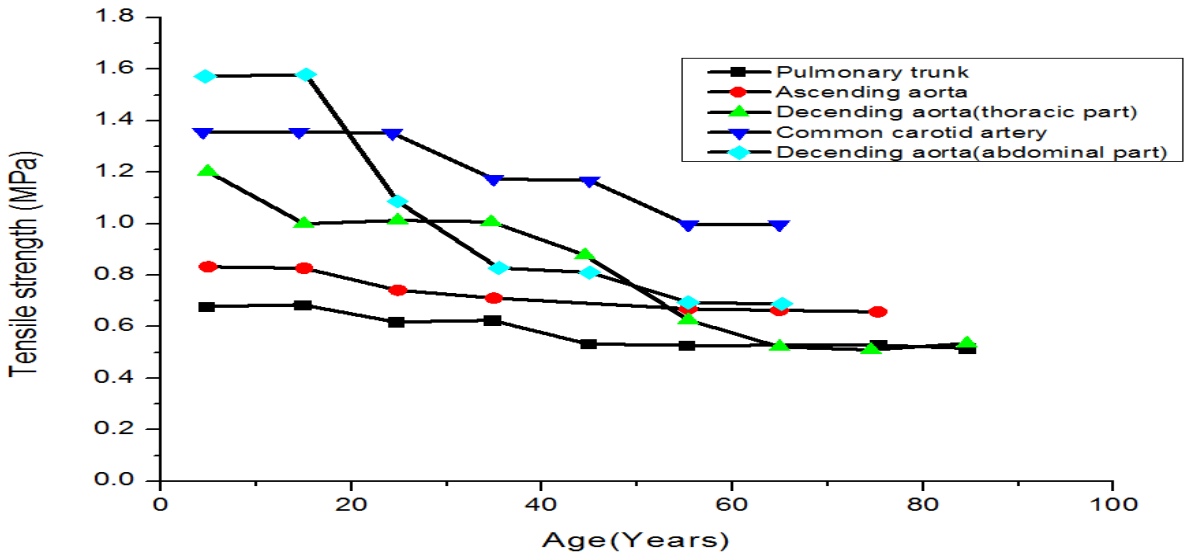

Figure 8-3 Age related changes in tensile strength of human arterial tissues (Zhou *et al.* 1996 and reproduced from Yamada 1970)

Table 8-1 Material properties assumed for the 70 years old female thorax model

Part	Material law	Material constants
Vertebrae/Rib Cancellous bone	Elastic-Plastic	ρ =1.0e-006 kg/mm^3, E=0.04 GPa, σ_y =0.002 GPa, E_{tan}=0.01 GPa,
Vertebrae/Rib Cortical bone	Elastic-Plastic	ρ =1.8e-006 kg/mm^3, E=9.8 GPa, σ_y =0.08 GPa, E_{tan}=1.35 GPa,
Thoracic disc	Elastic	ρ =1.1e-006 kg/mm^3, E=0.0364 GPa, γ =0.4
Aorta, intercostal muscle, veins	Elastic	ρ =1.2e-006 kg/mm^3, E=0.001 GPa, γ =0.45
Cartilage	Elastic	ρ =1.1e-006 kg/mm^3, E=0.05 GPa, γ =0.35
Pancreas	Elastic	ρ =1.1e-006 kg/mm^3, E=0.03 GPa, γ =0.45
Clavicle ligaments	Elastic	ρ =1.1e-006 kg/mm^3, E=0.104 GPa, γ =0.45
Stomach	Elastic fluid	ρ =1.0e-006 kg/mm^3, Bulk =1.4 GPa
Gallbladder	Elastic fluid	ρ =1.0e-006 kg/mm^3, Bulk =2.2 GPa
Blood	Elastic fluid	ρ =1.0e-006 kg/mm^3, Bulk =2.2 GPa
Lung	Elastic fluid	ρ =1.0e-006 kg/mm^3, Bulk = 1.4 GPa
Heart	Heart tissue	ρ=1.0e-06 kg/mm^3, P = 3.48 GPa
Spleen	Viscous foam	ρ=1.1e-06 kg/mm^3, E_i = 9.8e-5 GPa, E_v=0.0085, γ =0.45
Liver	Viscoelastic	ρ=6.0e-07 kg/mm^3, G_0=2.3e-4 GPa, G_t =4.3e-5GPa, Bulk=2.87e-3GPa, beta=0.635
Soft tissue filling	Soft tissue	ρ=1.1e-06 kg/mm^3, C_1= 7.2e-6 GPa, C_2=8.5e-6 GPa, Bulk = 0.01GPa
Flesh	Simplified rubber/foam	ρ=1.06e-06 kg/mm^3, damping coefficient = 0.1 Bulk = 0.5GPa, stress-strain curve
Intestine	Elastic	ρ =1.1e-006 kg/mm^3, E=0.03 GPa, γ =0.45

where ρ = density; E= Young's modulus; γ =Poisson's ratio; C_1, C_2 = hyper elastic coefficients, G_0 = short term shear modulus, G_t = long term shear modulus, P = Pressure, Ei=Initial Young modulus, ev= Viscous Young's modulus, σ_y = Yield stress, E_{tan} = Tangent modulus

Table 8-2 Threshold values for soft tissue injury prediction assumed for the 70 years old female model grounded on Shigeta *et al.* (2009)

Organ name	Injury Criteria	Threshold value	Reference
Lung	Pressure	± 10 kPa	Schaefer *et al.* (1958)
Liver	Strain	30%	Melvin *et al.* (1973)
Heart	Strain	30%	Yamada *et al.* (1970)
Blood vessel	Strain	100%	
Intestine	Strain	120%	

8.2. ISOLATED RIBCAGE LOADING

Although the constitutive material laws or stiffness characteristics of the ribs and soft tissues, listed in Table 8.1 for the 70 years old female, could affect the overall stiffness of the ribcage, this stiffness could also be affected by the interaction between the ribs and vertebrae. Therefore, it is important to model the costovertebral joints accurately. Current section of the study focuses on modeling the interface between ribs and vertebras.

8.2.1. Modeling of Costovertebral Joints

The joint between ribs and vertebra could affect the overall response of the ribcage during frontal loading. Kent *et al.* (2005) showed that the bone strain is affected by the joint rotation as shown in Figure 8-4. There are different strategies to model the costo-vertebral joints using FE models. It can be simulated by using spherical joints (Choi and Lee 1999) or by defining a surface to surface contact between vertebrae and ribs and by making 1-D ligaments between vertebra and ribs to control the overall stiffness behavior (Iwamoto *et al.* (2002)). In general, there are surrounding soft tissues as well as the muscles involved to anatomically define

the stiffness of these soft tissues, but in FE simulations, the overall stiffness response of these joints can be a challenge to meet.

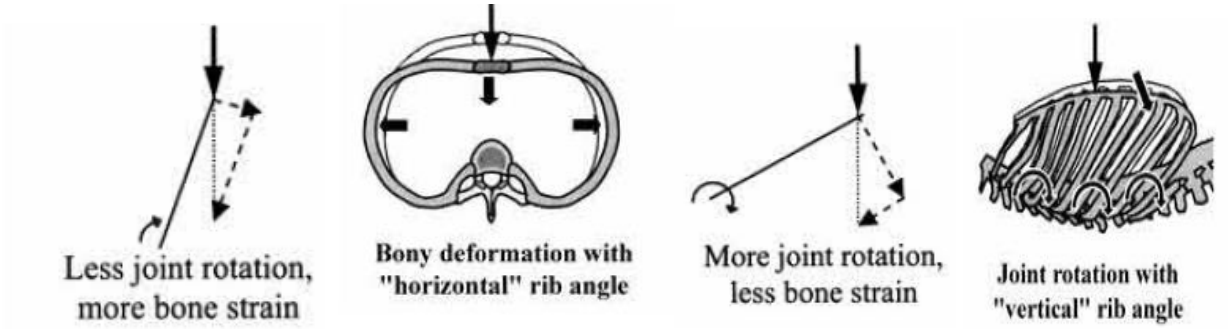

Figure 8-4 Influence of joint rotation on rib strain (Photo taken from Kent *et al.* (2005))

Li *et al.* (2010) optimized the overall modeling of these joints by changing the spherical joint stiffness, the costal cartilage elastic modulus, and the sternum cortical thickness for the GHBMC (Global Human Body Modeling Consortium) model in order to better match against rib ring tests done by Kinding *et al.* (2010). The experiment involved 1 male cadaver (44 years old) and 2 female cadavers (61 years and 63 years old). It was concluded in Li *et al.* study that the stiffness and the kinematic trends in the experimental study were more likely to be applicable to elderly subjects and to females. Therefore, for the current model, the interaction between the ribs and the vertebrae were modeled using similar spherical joints in the FE model and the joint stiffness was assigned through moment-angle curves as defined in the GHBMC model. Since there were no studies appeared in literature for defining the age dependent material properties of costal cartilage and the change in cortical bone thickness of sternum with age and gender, the costal cartilage properties and the cortical thickness of the sternum were also taken from the GHBMC model (Li *et al.* (2010)).

8.2.2. Validation against isolated ribcage loading

The overall behavior for the stiffness of costovertebral joint as well as the ribcage was validated against experimental data reported by Vezin and Bethet (2009). In this study, the

experiments were performed on isolated thoracic ribcages dissected from 4 un-embalmed PMHS (Post Mortem Human Subjects) specimens. A fixture was designed to hold the specimens at the rear end of the spine and a 9.5 kg duralumin circular tube fitted with a rigid rectangular aluminum pad (40 X 70 mm) with round edges was used to impact the specimen for speeds up to 2 m/s, as shown in Figure 8-5 (a). The 70 years old female ribcage model was simulated for the same loading condition as used in experiments, as shown in Figure 8-5 (b). The experimental matrix consisted of 3 F and 1 M specimens, but data related to elderly female specimens were taken into consideration for comparison of results predicted by the model.

The ribcage model was loaded using the displacement profile as recorded in the experiment for cadaver #2 with a peak velocity Vmax =1.67m/s. The authors did not report the displacement profiles for the other two female cadaveric tests. Hence, only one simulation was conducted. The model predicted force-deflection response matched the experimental data recorded for cadaver #2 reasonably well but behaved quite differently for data reported for the other two cadavers. The model predicted overall deformation of the post impact ribcage is shown in Figure 8-6 (a) and comparison between experimental and simulation force-deflection response is shown in Figure 8-6 (b). No rib fractures were recorded in the study, therefore, no comparison was made for the fracture prediction of ribs in the simulation also.

8.3. FRONTAL IMPACT VALIDATION

8.3.1. Hub loading

Kroell *et al.* (1971, 1974) performed pendulum impact on thorax of 37 cadaver specimens four decades ago, out of which 8 specimens were from females of different ages. The anthropomorphic details as well as different pendulum masses and speeds are listed in Table 8-3 for these specimens.

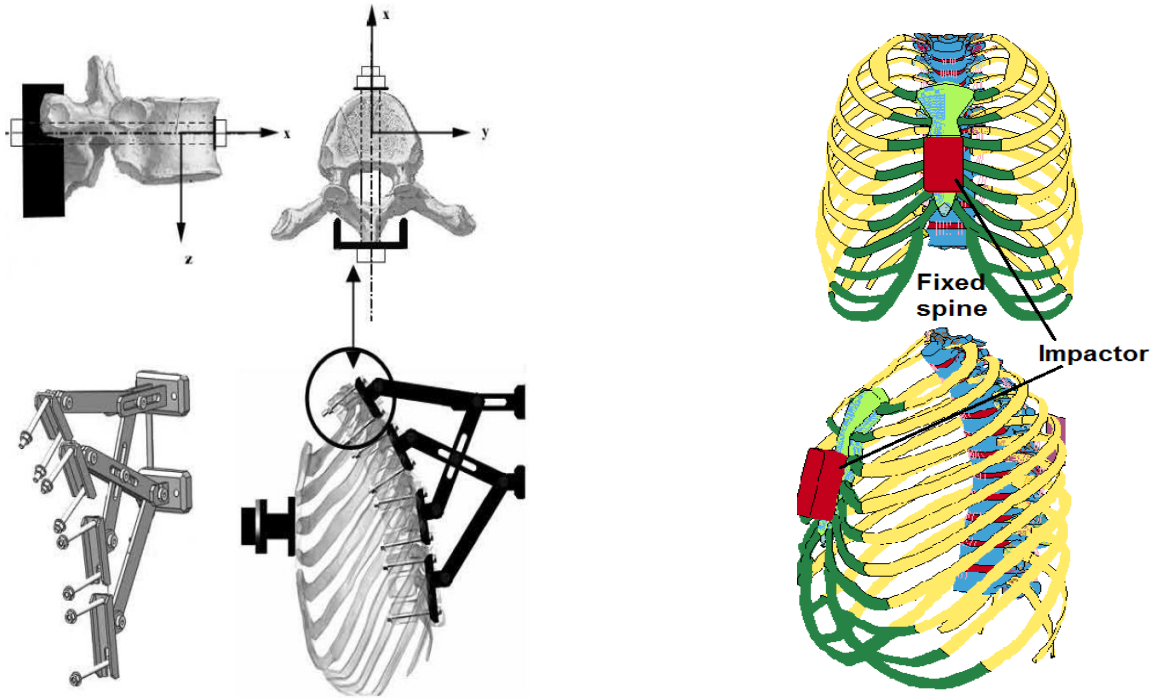

(a) (b)

Figure 8-5 (a) Experimental setup for isolated ribcage loading (Vezin and Bethet (2009)) and (b) Simulation setup frontal and lateral view (shell elements were hidden for clear view)

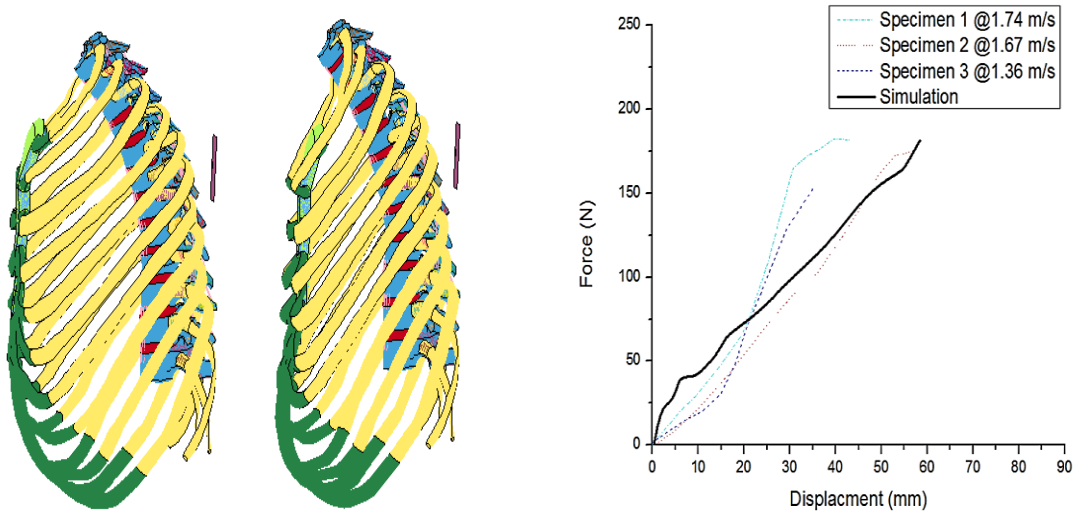

(a) (b)

Figure 8-6 (a) Deformation of the ribcage before (left) and after (right) impact and (b) Comparison between experiment and simulation force deflection curves

The impact setup is shown in Figure 8.7 (Left). The corresponding force and deflection characteristics of each specimen were retrieved for the FE model validation. The impactor mass used for specimen 30 FF was significantly lower than the other tests and the impact speeds used for specimen 30FF and 55FF were significantly higher than other tests, therefore these two specimens were excluded for response comparison.

Table 8-3 Pendulum impact experimental matrix for female specimens taken from Kroell *et al.* (1971, 1974)

Sr. No.	Experiment No.	Specimen No.	Age	Height (cms)	Weight (kg)	Pendulum mass (kg)	Impact velocity (m/s)	No of rib fractures	Soft tissue injuries	Reference
1	60	11FF	60	160.02	58.97	19.50	6.30	11	No	Kroell et al. (1971)
2	61	12FF	67	162.56	62.60	22.86	7.24	22	right lung contusion	
3	66	14FF	76	156.21	57.61	22.86	7.33	7	beneath sternal fractures-aortic, vena cava, right artium ruptures	
4	82	21FF	45	173.99	68.49	23.59	6.84	18	no	
5	85	23FF	58	162.56	61.23	19.50	7.73	23	pleura punctures below rib fractures	
6	92	30FF	52	156.21	40.82	1.59	13.23	3	no	Kroell et al. (1974)
7	190	54FF	49	162.56	37.19	19.55	6.71	7	left liver lobe fractures, aortic tear	
8	191	55FF	46	173.99	81.19	19.55	9.92	8	pericardial and left ventricle laceration, aortic valve muscle severed	

For the simulation, a unpadded pendulum with a diameter of 152 mm with round edges and a mass of 19.5 kg was impacted at the mid sternum position of the model at a velocity of 7 m/s. The overall force and deflection response was compared with the experimental data. Although no mass scaling was used to account for age effects, the mass scaling using equal stress equal velocity approach (Petitjean *et al*. (2015)) was done in the cadaver test data so that inertia

effect can be comparable between the experimental and simulation results. The kinematics of simulation as well as cross sectional view of thoracic deformation at fourth level of vertebra at an interval of 6 ms are shown in Figure 8-8 and Figure 8-9 respectively. A comparison between the experimental and simulation results for force-deflection is shown in Figure 8-10.

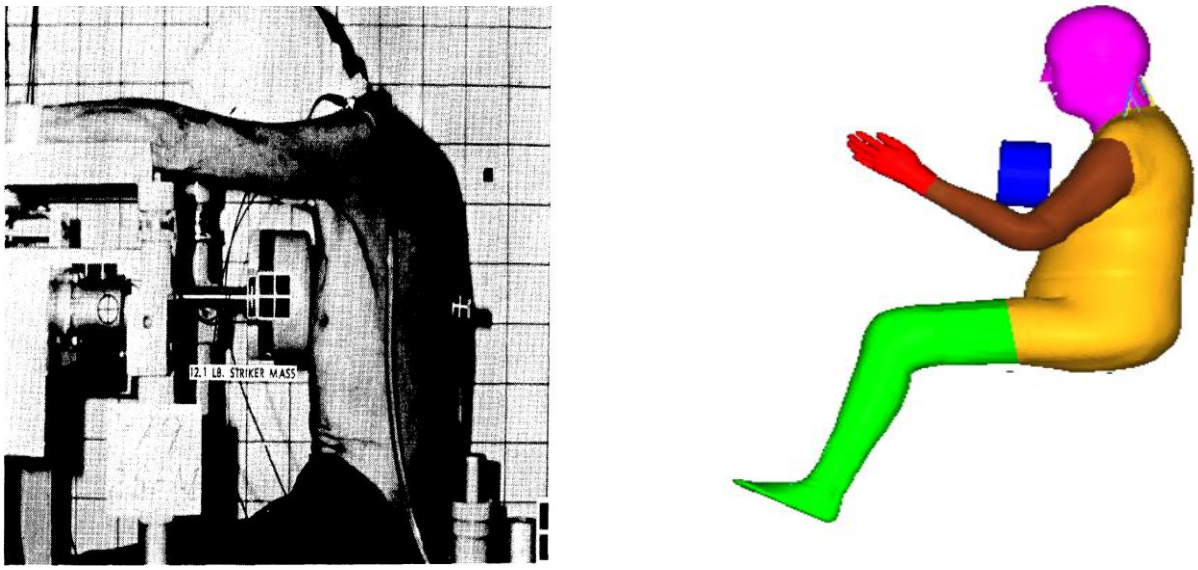

Figure 8-7 Hub loading experimental setup (Kroell *et al.* (1971) (Left) and hub loading simulation setup (Right)

The injuries related to rib fracture as well as soft tissues were reported in the experiments conducted by Kroell *et al* (1971, 1974). Rib fractures were common in all the experiments and different kind of soft tissue injuries were mainly reported for lung contusions, liver lobe ruptures and heart tissue lacerations with aortic tears. The current 70 years female model was able to predict rib fractures (number =11) as shown in Figure 8-11 as well as soft tissue injuries for the lungs, heart, and liver as shown in Figures 8-12, 8-13, and 8-14 respectively.

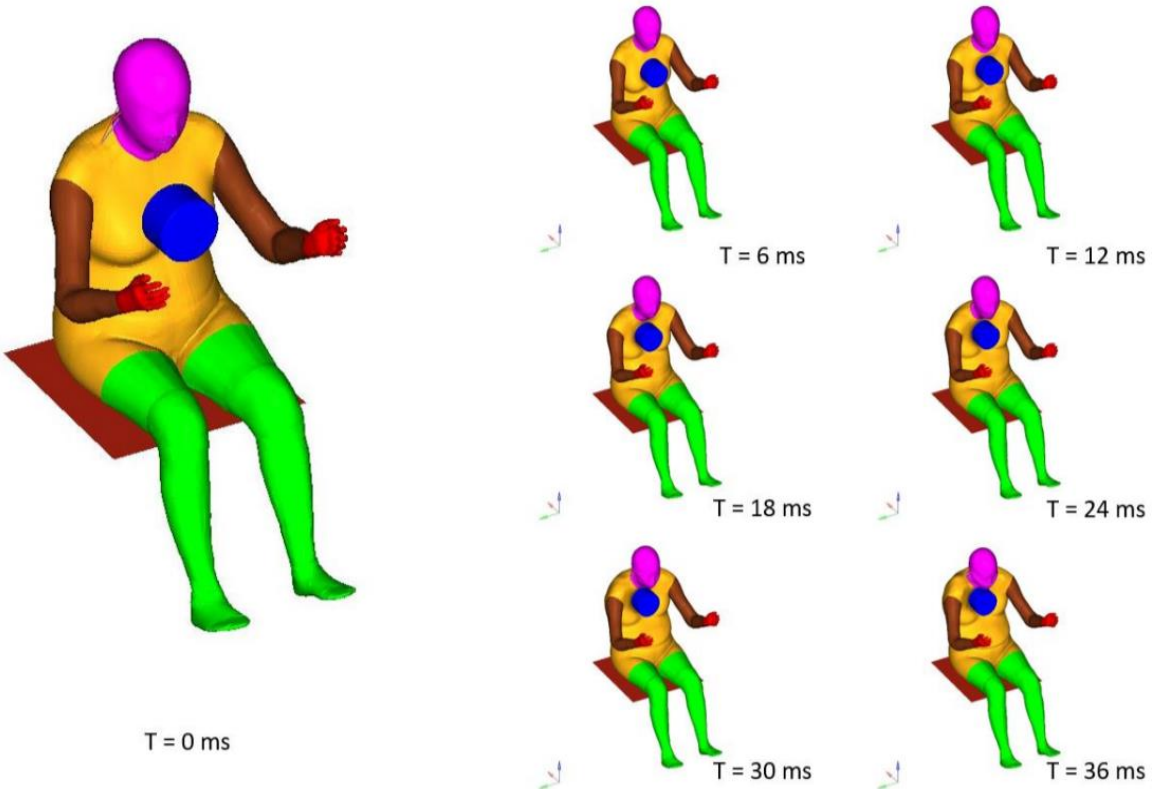

Figure 8-8 Kinematics of Kroell's hub impact simulation at every 6 ms

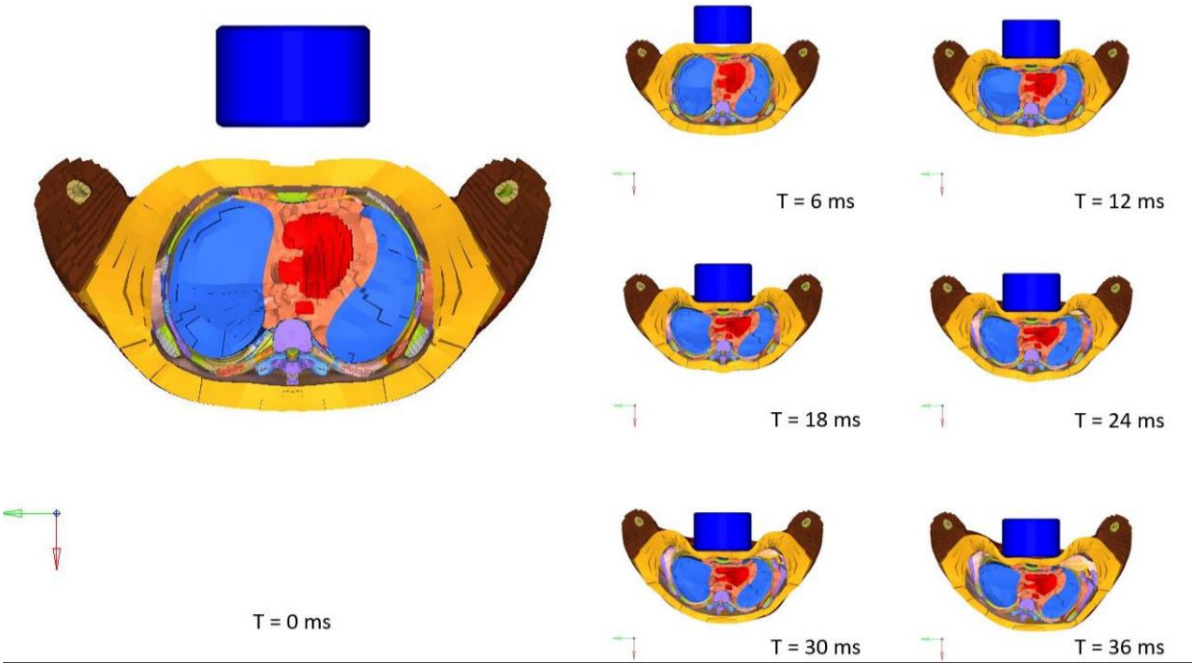

Figure 8-9 Cross-sectional view of thoracic deflections at 4th level of vertebra at every 6 ms

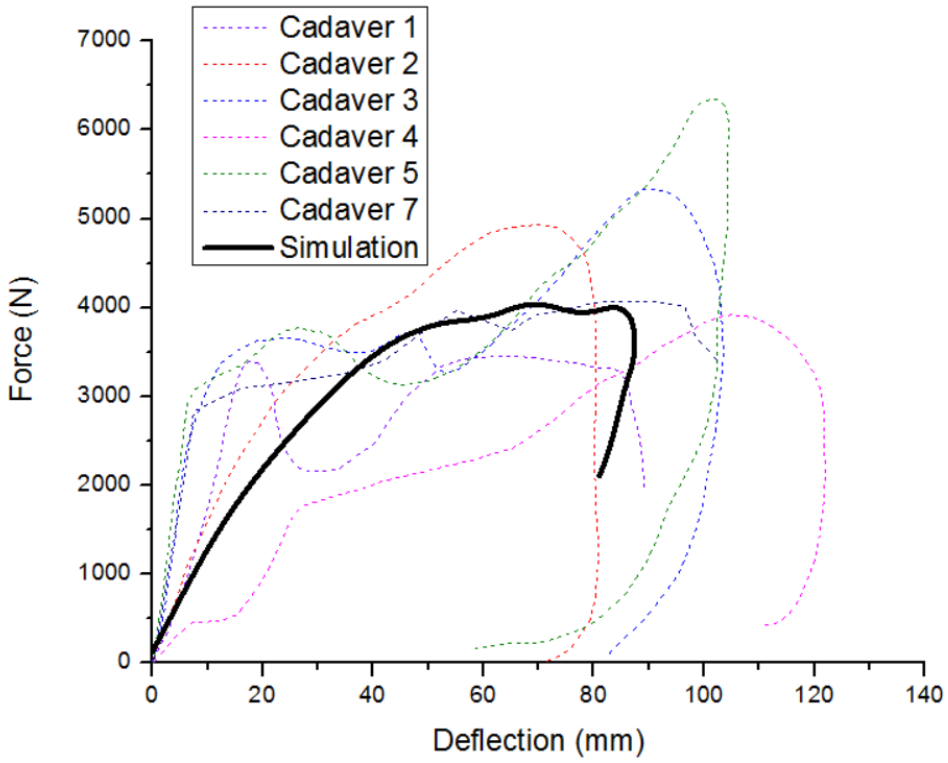

Figure 8-10 Comparison of force vs chest deflection between experimental and simulation results for hub loading (Kroell's experiments)

According to the threshold value mentioned in Table 8-2, 60% of the lungs volume was above 10 kPa critical pressure volume, showing a greater chance for predicting lungs damage in such loading condition. Similarly, 90% of the volume for the heart and upper aortic tissues elements was above the pre-set 0.3 strain threshold value, again predicting higher possibility of getting ruptured or lacerated. For the liver, volume of failed elements for the 0.3 strain threshold value was found to be only 22%, showing a lower probability of having such injury in these kind of loading condition. It should be noted that the failure in the liver elements are in the later stage of simulation, when the abdominal portion of the body moves along with the upper thorax causing strain in the abdominal organs. For estimating the probability of sustaining soft tissue

injuries, the critical volume value for failure can be used as a simulation based parameter and can be divided into the levels as shown in Table 8-4.

Table 8-4 Volume failed at critical threshold value vs probability of sustaining injury

Volume failed at critical threshold value	Probability of getting injury
> 70 %	Highest
35-70%	Medium
< 35 %	Lowest

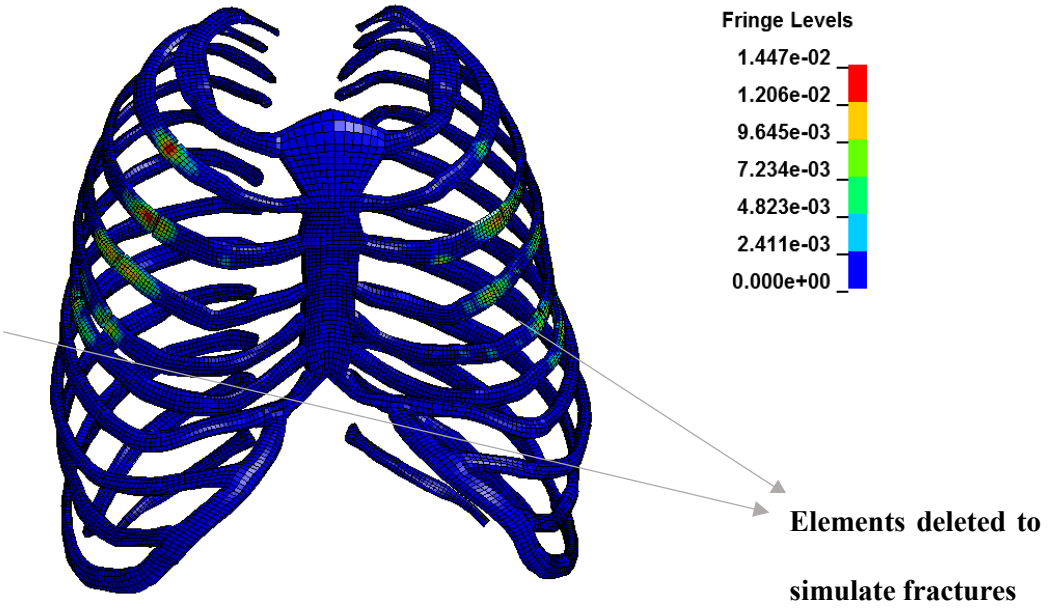

Figure 8-11 Plastic strain contours in the thorax rib skeleton and 11 simulated fracture locations spotted with the help of maximum plastic strain based element deletion

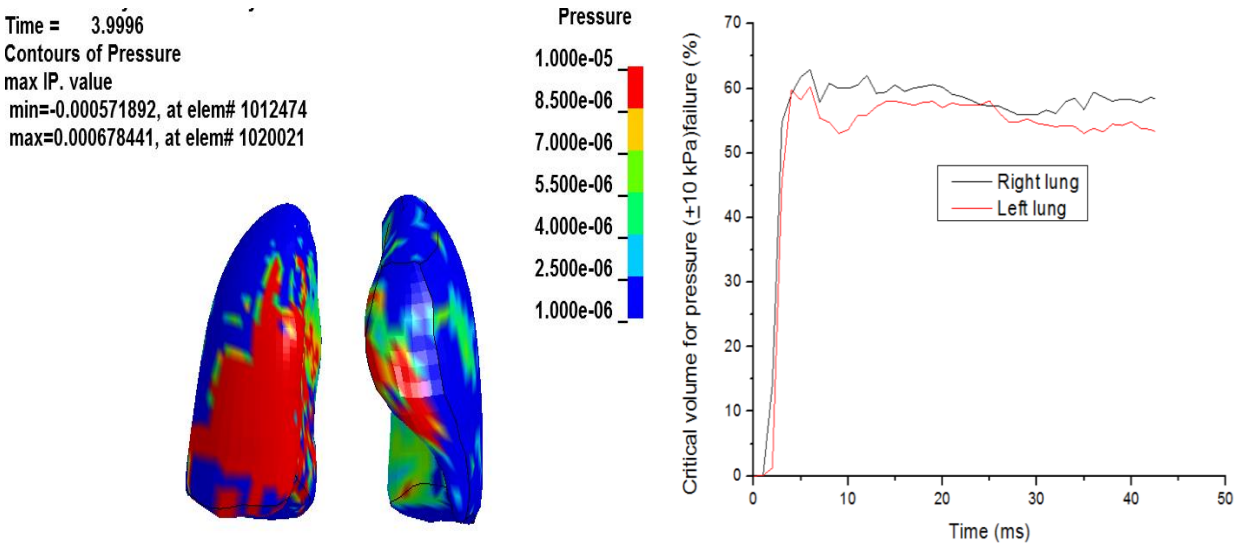

Figure 8-12 Pressure contours for lungs (Red color region > 10 kPa) (Left) and critical volume history (Peak value = 60%) history for pressure failure (at 10 kPa threshold) from simulation output (Right)

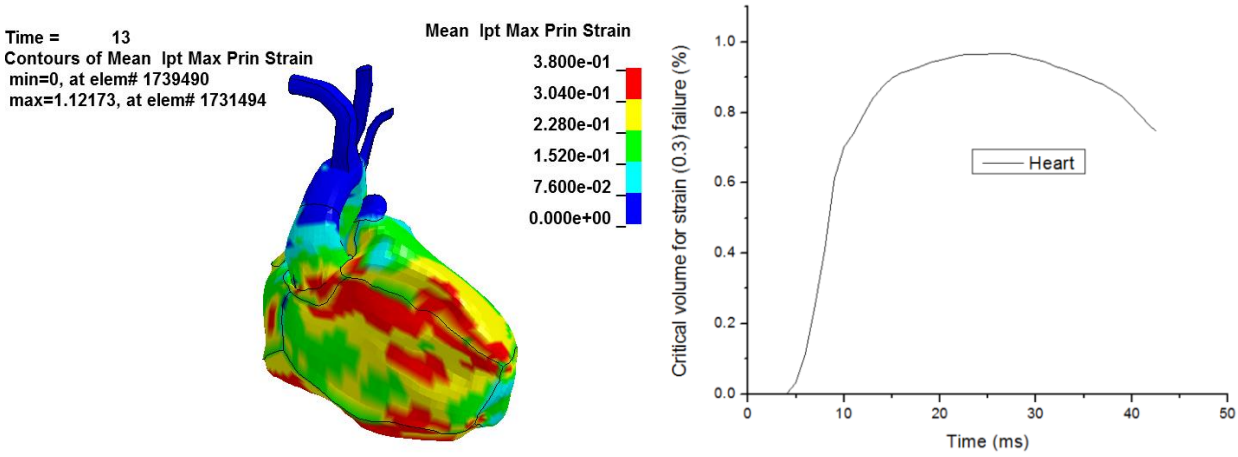

Figure 8-13 Strain contours for the heart (Red color region > 0.3 strain) (Left) and critical volume history (Peak value = 90%) history for the strain failure (0.3 threshold) from simulation output (Right)

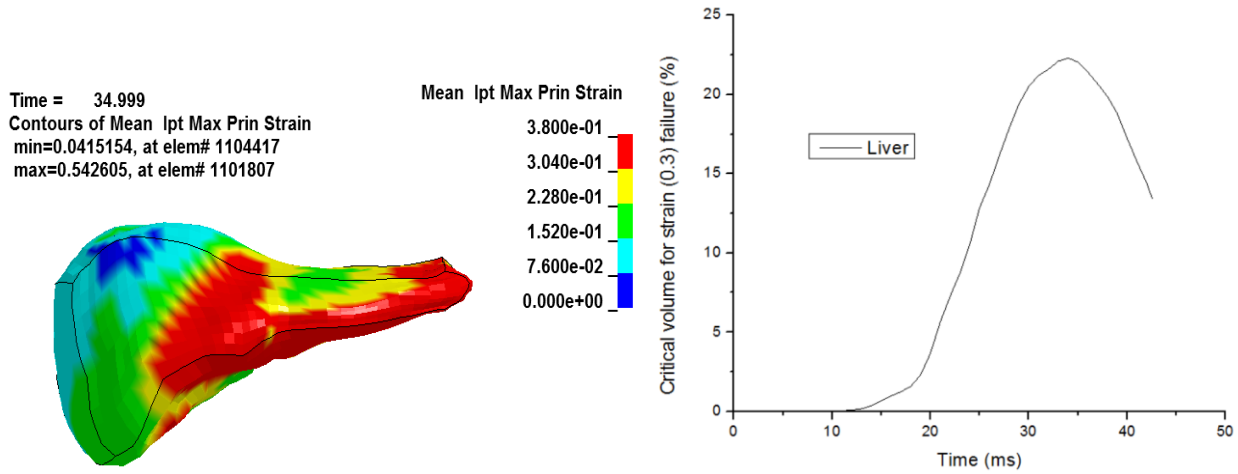

Figure 8-14 Strain contours for the liver (Red color region > 0.3 strain) (Left) and critical volume history (Peak value = 22%) for strain failure (0.3 threshold) from simulation output (Right)

Later, Kent *et al.* (2004) performed thorax impact test for hub loading condition on 15 human cadaver specimens. The test setup used for the experiment is shown in Figure 8-15 (Left). Out of these specimens, six specimens were of elderly female with ages from 60-80 years. The data presented in the publication was scaled to 50th percentile male population specimens, but the original data related to the six elderly female cadavers were kindly provided by the authors through personal communication. The boundary conditions in this hub loading were different than Kroell *et al.* (1971, 1974) experiments. In these experiments, a load cell was mounted at the posterior end of the thorax or the posterior end of the thorax was fixed and the front end of the thorax was loaded through a platform driven by steel cables. The corresponding chest deflection as well as the force at the posterior end was measured. The same setup was simulated by loading the front end of the chest with the mean chest deflection history. Before that, a constant gravity load was applied to the model so that it can initiated the proper contact with posterior loading plate for a total of 150 milliseconds (ms).

The comparison of force vs deflection for the experimental and simulation results is shown in Figure 8-16. Only response related to female cadavers with ages greater than 60 years old were chosen from the experimental data for model comparison. Except the initial stage, the model predicted responses were found to be within one standard deviation corridors for chest deflection (Figure 8-16).

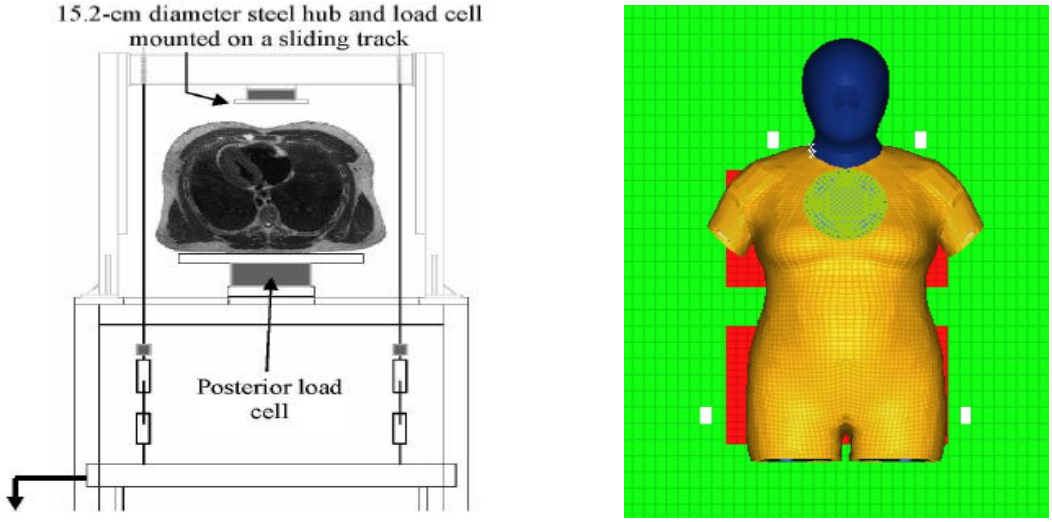

Figure 8-15 Hub loading experimental setup (Kent *et al.* (2004)) and simulation setup

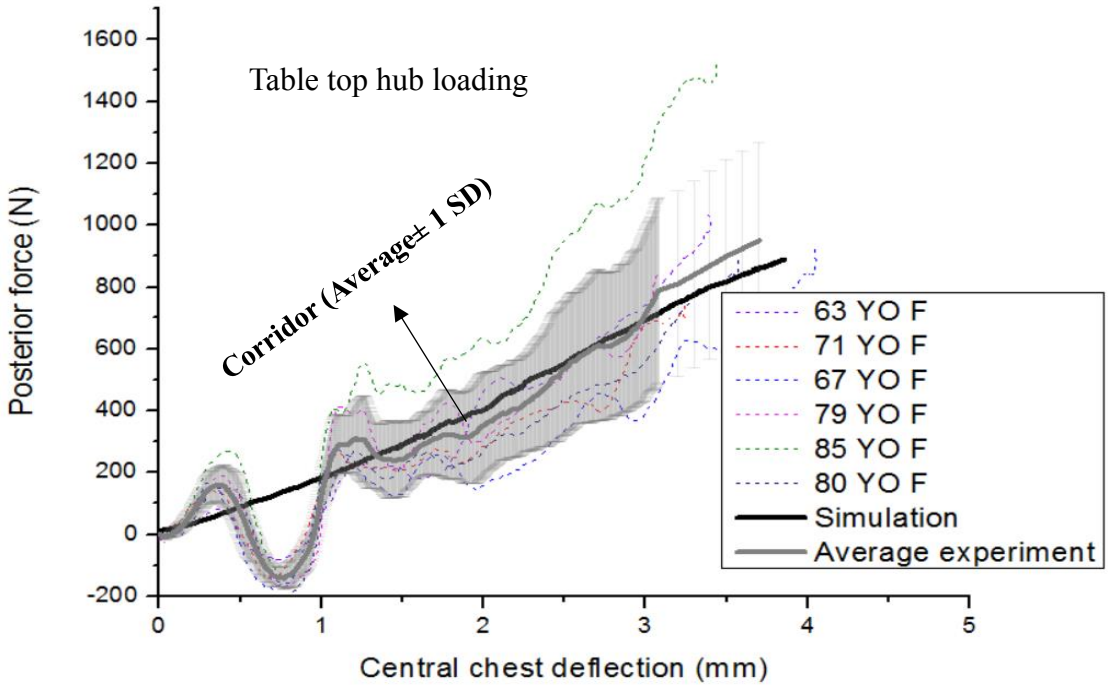

Figure 8-16 Comparison of force vs chest deflection between experiments and the simulation for table top hub loading

In the tests done by Kent, there were an initial spike in the experimental force-deflection curves; even the mass compensating of the mass of the hub was made. It was mentioned in the publication (Kent et al. (2004)) that these spikes are due to the results of accelerating the effective mass of the thorax. These spikes couldn't be achieved in the simulations, but the overall stiffness of the thorax was compared well after this initial spike phase. Since there were no rib fracture mentioned in the experiment and the soft tissue injuries were also not reported, no comparison of injuries were made for Kent's experiment. But it should be noted that no elements were deleted during the simulation of Kent loading with the pre-set threshold strain value.

8.3.2. Belt loading

Kent *et al.* (2004) also presented the test results for belt loading in different configurations (diagonal, double diagonal, and distributed) and the force deflection measurements were made similar to the hub loading. Figure 8-17 shows the experimental setup as well as the different belt configurations used during the testing. For the simulation, the belt routing was done in Hypermesh 14.0. 2-D elements of belt were assigned material Mat_Fabric properties and 1-D elements at the end of belts were modeled with seatbelt elements with material Mat_Seatbelt. The relevant cards were taken from LSTC practice examples given for belt loading. In the experiments, the belt was rolled on pulleys as shown in Figure 8.17 (left) while pushing downwards. Similar setup of pulley was attained by using Seatbelt_slipring elements through which belt slips down in the loading direction. The prescribed motion was added at the end of seatbelt elements to mimic the exact loading condition as in experiment. Figure 8-18 shows the simulation setups.

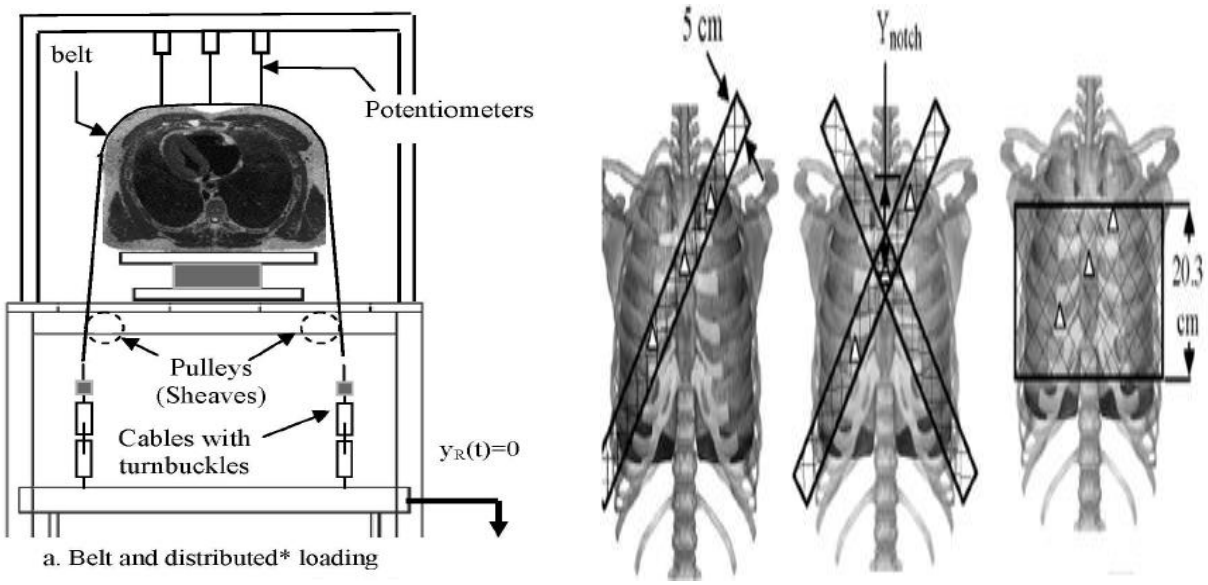

Figure 8-17 Test Setup for belt loading (Kent *et al.* 2004) (Left) and different belt position (diagonal, double diagonal, and distributed) during the experiments (Right)

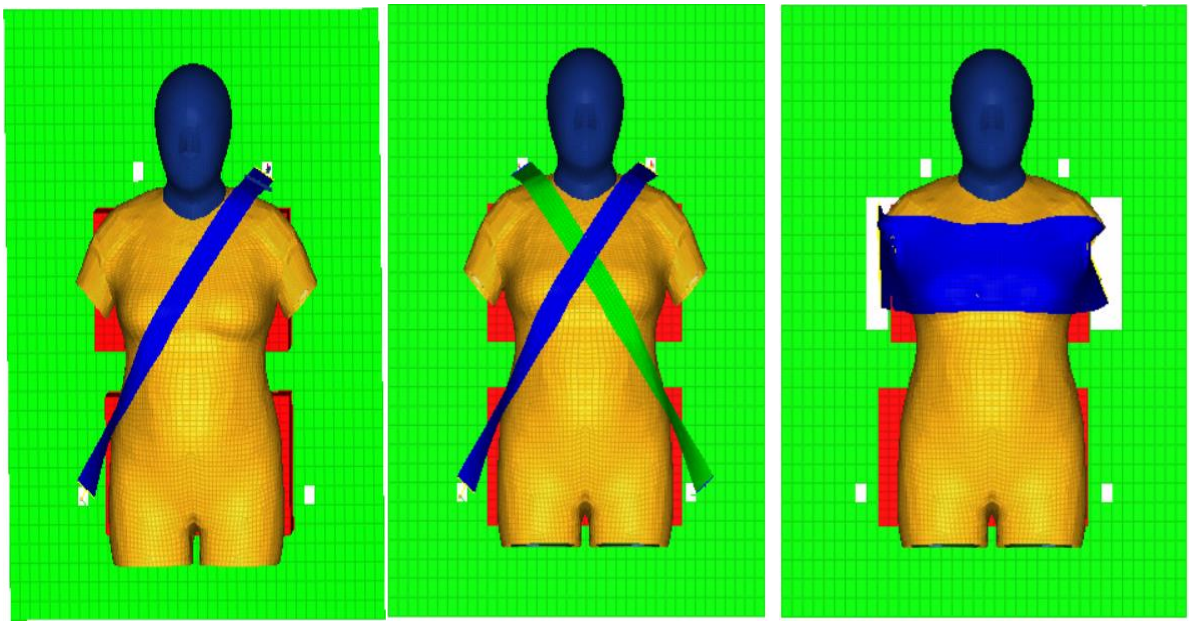

(a) (b) (c)

Figure 8-18 Simulation setups for different belt loading conditions (a) diagonal belt (b) double diagonal belt, and (c) distributed belt

The comparison of force vs deflection for the experimental data as well as for simulation results is shown in Figure 8-19. The average response of the experimental data was retrieved similar to the hub loading. The model predicted responses were found to be within one standard deviation corridors for average force and chest deflection of experiment.

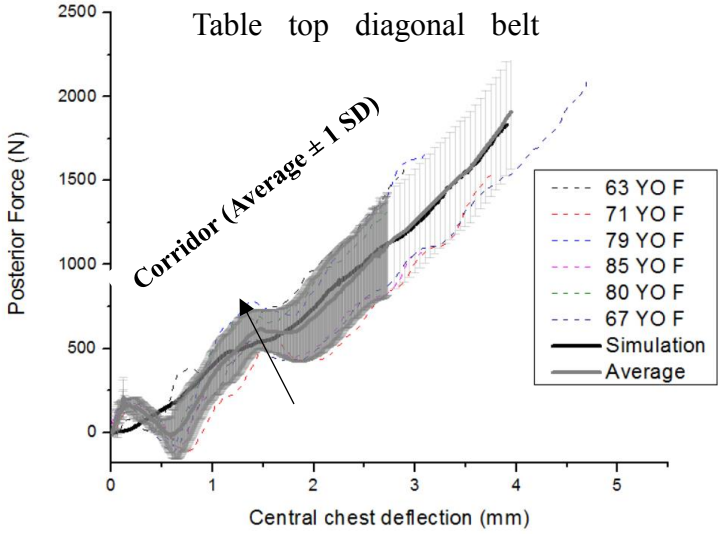

(a)

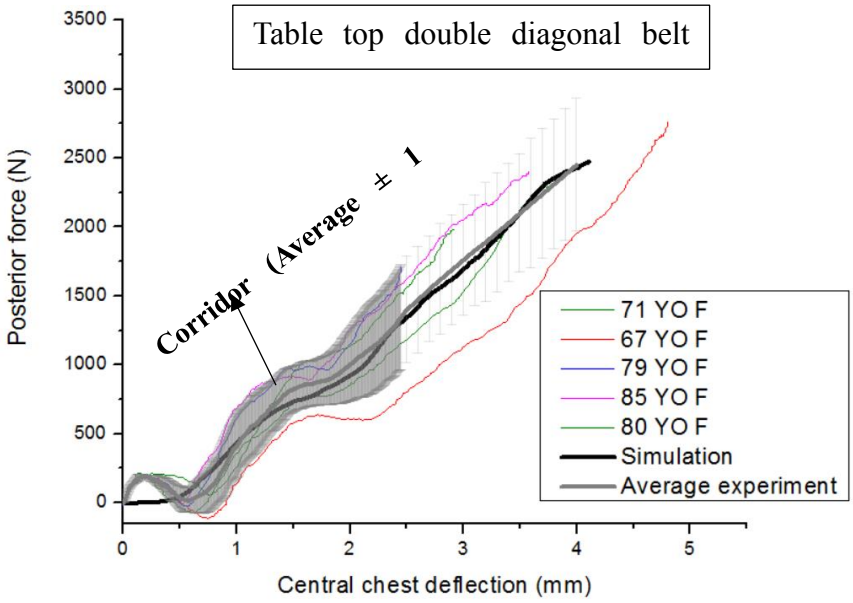

(b)

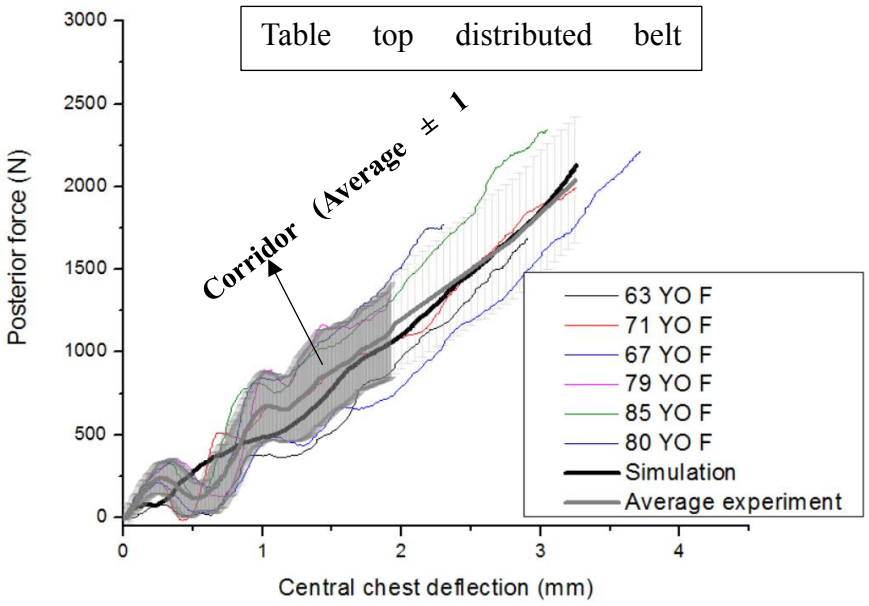

(c)

Figure 8-19 Comparison of force vs chest deflection between experiments and the simulation for (a) diagonal belt loading, (b) double diagonal belt loading, and (c) distributed loading

8.4. LATERAL IMPACT VALIDATION

8.4.1. Lateral impact test

Talantikinte *et al.* (1998) presented the thoracic responses for 11 cadavers impacted in a lateral direction with a 15 cm diameter impactor at a speed of around 6 m/s. Out of these 11 cadavers, only three specimens were females as shown in Table 8-5. The experimental impact setup is shown in Figure 8-20 (Left) and the simulation setup is shown in Figure 8-20 (Right). Since the cadaver arms were tied up in the testing setup, no arms were included in the simulation setup so that the impactor can impact at the described location. The arms mass of 7 kg were compensated for the experimental response comparison. In addition, the flesh near the shoulder region was compressed inward for approximately 5 mm to provide a good contact condition during the simulation. The kinematics of 70 years old female model during simulation for longitudinal lateral impact is shown in Figure 8-21. The corresponding force and deflection

characteristics of each specimen were retrieved for FE model validation and compared with simulation results as shown in Figure 8-22. Again, the mass scaling using equal stress equal velocity approach (Petitjean et al. (2015)) was done in the cadavers so that inertia affect can be comparable between the experimental and simulation results.

Table 8-5 Longitudinal lateral impact experimental matrix for female specimens from Talantikinte *et al.* (1998)

Sr. No.	Experiment No.	Specimen No.	Age	Height (cms)	Weight (kg)	Pendulum mass (kg)	Impact velocity (m/s)	No of rib fractures	Reference
1	60	LCT02	53	164	78.00	16.00	5.93	10	Talantikinte et al. 1998))
2	61	LCT03	80	157	30.00	16.00	6.06	18	
3	66	LCT04	93	157	43.00	12.00	6.00	16	

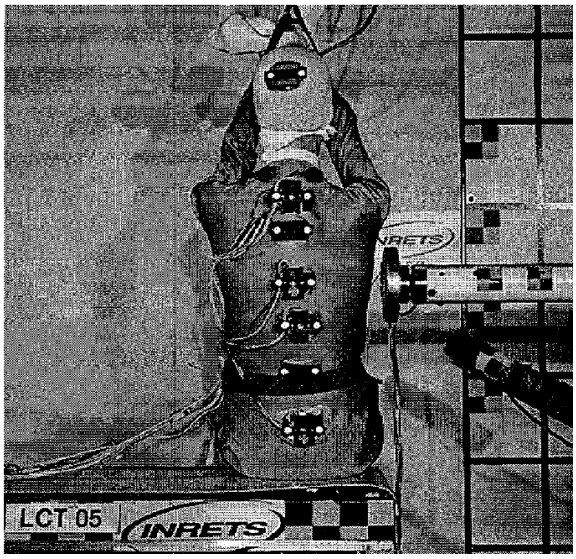

Figure 8-20 Longitudinal lateral loading experimental setup (Talantikite *et al.* (1998)) (Left) and longitudinal lateral loading simulation setup

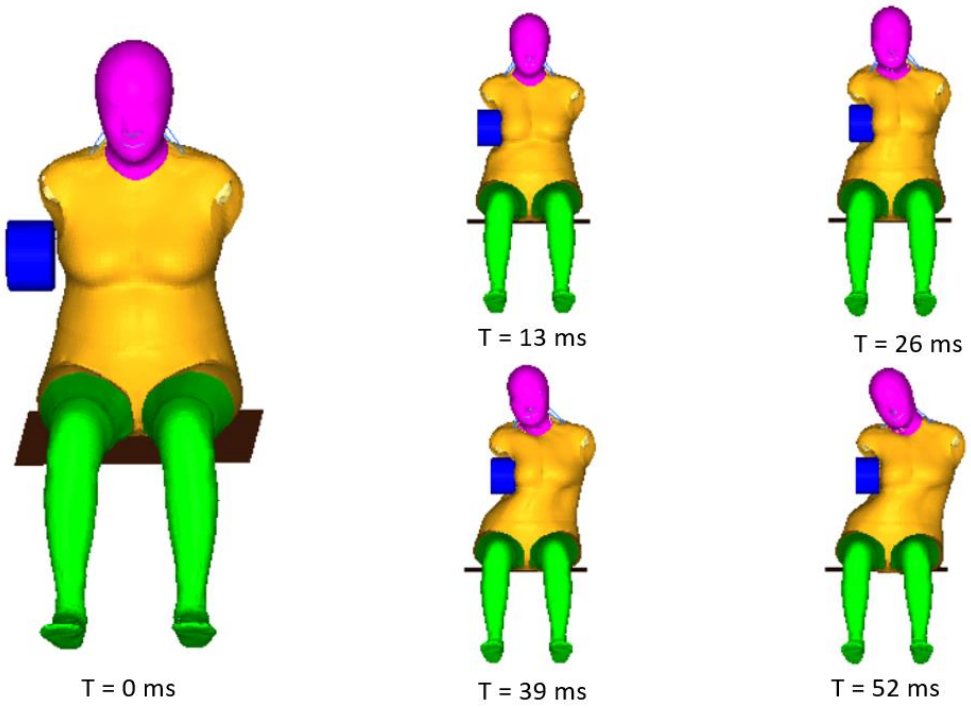

Figure 8-21 Kinematics of longitudinal lateral impact in simulations at every 13 ms

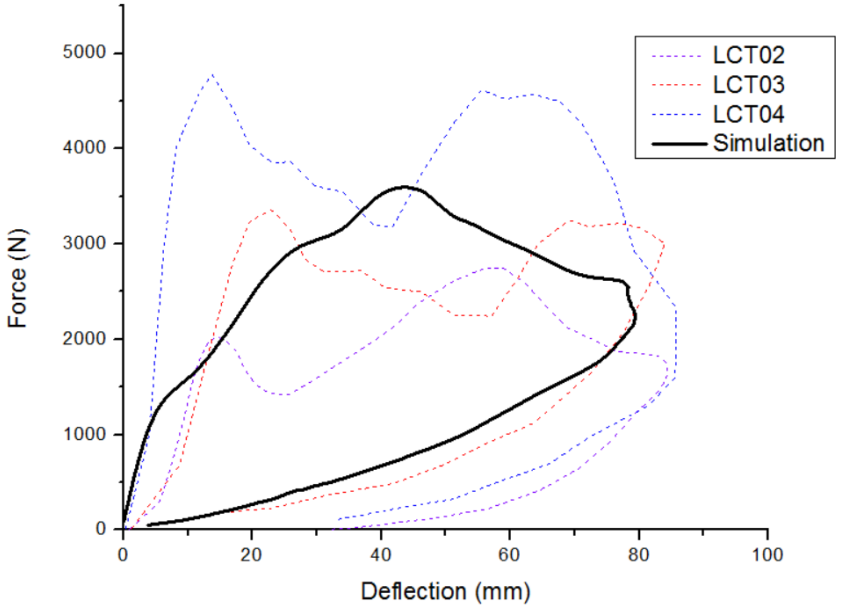

Figure 8-22 Comparison of force vs chest deflection between experiments and the simulation for lateral pendulum loading test

Along with thorax validation, it is important to validate abdomen as well as pelvic portion of the upper body part as the stiffness of these components can affect the overall response of the thoracic viscera. Therefore, additional simulations were run on abdomen as well as pelvic level so that proper stiffness characteristics can be assured for these components in upper body model.

8.5. ABDOMEN AND PELVIC IMPACT VALIDATION

Cavanaugh et al. (1986) described the stiffness characteristics of the lower abdomen by impacting rigid bar in anterior posterior direction to the cadaveric specimens. The mass of the impactor was 31.52 kg and the initial velocity of the impactor was 7.24 m/s during the tests. The experimental impact setup is shown in Figure 8-23 (Left) and the simulation setup is shown in Figure 8-23 (Right). The kinematics of 70 years old female model during simulation for abdomen impact is shown in Figure 8-24. The corresponding force and deflection characteristics of elderly female specimens were retrieved for FE model validation and compared with simulation results as shown in Figure 8-25. The model predicted result were in the experimental corridor

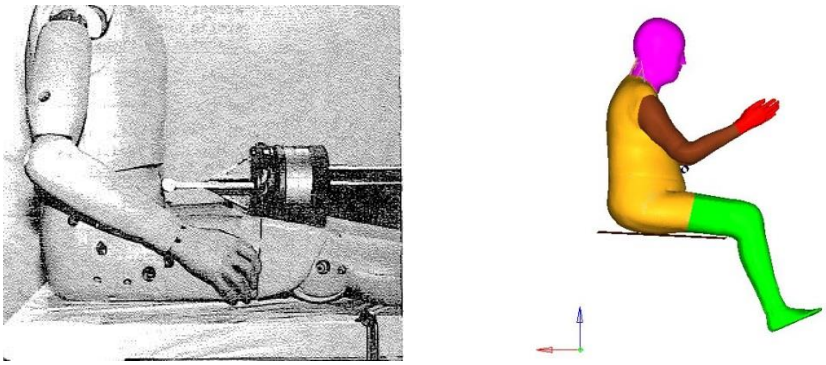

Figure 8-23 Experimental (Left) and simulation (Right) setup for abdomen rigid bar impact

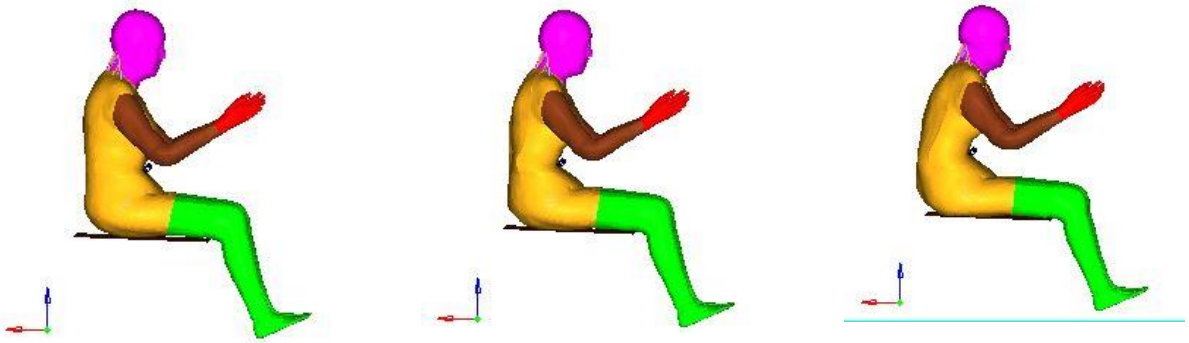

T= 10 ms T= 20 ms T= 30 ms

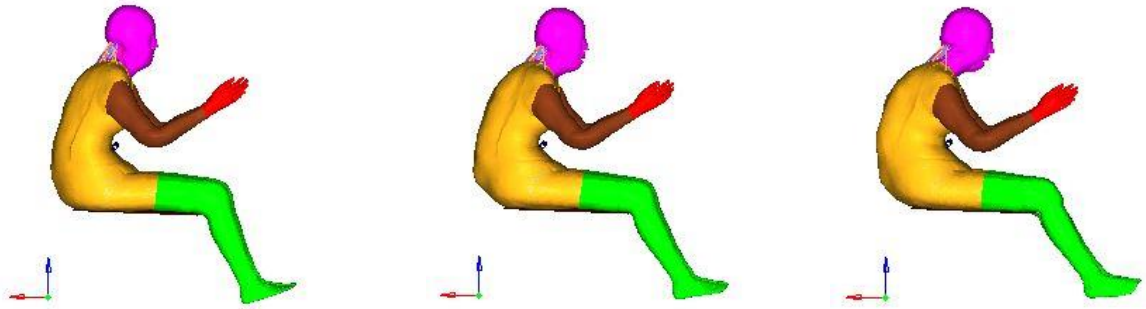

T= 40 ms T= 50 ms T= 60 ms

Figure 8-24 Kinematics of rigid bar abdomen impact in simulations at every 10 ms

Cesari et al. (1980) performed tests on cadavers to describe the pelvic tolerance in lateral impact by impacting a pendulum at iliac wing and greater trochanter level. The front end of the impactor section was of spherical profile with 20 cm diameter and the total mass of the impactor was 17.3 kg. The impactor speed was 5.83 m/s and 7.2 m/s. The experimental impact setup is shown in Figure 8-26 (Left) and the simulation setup is shown in Figure 8-27 (Right). There was only one elderly female cadaver from each speed category with similar anthropomorphic details as 70 years old female model. The kinematics of 70 years old female model during simulation for lateral pelvic impact is shown in Figure 8-28. The response was retrieved in terms of peak force from these cadaveric tests and was compared with peak simulation value as shown in Figure 8-29 as the corresponding force time histories were not available from these tests.

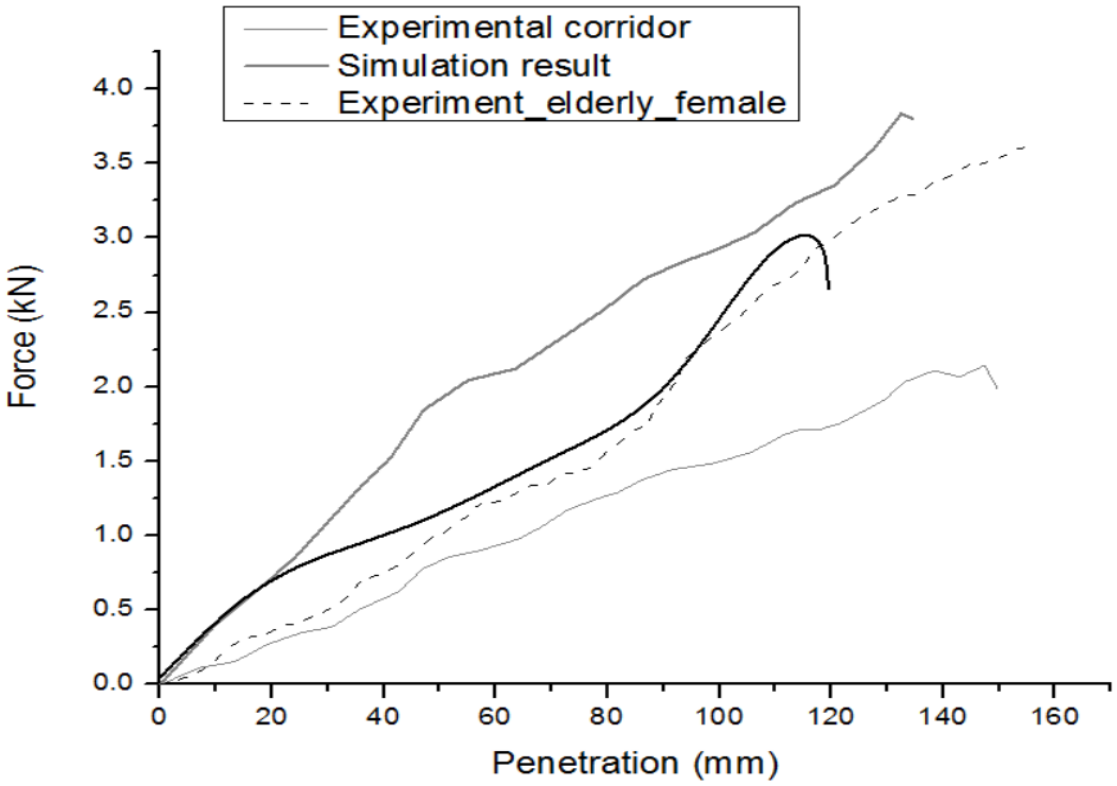

Figure 8-25 Comparison of force vs penetration between experiment and the simulation for rigid bar abdomen test

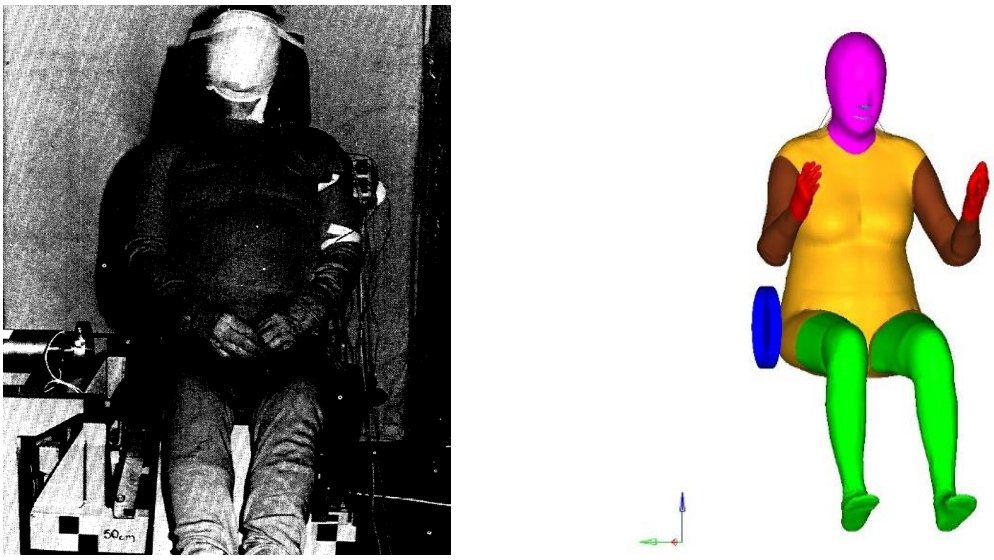

Figure 8-26 Experimental (Left) and simulation (Right) setup for pelvic lateral impact

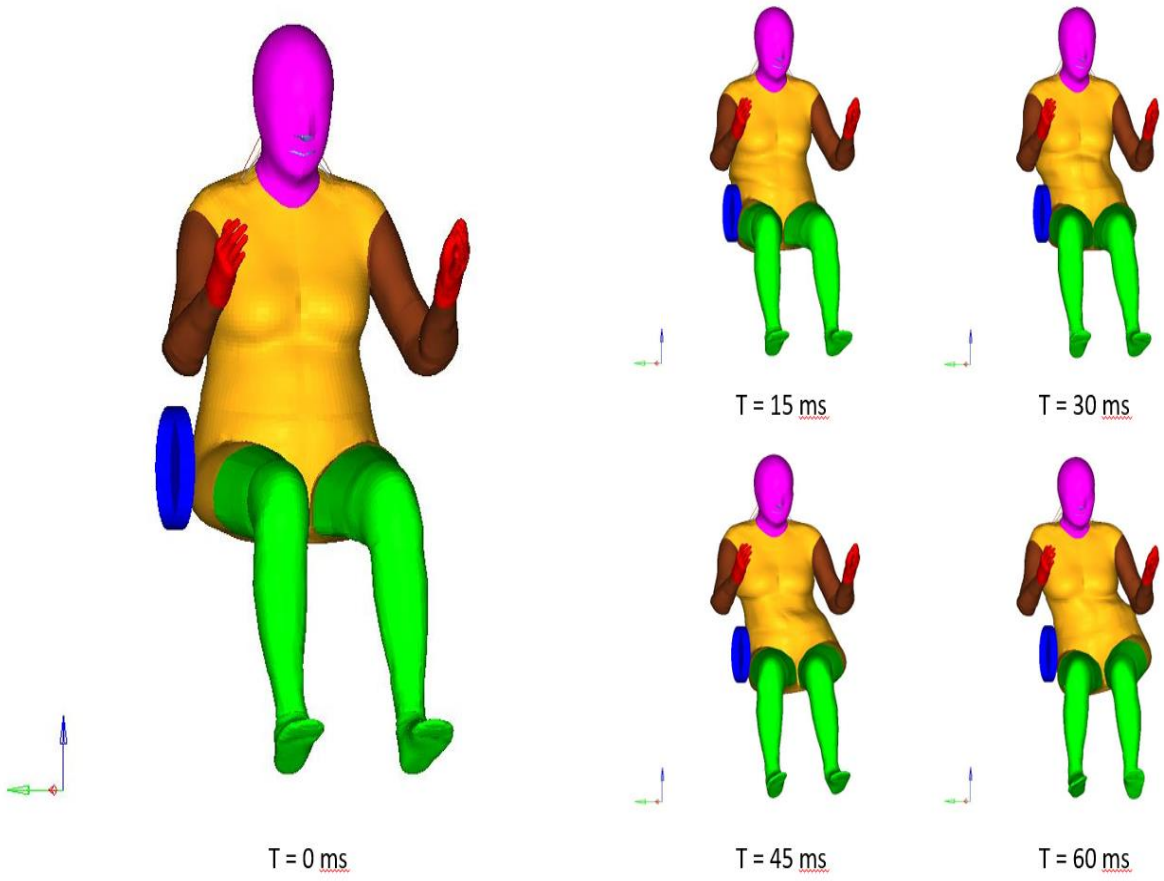

Figure 8-27 Kinematics of lateral pelvic impact in simulations at every 15 ms

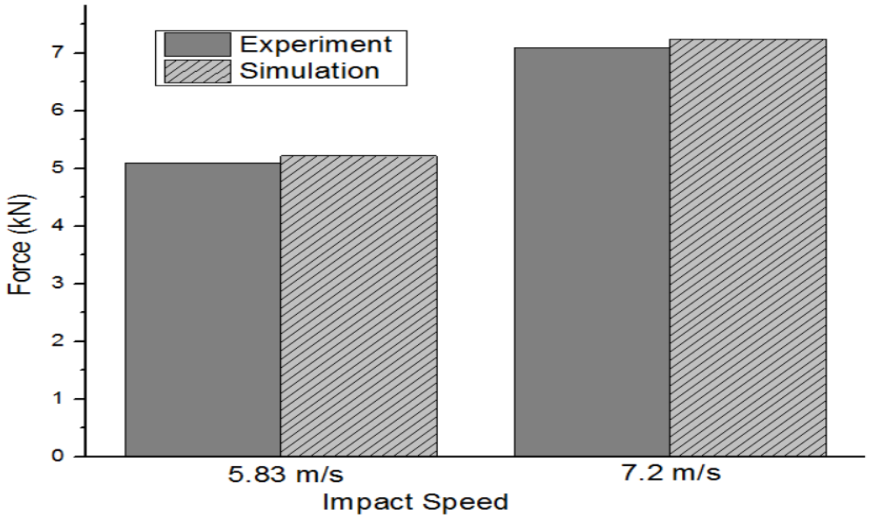

Figure 8-28 Comparison of peak force between experiment and the simulation for lateral pelvic impact

8.6. CONCLUSION

Laboratory experimental results pertaining to various configurations were used to validate the developed 70 years old female model in both frontal and lateral impact conditions. The simulations results showed that the developed model is capable of producing the responses similar to those observed in experiments. Further efforts will be made to use the model in frontal and side impact conditions in sled impacts and the responses will be compared with the available experimental data. A parametric study will also be conducted in next chapter to see the effect of prime factors such as rib angle, cortical thickness change etc. in peak force and rib fractures produced by the model.

CHAPTER 9. APPLICATION OF THE DEVELOPED FE MODEL

While talking about data obtained from real world crash incidents or laboratory experiments with cadavers, the change in material properties of thorax associated with age and gender suggests that impact response curves of the thorax should be different for elderly females compared to young males or children. This line of thinking has been supported by the studies reported by Laituri *et al.* (2005) and Kent *et al.* (2005) on PMHS (Post Mortem Human Subjects) studies. The probability curves (as shown in Figure 9-1) for thoracic injuries in belted young occupants in frontal impacts are different from those in belted elderly people. People above the age 70 have a higher risk of rib fracture than people who are 30 years of age with the same chest deflection. Although the difference between the response curve of females and males has not been shown in the study separately, it is conjectured that the response curve for female would be different from that for male on the basis of the difference in geometrical details and bone properties between the two genders. Further, the risk curve for 70 years old occupants is not realistic as zero chest deflection has a 15% risk of having rib fracture for this segment of population.

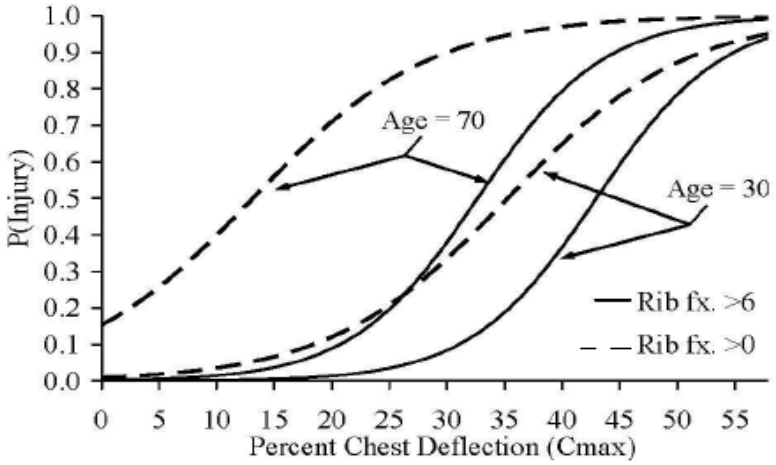

Figure 9-1 Probability of rib fracture based on percent chest deflection or response curves of PMHS specimens (Kent *et al.* (2005))

9.1. SIDE AND FRONTAL SLED SIMULATION

Once the elderly female FE model is fully developed and validated, it is used as a surrogate for crash simulations. Belt loading with pre-tensioner is one of the key factors that makes elderly female more suspicious to injuries during frontal impact because of the lower injury tolerance and more concentrated deformation of the thorax along the belt line. Various researchers have completed studies on belt loads that can be tolerable by crash victims (Yoganandan *et al.* (1993), Morgan *et al.* (1994), Kallieris *et al.* (1995), Otte (1995), Bendjellal *et al.* (1997), Foret-Bruno *et al.* (1998), Kuppa *et al.* (1998)). For an average adult male, the belt loading that can be tolerated, is concluded to be about 4-6 kN. Also, the firing time of the pre-tensioner or the magnitude of the applied load plays an important role for the safety of thorax. Airbag loading also presents a risk of thoracic injury for elderly female. Factors such as the time of ignition, the reaction time of inflator, and gas dynamic behavior also play an important role in determining the risk of crash induced injury.

Experimental data of one cadaveric test subjected to 3-point belt loading due to frontal sled impact were taken from NHTSA biomechanics database for comparison with the behaviors predicted by the developed 70 year old female model. For side impact sled testing, recently conducted tests at UMTRI (Wood *et al.* (2014)) with focus on elderly females were reconstructed to co-relate the behavior of the 70 years old female model.

9.1.1. Frontal Sled Simulation

Case ID B2895, which was conducted at Medical College of Wisconsin, was chosen from the project ‘Human surrogate test with three point seatbelt restraint and chest-bands’ funded by

NHTSA. In this test, an un-embalmed female cadaver, 67 years of age, 68 kg of weight, and 1.65 meters overall height was restrained by a three-point belt and seated in driver position of a 1986 Ford Tempo truck. The mean deceleration of the sled was reported to be approximately 6.8 g's with a pulse width of 102 ms.

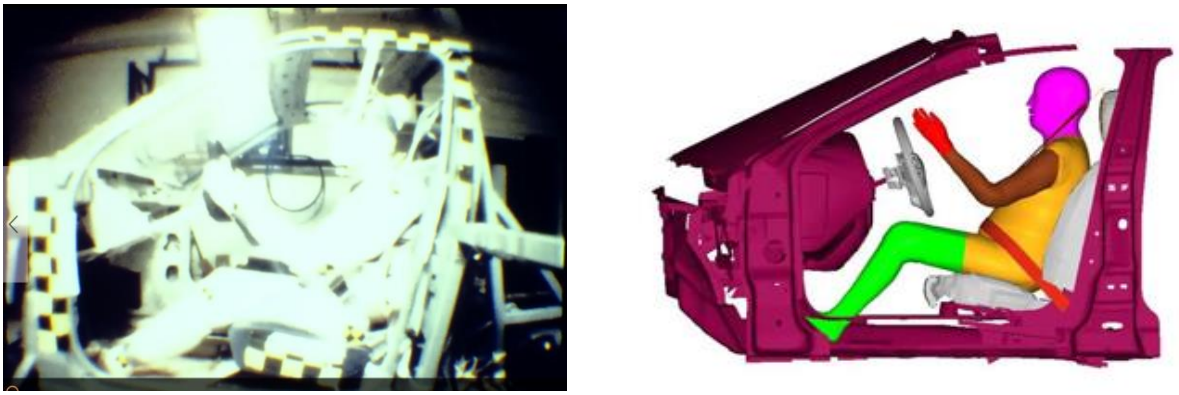

Figure 9-2 Experimental and simulation setups for frontal sled impact

The FE mesh for 1986 Ford Tempo could not be found, but FE mesh of a similar vehicle, retrieved from NHTSA website (http://www.nhtsa.gov/Research/Crashworthiness/Lsdyna_FE_Models), was scaled up as per dimensions calculated from the video markers. The 70 years old female model was positioned in that scaled FE mesh as per the measurements provided in the report. The experimental and the simulation setups for the frontal sled are shown in Figure 9-2. It should be noted that the front end of vehicle omitted in the experiment and simulation does not affect the kinematics or injury pattern of the cadaver. The same sled deceleration pulse was applied to the FE vehicle model as prescribed in the experiment. The model predicted kinematics is shown in Figure 9-3. The 70 years old female model subjected to the same sled pulse predicted similar peak shoulder and lap belt forces as measured in experiments (Figure 9-4). The simulation predicted peak shoulder and lap belt force was found to be 8.7 % and 5.5% higher than the peak experimental values, respectively. The experiment used two chest bands instrumented at T4 and T7 levels to

characterize the deformation pattern of the chest. It was not suitable to compare the corresponding results in simulation since the current model geometry was based on scans of volunteers while the cadaver used in this experiment might have different soft tissues covering the rib skeleton. Additionally, the deformation patterns measured through chest bands include the soft tissue deformations as well. Further, during the case there was 1 rib fracture reported at an anterior section of the 3rd left rib. The simulation also predicted 1 rib fracture, but it was located at a middle section of the 1st left rib as shown in Figure 9-5.

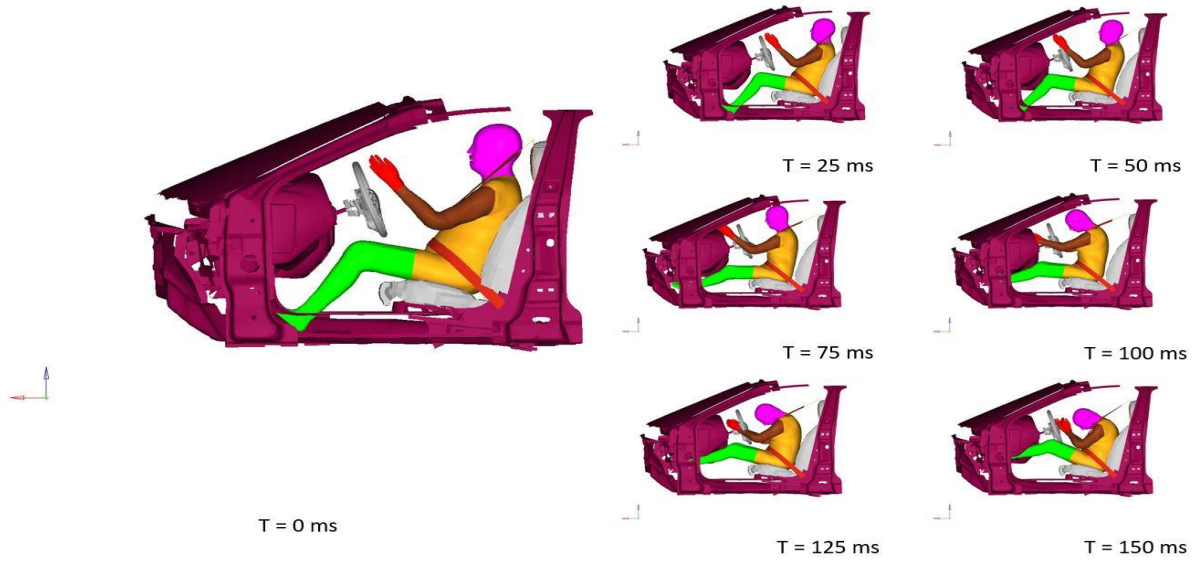

Figure 9-3 Kinematics response of frontal sled results predicted by the 70 years old female model

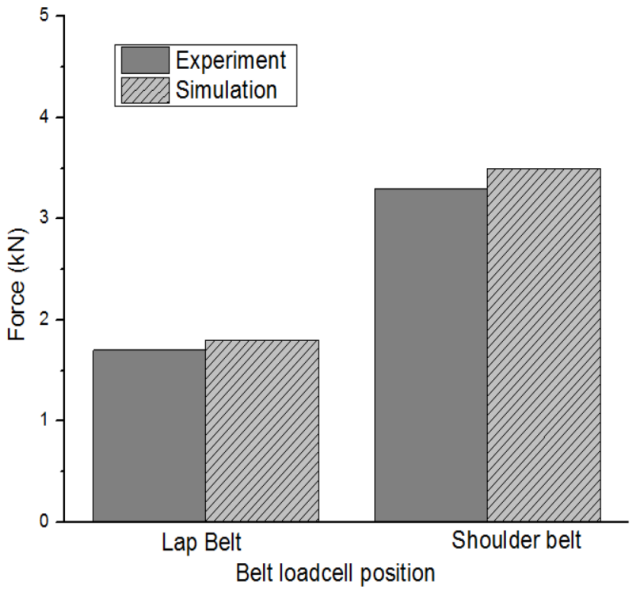

Figure 9-4 Comparison of experimentally obtained and model-predicted peak lap belt and shoulder belt forces

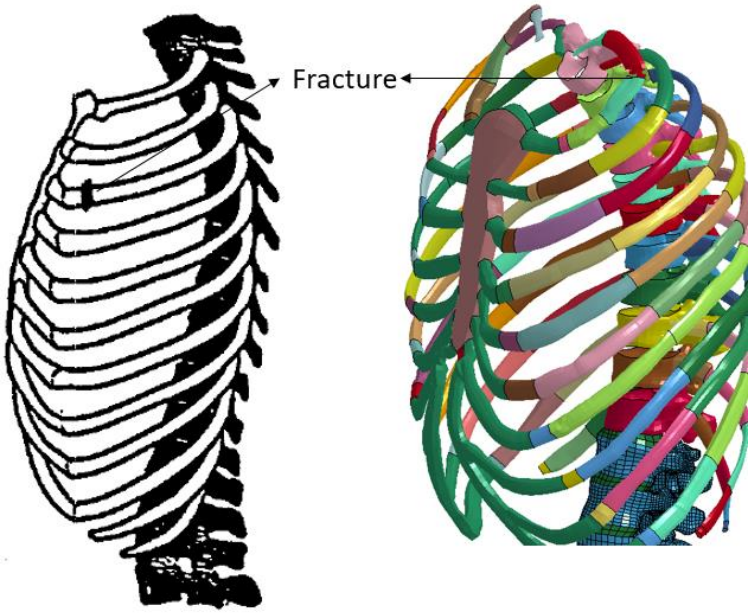

Figure 9-5 Comparison of fracture locations in experiment (left) and simulation (right)

9.1.2. Side Sled simulation

Recently, Wood *et al*. (2014) presented biomechanical responses of eight elderly (2M, 6F) cadavers in lateral impact. Full body cadavers were subjected to UMTRI's multi-segmented dual-sled impactor. The sled acceleration pulse was controlled with Hexcel structures whose deformation provided a speed of 3 m/s and 6 m/s at the time of impact. This setup can reproduce a loading condition similar to a T-bone type side impact to a nearside occupant. All cadavers were instrumented with chest bands at T7 and T10 levels, strain gauges and accelerometers at T1, T7, T10, and sacrum levels. The dual sled system consisted of a 725 kg bullet sled to which a padded segmented impact load cell wall was attached. A second target occupant sled, 360 kg in weight, on which the cadaveric specimens were seated, was impacted by the bullet sled at a preset speed. Adjustable plates attached to bullet sled were used to measure the load applied to the subject's head, shoulder, thorax, abdomen, and pelvic levels. The vertical position of the load cells can be adjusted to match the desired region of interest.

A fully validated model of UMTRI's multi-segmented bullet and target sleds was retrieved from the group through the courtesy of Dr. Jingwen Hu. The experimental setup of the dual-sled side impact apparatus is shown in Figure 9-6. In this experimental series, the PMHS was positioned with both arms pointing upwards. However, the authors did not disclose the positioning method. As such, the original arm positions used to develop the 70 years old female model were used as the pre-impact position. Further, the 70 years old female model was seated in the sled assembly as shown in the first frame of Figure 9-7. The sled was simulated for the 3 m/s velocity cases and the experimental force time histories were obtained for all six female cadavers.

The kinematics of the 70 years old female model during simulation for the lateral sled impact is shown in Figure 9-7. The corresponding force time characteristics of each specimen were retrieved for comparisons with simulation results and FE model validation as shown in Figure 9-8. Again, the mass scaling using equal stress equal velocity approach (Petitjean *et al*. (2015)) was done in the cadaveric data so that inertia affect can be comparable between the experimental and simulation results. The force-time responses predicted by the numerical simulation of the 70 years old female model lied within the corridor generated through the UMTRI experiments for elderly female cadavers. The peak thoracic impact force predicted by the model was 5% higher than that of the average experimentally obtained impact force. Some rib fractures were reported during the experiments and summarized in Table 9-1. Further, the comparison of rib fracture locations was made between the experiments and simulation as shown in Figure 9-9. The rib fracture locations and numbers were found to be similar in one of the tests with ID NBA1109A (highlighted in Table 9-1). Overall, the average numbers of rib fractures produced during the experiments were 3, while a total of 4 rib fractures were predicted by the model.

Figure 9-6 Experimental set-up for the dual-sled side impact (Woods *et al.* (2014))

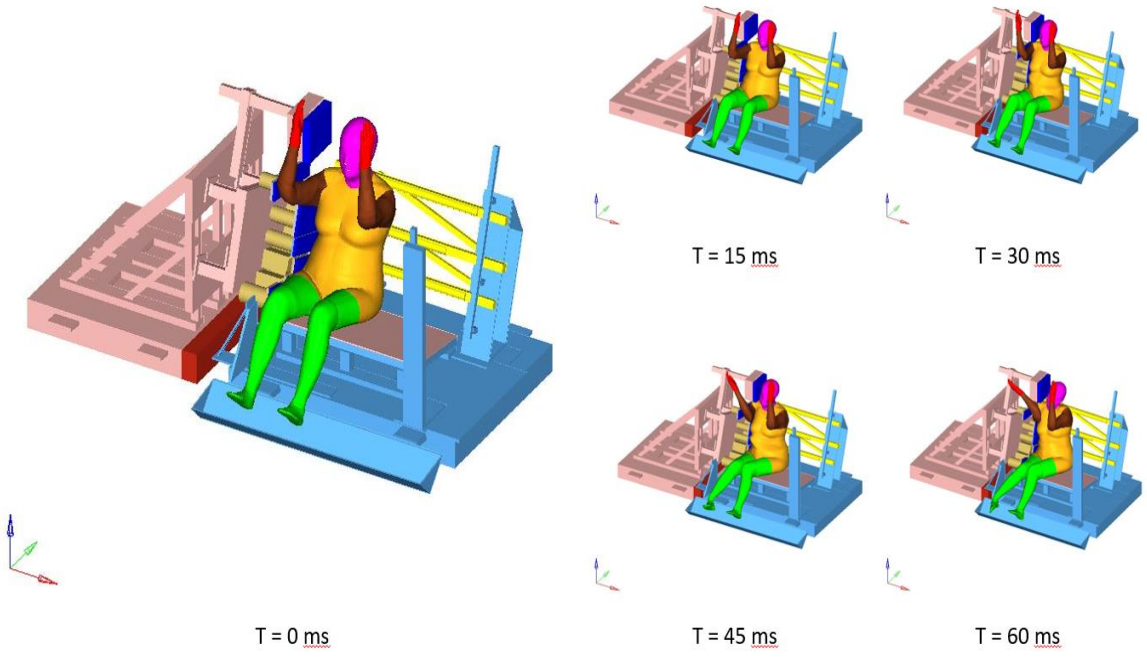

Figure 9-7 Kinematic sequences of the lateral dual-sled test simulation

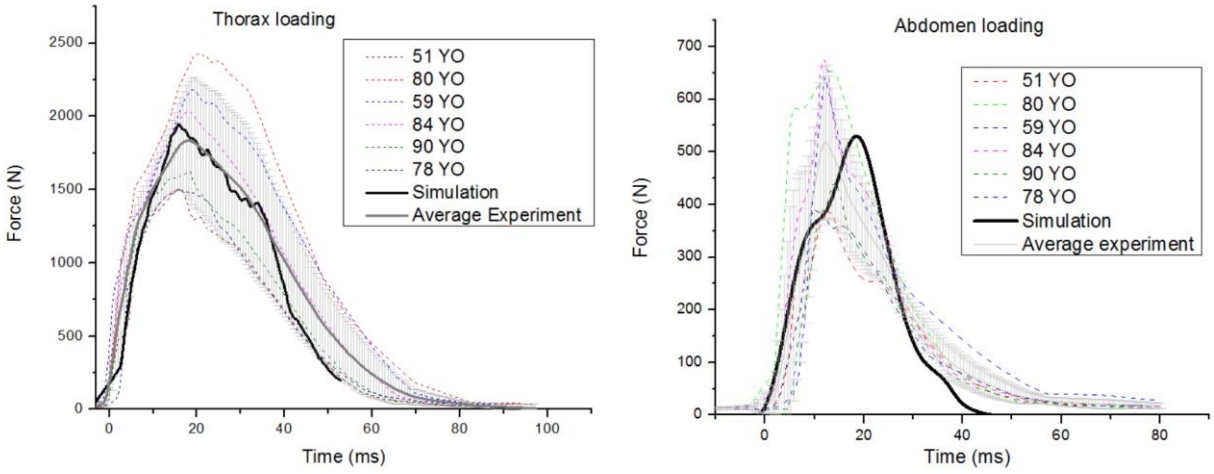

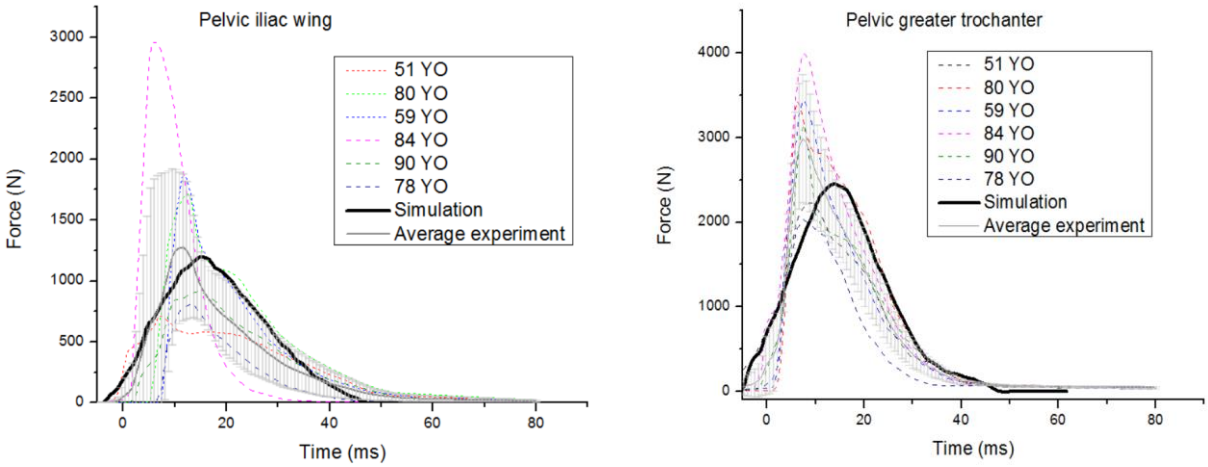

Figure 9-8 Comparison of force time histories of experimental and simulation results

Please note that the struck side in the experiment for cadaver NBA 1109A was the left side of the cadaver, while in simulation the struck side was located on the right side. Despite this fact, rib fractures were compared for the struck side only for both simulation and experiment. Overall for both frontal and side sled impacts, the 70 years old female model predictions lied in the corridors described by corresponding experiments. Further detailed investigation of different injury patterns can be explored, if needed, during such loading conditions. In the following section, this validated model is used to parametrically study the effect of structural and anatomical changes on impact responses.

Table 9-1 Rib fracture during lateral sled experiments (Reproduced from Wood *et al*. (2014))

Subject ID	Subject details	No of rib fracture	Rib levels and locations L-lateral, P-Posterior AL-Anterior-lateral
NBA1109A	Female, 51 years, 68 kg, 157 cm	4	4L, 5L, 6L , 7L
NBA1110A	Female, 80 years, 39 kg, 167 cm	1	4 L
NBA 1211	Female, 59 years, 44 kg, 163 cm	2	4L, 7L

NBA1212	Female, 84 years, 48 kg, 168 cm	3	3AL,4AL,6L
NBA 1214	Female, 90 years, 64 kg, 160 cm	3	5P, 6P, 7P
NBA1215 A	Female, 78 years, 68 kg, 160 cm	4	4L, 5L, 5AL, 6AL
Average experiments		3	-
Simulation prediction		4	4L, 5L, 6L , 7L

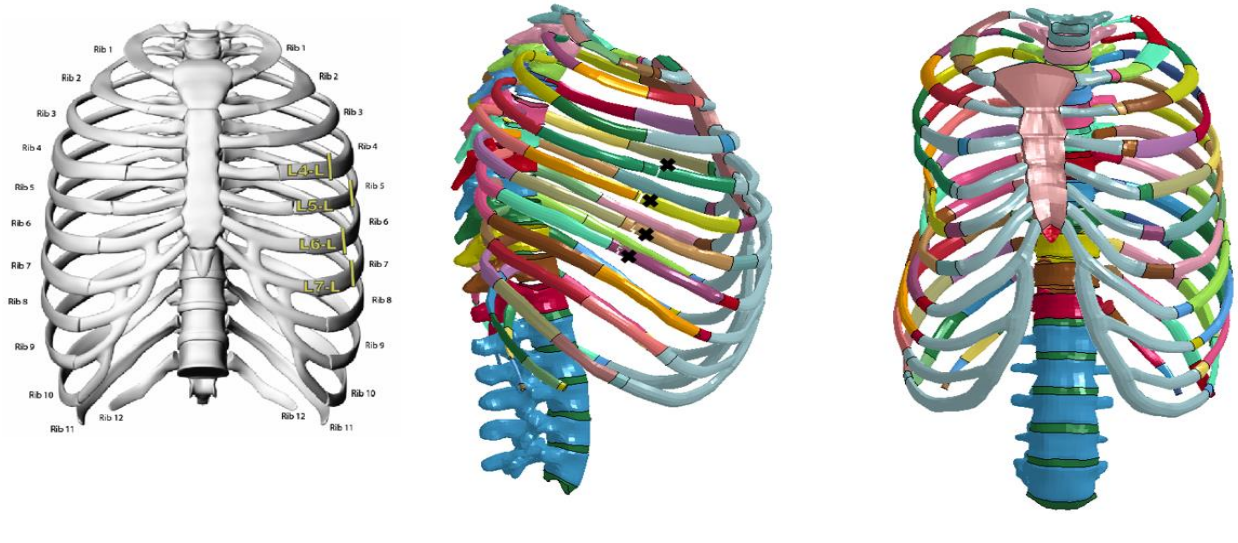

(a) (b) (c)

Figure 9-9 (a) Rib fracture locations for Cadaver ID NBA1109A (Reproduced from Wood *et al*. (2014)), (b) rib fracture locations predicted by the model (lateral view), and (c) Model-predicted deformation pattern of the ribcage for the struck side (frontal view)

9.2. PARAMETRIC STUDY TO INVESTIGATE THE EFFECTS OF STRUCTURAL AND ANATOMICAL RELATED DIFFERENCES

It is well evident from safety facts mentioned previously that the response of elderly female during similar type of crashes is quite different from that of adult male or younger females. Therefore, it is important to study the effects of various factors that contribute towards change in impact responses observed in the ribcage of the 70 years old female model. Kent *et al.*

(2005b) showed that the rib cage morphology, such as the rib angle, affects the force deflection response as well as injury tolerance.

In order to quantify the effects of morphological differences, the angle of the ribs was changed to include ±3º and ±6º deviations from the baseline model. The overall range for rib angles in females was found to be 12 degrees, based on a previous study reported by Bellemere *et al*. (2003) as shown in Table 4.1. Therefore, the overall range was selected as -6º to +6º from the current model with a 3º interval.

Two factors were selected to study the effects of structural responses, namely the material properties and thickness of the rib cortical bone. As shown in literature, the rib stiffness changed by 30% by the age of 75 (Kent *et al*. 2005b). Thus, the material properties (Young's modulus, yield stress, and tangent modulus) of the rib cortical bone were changed from -30% to +30% of the baseline model with 10% increment to determine the effect of material properties. As reported in Chapter 5, the range in the cortical bone thickness was predicted to have up to 40% of variation. Thus, the cortical thickness value was changed from -40% to +40% of the baseline model at an interval of 10%.

Also, to investigate the effect of the stiffness of the thoracic viscera and the soft tissues, the stiffness (Young's modulus and Hyper-elastic coefficients) of the tetra element filling materials as well as of the blood filled veins and arteries were changed by ±25% and ±50% of the baseline model. The range was selected based on a previous study (Yamada (1970)), as shown in Figure 8-3, where the tensile strength of the arterial tissue were changed from 1.2 MPa to 0.6 MPa.

A complete detail of all the factors and levels is shown in Table 9-2. Overall, the parametric study considered five levels of the rib angels, seven levels of rib cortical material properties, nine levels of rib cortical thickness, and five levels of thoracic viscera stiffness.

Table 9-2 Four factors with corresponding levels for parametric study

Factor Name	Minimum	Maximum	Interval	Level
Rib angle	-6°	6°	3°	5
Rib cortical mechanical properties	-30%	30%	10%	7
Rib cortical thickness	-40%	40%	10%	9
Thoracic viscera (soft tissue) properties	-50%	50%	25%	5
Total potential number of simulations				1,575

9.2.1. Methods

To change the rib angle, a point located at the posterior end of the vertebral body was assumed to be the center of rotation as shown in Figure 9-10 (a). Firstly, each rib was rotated individually about the center of rotation at its corresponding vertebral end. Since the rib bony elements changed position due to rotations, the corresponding 2-D elements connecting any two adjacent ribs became distorted (Figure 9-10 (b)). Therefore, these elements were deleted and re-meshed to ensure proper connectivity. The element mesh size was taken as the same (3 mm) for each case when re-meshing 2-D elements representing intercostal muscles. The mesh also became distorted at the rib-cartilage junction. Therefore, the 3-D elements representing the cartilage were re-meshed by keeping the sternum connecting end the same as in the baseline model (Figure 9-10 (b) right). The sternum position was consistent throughout the cases. At +6

degree rotation, the ribs protruded inside the flesh due to excessive rotation. Therefore, the inner surface of flesh solid elements was changed at those junctions where interference was found.

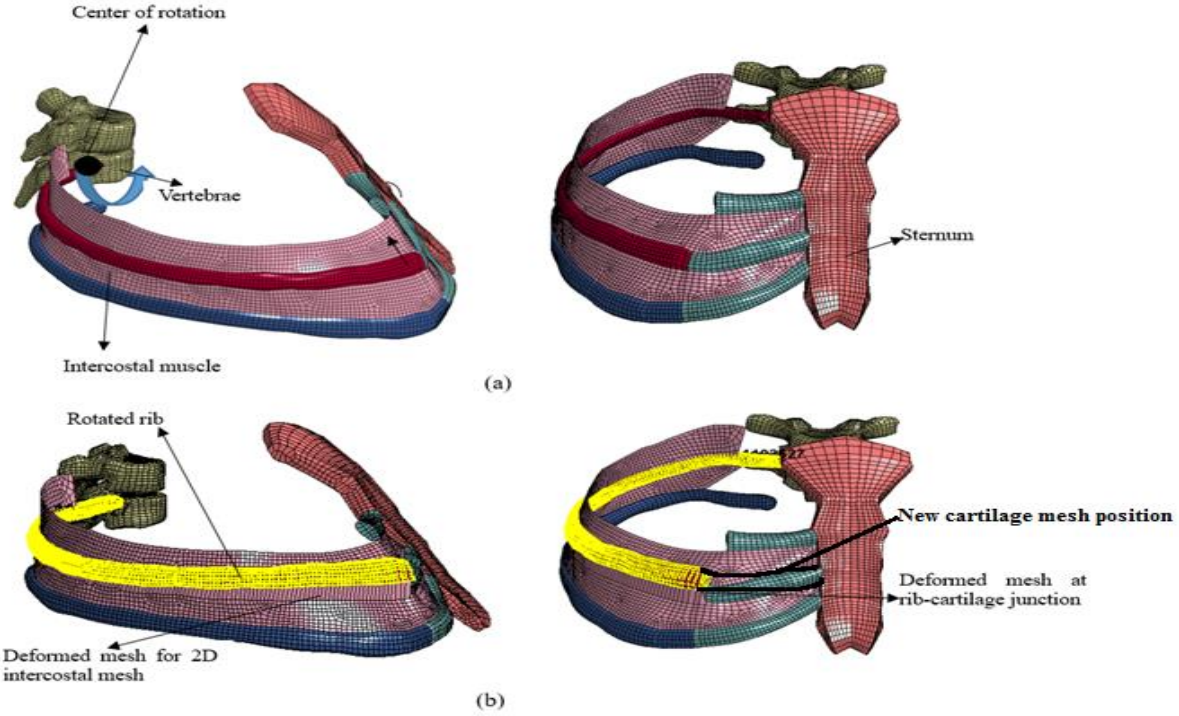

Figure 9-10 Methods for changing the rib angle and associated mesh

Aside from changing the mesh, the corresponding changes in structural parameters from the baseline model to each level were done by assigning corresponding keywords when setting up the simulations for designs of computer experiments (DOCEs). The parameter values at each level for the three factors: (a) rib cortical material properties, (b) thoracic soft tissue viscera properties , and (c) rib cortical thicknesses are shown in Table 9-3 (a), (b), and (c), respectively. Since the ribs were modeled with multiple (10) sections with different thickness throughout the length, therefore the corresponding changes were done for each thickness value.

Table 9-3 Corresponding changes in parameters from the baseline model at each interval used in DOCEs for: (a) rib cortical bone material properties, (b) rib cortical thickness (at each section), and (c) thoracic soft tissue viscera properties

(a)

Parameter	Baseline	30%	20%	10%	-10%	-20%	-30%
Elastic modulus (GPa)	9.8	12.74	11.76	10.78	8.82	7.84	6.86
Yield stress (GPa)	0.08	0.104	0.096	0.088	0.072	0.064	0.056
Tangent modulus (GPa)	1.35	1.755	1.62	1.485	1.215	1.08	0.945

(b)

	Parameter	Baseline	50%	25%	-25%	-50%
Tetra filled soft tissue Viscera	Hyper-elastic constant C1	7.20E-06	1.08E-05	9.00E-06	5.40E-06	3.60E-06
	Hyper-elastic constant C2	8.50E-06	1.28E-05	1.06E-05	6.38E-06	4.25E-06
Blood filled vessels	Elastic modulus (GPa)	0.05	7.50E-02	6.25E-02	3.75E-02	2.50E-02

(c)

Thickness		Baseline thickness	40%	30%	20%	10%	-10%	-20%	-30%	-40%
Rib cortical bone (mm)	1	0.95	1.33	1.235	1.14	1.045	0.855	0.76	0.665	0.57
	2	0.92	1.288	1.196	1.104	1.012	0.828	0.736	0.644	0.552
	3	0.68	0.952	0.884	0.816	0.748	0.612	0.544	0.476	0.408
	4	1.2	1.68	1.56	1.44	1.32	1.08	0.96	0.84	0.72
	5	1.15	1.61	1.495	1.38	1.265	1.035	0.92	0.805	0.69
	6	1.035	1.449	1.3455	1.242	1.1385	0.9315	0.828	0.7245	0.621
	7	1.175	1.645	1.5275	1.41	1.2925	1.0575	0.94	0.8225	0.705
	8	1.075	1.505	1.3975	1.29	1.1825	0.9675	0.86	0.7525	0.645
	9	0.815	1.141	1.0595	0.978	0.8965	0.7335	0.652	0.5705	0.489
	10	0.84	1.176	1.092	1.008	0.924	0.756	0.672	0.588	0.504

Since the design space for full factorial simulations is too large (1,575 simulations), a Latin Hypercube sampling method (Tille (2005)) was used to reduce the number of designs (or simulations) to 200 designs by using the software modeFrontier version 2014 (Esteco North America, Novi, MI). A uniform Latin Hypercube method is useful when a random sampling space is needed and it guarantees a relatively uniform distribution over each dimension. The sampling of designs is shown in Figure 9.11 with 3 variables, *i.e*. the rib cortical thickness (x-axis), thoracic viscera stiffness (y-axis), and rib angle (z-axis). These data points formed a design space with 200 DOCEs for further analysis. The table for all 200 DOCEs is shown in Appendix

D. After completing all DOCE simulations, the main effect analysis was run to identify the effect due to each individual independent variable. The "main effect" is the effect of one of independent variables on the dependent variables by ignoring other independent variables. The software package modeFrontier version 2014 (Esteco North America, Novi, MI) was used to study these effects and plotting main effects charts.

To study the interactions between independent variables, the problem was found to be very complex due to multi-level interactions between independent variables. Therefore, an advanced data mining approach, the Decision Tree method (Zhu *et al*. (2016), was used to study the consistent patterns and/or systematic relationships between combined independent variables and dependent variables. A decision tree is a graphical support tool which generates tree like structure to identify the relationships or interactions between variables. Using this method, a dependent variable can be predicted through linear combinations of independent variables instead of running the lengthy FE simulation. WEKA software (http://www.cs.waikato.ac.nz/ml/weka/) was used to generate such decision tree for each dependent variable to identify the interactions between independent variables.

9.2.2. Calculations

All 200 DOCE cases were set up to simulate the hub loading conditions of Kroell *et al*. (1971), as shown in Figure 8-8, using LS-DYNA version 7.1.1. Each simulation was run for 30 ms of simulation time and took approximately 8 hours of execution time (with less than 5% mass scaling) using 8 nodes with single processer on a local machine running the Windows 10 operating system. The total number of model-predicted rib fractures were taken as the output variable. Besides the total number of rib fractures, other parameters such as the peak force, peak

deflection, and total energy at peak deflection (peak energy) were also taken into consideration as dependent output variables

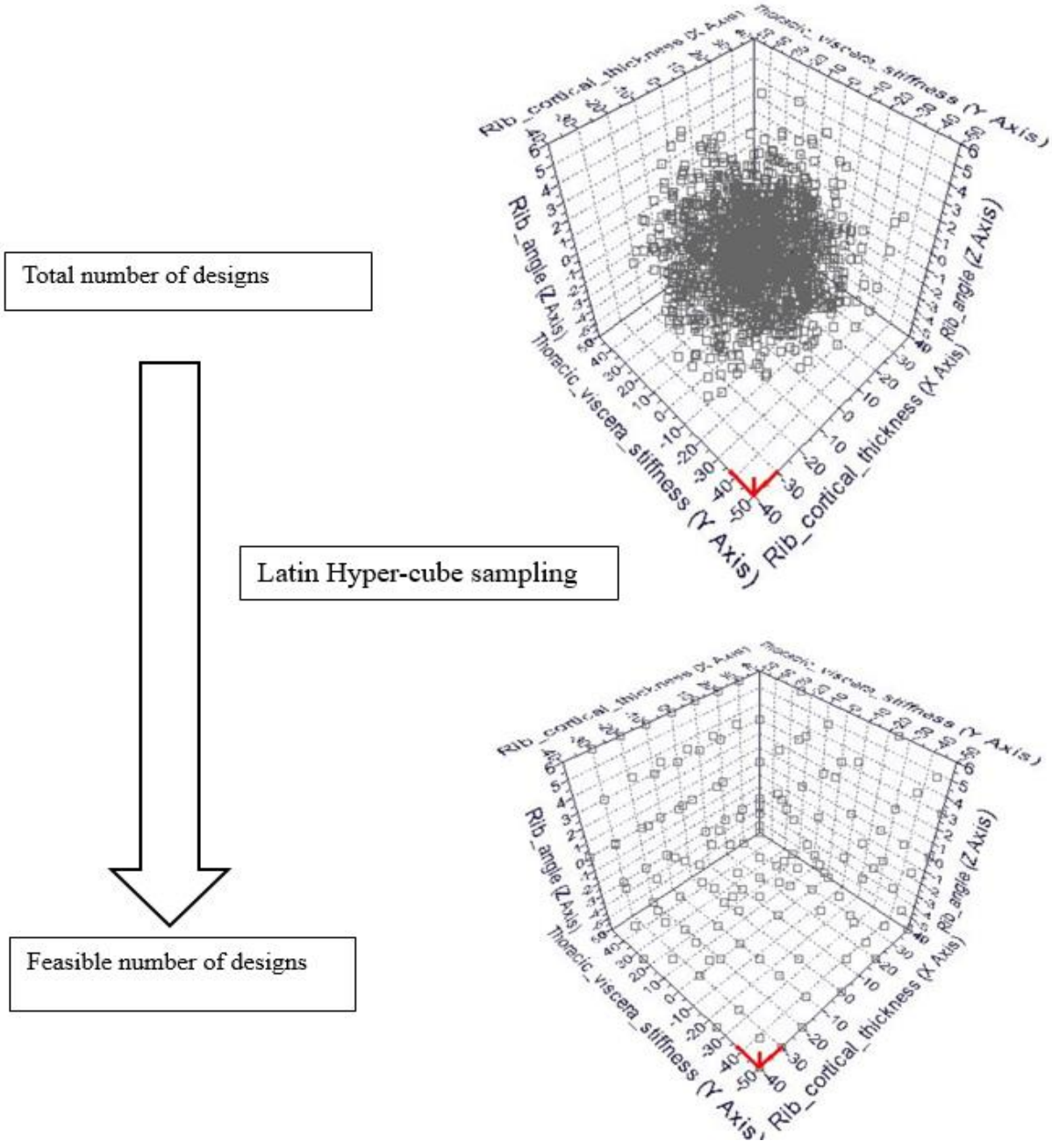

Figure 9-11 Total number of DOCEs and random sampling for designs using Latin Hypercube method for three variables: the rib cortical thickness (x-axis), thoracic viscera stiffness (y-axis), and rib angle (z-axis)

The number of fractured rib elements were calculated from the total number of cortical shell elements failed as reported in the *messag file, which was written after each simulation run, whereas the total number of rib fracture locations were determined by counting manually the number of failed element clusters from animation (d3plots). For example, in case number 35, the total number of shell elements failed were 92, but the corresponding fracture locations were counted as 8 from the animation (d3plots) as shown in Figure 9-12. The force and deflection time histories were retrieved through post processing of history files from simulation, the energy was calculated by integrating the force and deflection curves and then, the peak values were reported for analysis. The cumulative rib fractures were counted at the time step when maximum force and deflection was calculated so that consistent outputs are generated for all DOCEs. The complete set of DOCEs and the corresponding output variables achieved through simulations are summarized in Appendix D.

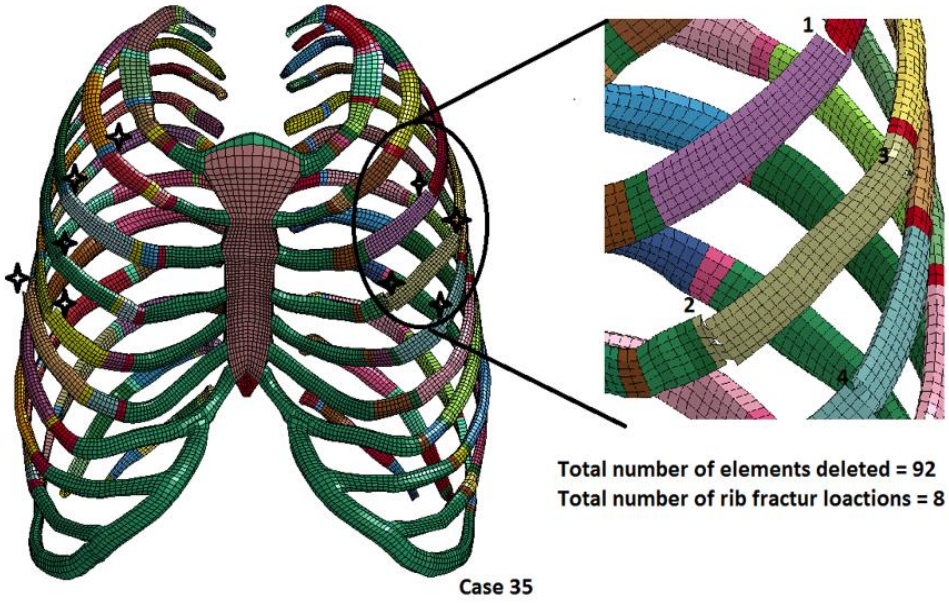

Figure 9-12 Snapshot showing the method used for counting the number of rib fracture locations for Case number 35

9.2.3. Results of Main Effect Analysis

The main effect chart also called design of experiments (DOE) main effect plot is a sequence of box-whiskers plot (shown in Figure 9-13) useful for determining the ranking list of important factors. Every experimental design is considered with all input factors set at two levels, called "high" [+] and "low" [-], respectively. The data are split into two equal-sized groups and a mean value is generated for these two groups to see if the mean is increasing or decreasing over the design change. The means for a single factor are connected by a straight line. A factor is said to be important if it leads to significant shift in the location of the response variable or if it leads to a significant change in variation going from "-" of the factor to the "+" setting of the factor (modeFrontier manual).

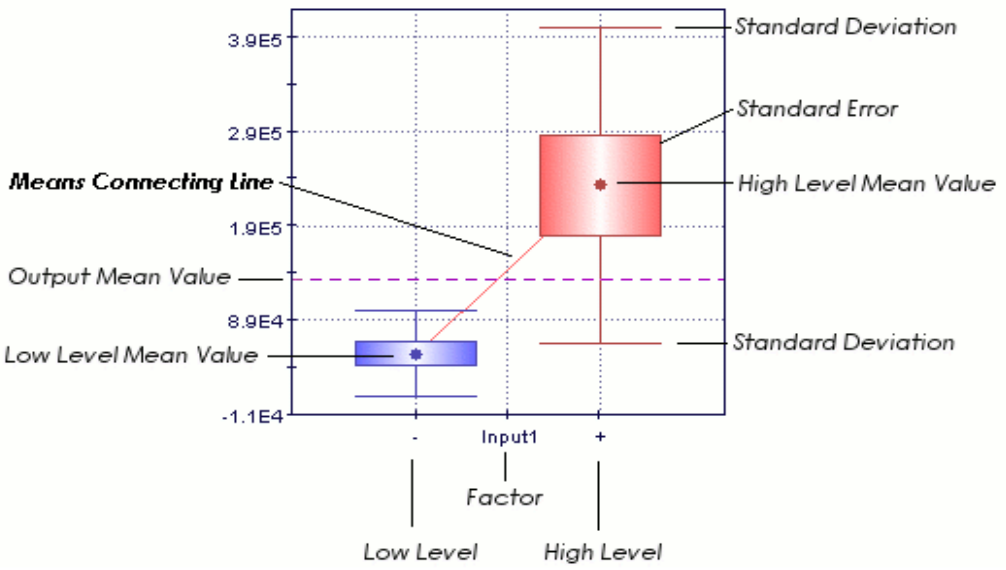

Figure 9-13 Exemplary box-whiskers plot (Reproduced from modeFrontier manual)

In Figure 9-13, the horizontal dotted line represents the overall output mean value, while the dot in the center of each box represents the mean value calculated only for the levels within that box. The box itself represents the standard error of the mean. The whiskers (the horizontal lines above and below the box) represent the standard deviation.

In this dissertation, the same idea used for DOE main effects analyses is applied for analyzing the DOCE results. The results of main effects analyses for the current set of data are shown in Figures 9-14, 15, 16, and 17 for each independent variable (Rib angle, rib cortical material properties, rib cortical thickness, and thoracic viscera stiffness). Figure 9-14 shows the main effect of the rib angle. The analysis results showed that the peak deflection was the most affected (highest slope) output variable, followed by the peak energy (higher slope), the peak force (lower slope), and number of rib fractures (lowest slope).

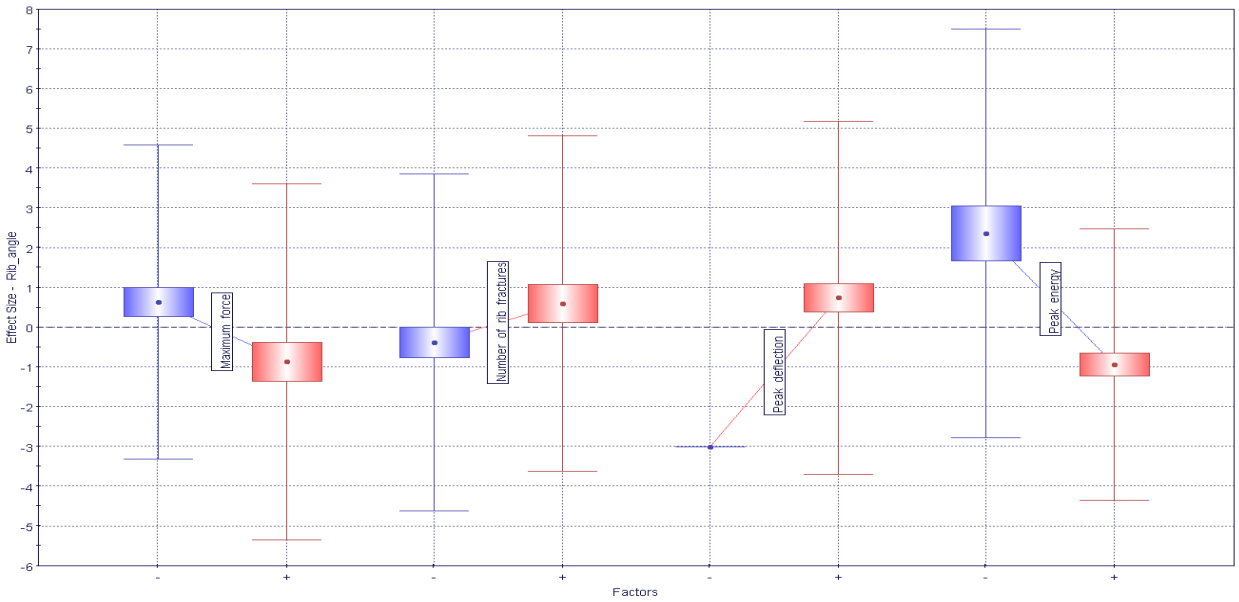

Figure 9-14 Main effect analysis of the rib angle

where maximum force, peak deflection and peak energy units are in kN, mm and J, respectively

The main effect chart of the rib cortical material properties (Figure 9-15) shows that the number of rib fractures was the most affected (highest slope) output variable, followed by the peak energy (higher slope), the maximum force (lower slope), and the peak deflection (lowest slope).

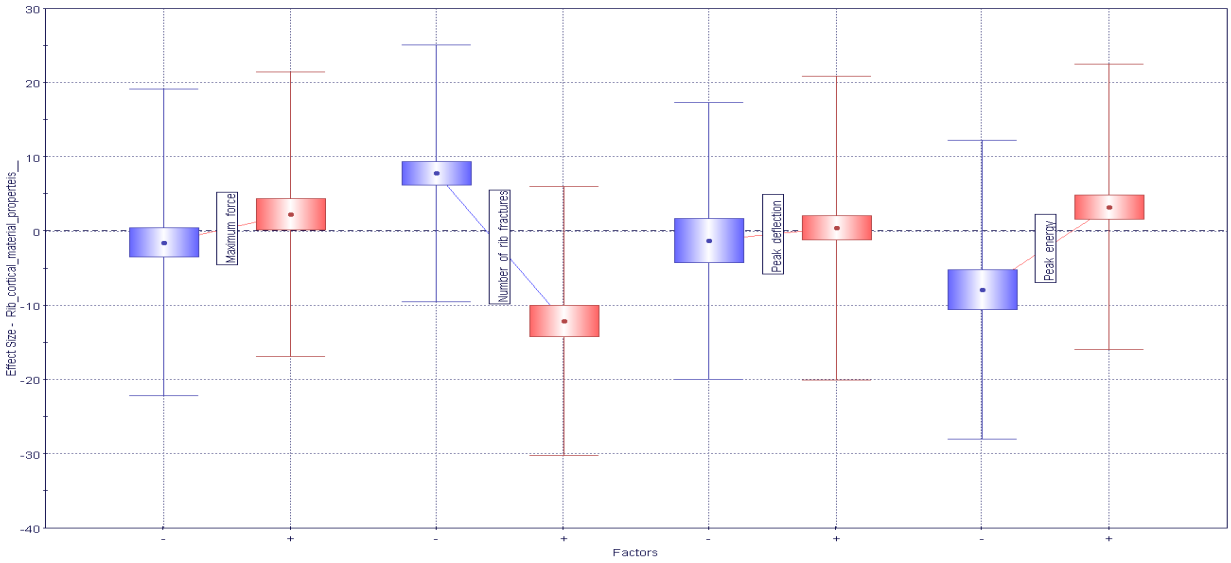

Figure 9-15 Main effect analysis of rib the cortical mechanical properties

where maximum force, peak deflection and peak energy units are in kN, mm and J, respectively

The main effect chart of the rib cortical thickness (Figure 9-16) shows that the number of rib fractures was the most affected (highest slope) output variable followed by the maximum force (higher slope), and the peak deflection (lower slope). Peak energy did not get affected by change in this parameter since the slope was almost zero for this output variable.

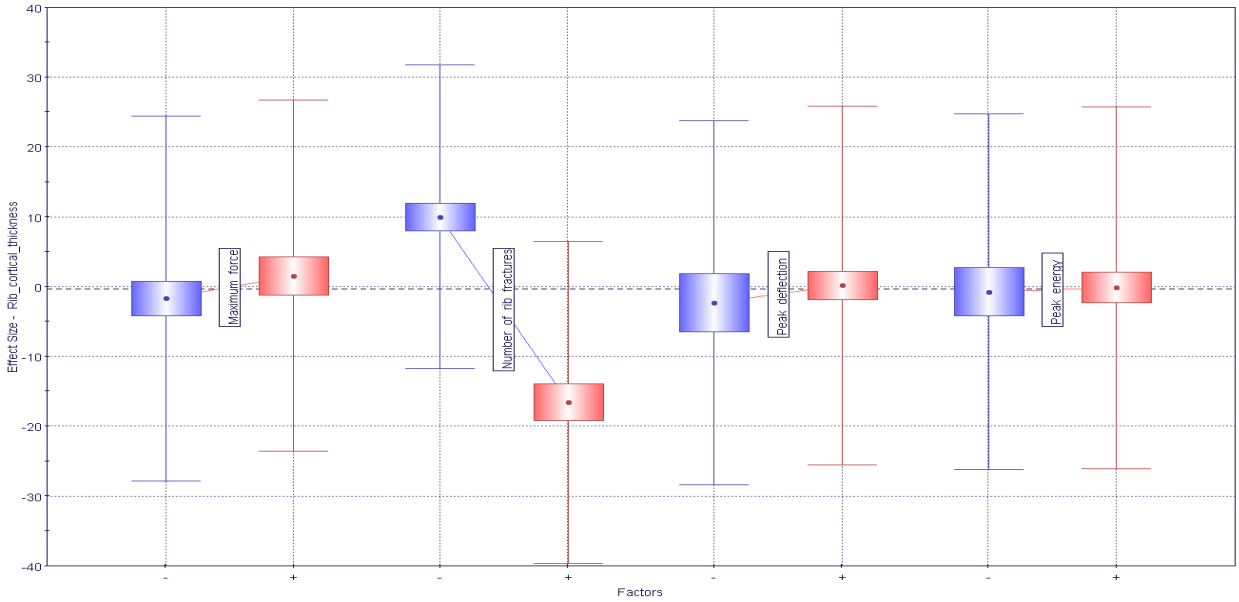

Figure 9-16 Main effect analysis of the rib cortical thickness

where maximum force, peak deflection and peak energy units are in kN, mm and J, respectively

Also, the main effect chart of thoracic viscera stiffness (Figure 9-17) shows that the peak energy was the most affected (highest slope) output variable, followed by the peak force (higher slope), and the number of rib fractures (lower slope). The peak deflection was not affected by changes in this parameter since the slope was almost zero for this output variable.

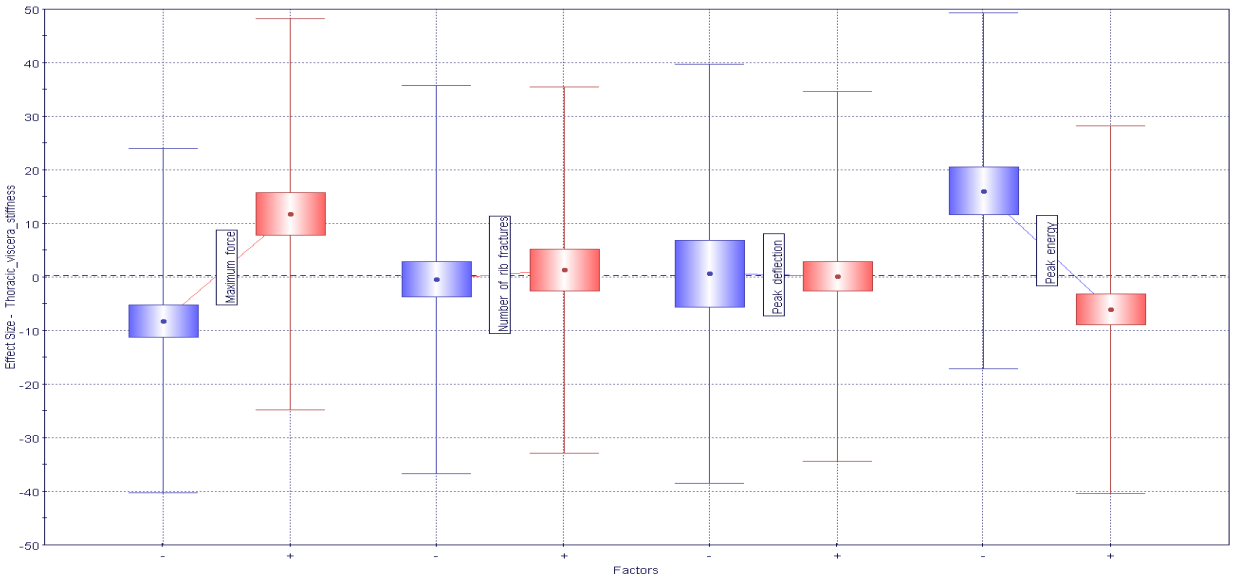

Figure 9-17 Main effect analysis of the thoracic viscera stiffness

where maximum force, peak deflection and peak energy units are in kN, mm and J, respectively

The effects due to increase of an independent variable on the polarity of the slopes of the four dependent variables are summarized in Table 9-5. A positive polarity (↑) means that a change of the factor from "-" to "+" values exhibits an increasing trend. In contrast, a negative polarity (↓) means that change of factor from "-" to "+" values exhibits a decreasing trend. Whereas the approximate symbol (≈) means that no increasing or decreasing trend could be noticed. The number of symbols represents the ranking for each dependent variable. For example, Row 1 of Table 9-5 indicates that an increase in the rib angle (↑), the most affected output variable was the peak deflection as indicated by the (↑↑↑↑) symbol. The next affected

output variable was the peak energy, which had a decreasing effect (↓↓↓). Further, the maximum force had a decreasing effect (↓↓) and lastly, the number of rib fractures had an increasing effect (↑).

Table 9-5 Results of the DOCE main effects analyses (ranking wise). The higher the number of arrows indicates a higher ranking for that factor

Parameters	Maximum force (kN)	Peak deflection (mm)	Peak Energy (Nm)	Number of rib fractures
Change in rib angle (↑)	↓↓	↑↑↑↑	↓↓↓	↑
Change in rib cortical material properties (↑)	↑↑	↑	↑↑↑	↓↓↓↓
Change in rib cortical thickness (↑)	↑↑↑	↑↑	≈	↓↓↓↓
Change in thoracic viscera stiffness (↑)	↑↑↑	≈	↓↓↓↓	↑↑

Where "↑" = increase, "↓" = decrease, and "≈" = no effect. More symbols: higher ranking

The results of the main effects analyses for the highest ranking output variable showed that the peak deflection increased with straighter ribs (increase in rib angle). With the increase in the rib stiffness (either by increasing the rib cortical mechanical properties or by increase in rib cortical thickness), the number of rib fractures decreased. With the increase in thoracic viscera stiffness, the peak energy decreased.

Further, a 3-D contours graph was plotted (Figure 9-18) to show the combined effect of changing the rib cortical thickness and rib cortical mechanical properties on the number of rib fractures. Overall, it can be seen that decreasing the rib cortical bone mechanical properties and cortical thickness together produced the highest number of rib fractures as seen in the red contours of the plot. On the contrary, increasing both independent variables produced lesser number of rib fractures. Some minor discontinuities in the contours plot were due to other contributing independent variables, such as changing the rib angle.

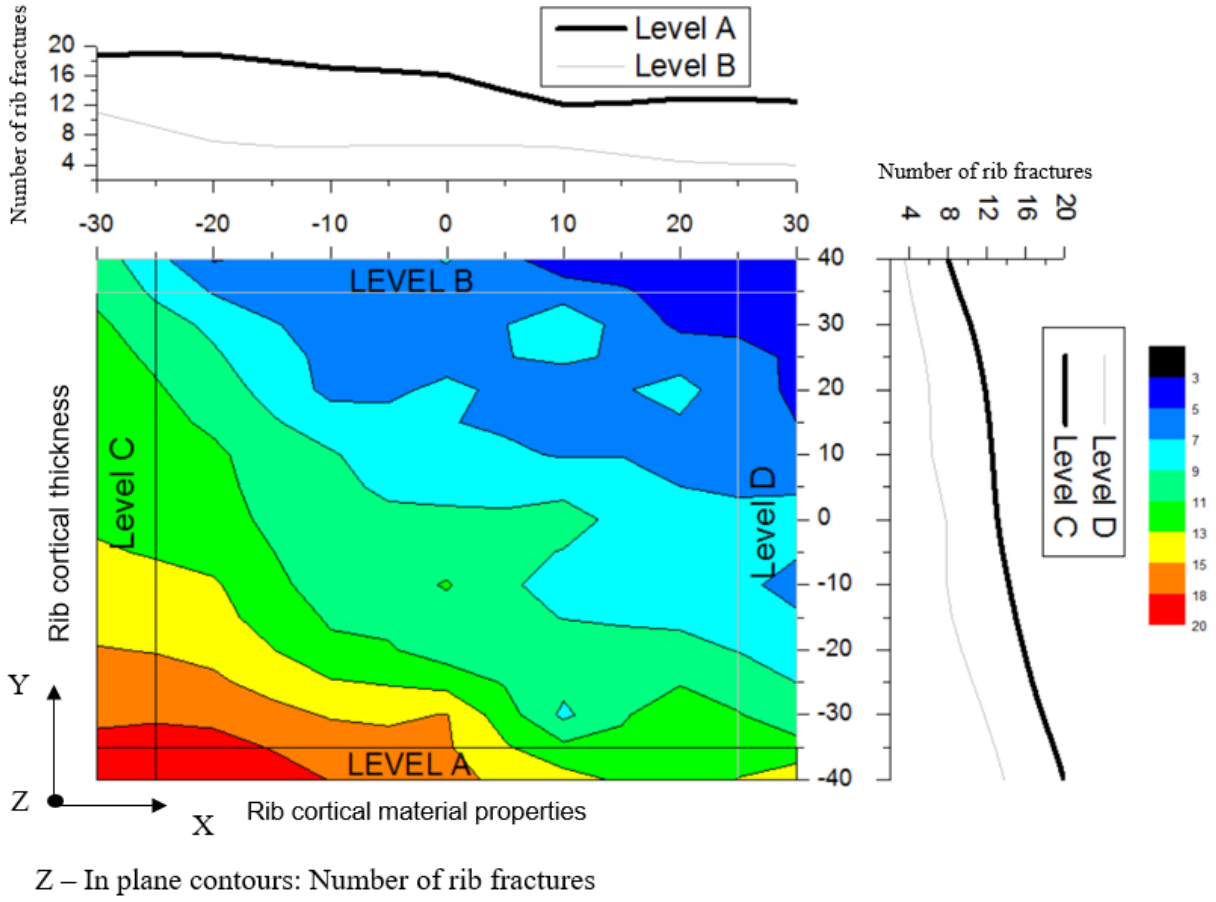

Figure 9-18 3-D contours plotting for the number of rib fractures versus changes in the rib cortical thickness and rib cortical mechanical properties

From a statistical point of view, a person who has the baseline cortical bone thickness may have rib material properties that are anywhere between ±30% of the baseline rib mechanical properties. Similarly, a person with the baseline rib angle may have a rib cortical thickness that is anywhere between ±40% of the baseline thickness. If the full factorial simulations were conducted, it may be possible to take this population, which consists of 1,575 subjects, for statistical analyses in order to understand the interactions between independent variables and dependent variables. Even so, the number of subjects may not be enough to conduct statistical analyses, because the intervals selected for each independent variable may be too large to represent the real-world population. Because calculating the full factorial with 1,575 simulations is already too much to handle, it was determined that studying such statistical interactions was beyond the scope of this dissertation.

Figure 9-18 shows that the effect of changing the rib cortical material properties on the number of model-predicted number of rib fractures depends on which level of the rib cortical thickness. This phenomenon confirms the fact that there are interactions between the independent variables. Since these interactions are found to be complicated, implicit, and hidden within the large amount of simulation dataset, advanced approaches like “data mining” (Kantardzic (2003); Han *et al.* (2006); Witten and Frank (2011) was used to further determine these interactions. Data mining approach is an analytical process designed to search consistent patterns and/or systematic relationships between variables and to extract useful information contained in big-datasets. This methodology has been widely used in many areas, such as, in business, medical science, and computer vision (Kantardzic (2003); Han *et al.* (2006); Witten and Frank (2011)). Recently, Zhu *et al*. (2015, 2016) used this approach in injury biomechanics to study the effect of structural parameters on the biomechanical response of the head.

In the current research, each dependent output variable's relationship was determined by considering the interactions between the independent variables based on decision tree method of data mining approach. Decision tree is a decision support tool that uses a tree-like graph to model decisions and their possible consequences. The logic is very similar to a set of 'if-then' decision makings in the top-down sequence. The decision tree was built based on M5P algorithm with the help of WEKA (http://www.cs.waikato.ac.nz/ml/weka/) software as shown in Figure 9-19 (a). This software is available in the public domain so that researchers can use it to analyze big datasets. In the tree, the top node is the factor which has the greatest impact on output variable. In each leaf node, a decision rule is obtained by linear regression and it describes the relationship between the output variable and independent variables.

For analyzing the output (dependent) variable maximum force (F_{max}), the rib angle was found to be the factor that has the greatest impact and served as the top node in the decision tree analysis as shown in Figure 9-19(a). The linear regression models based on decision rule is illustrated in Figure 9-19 (b).

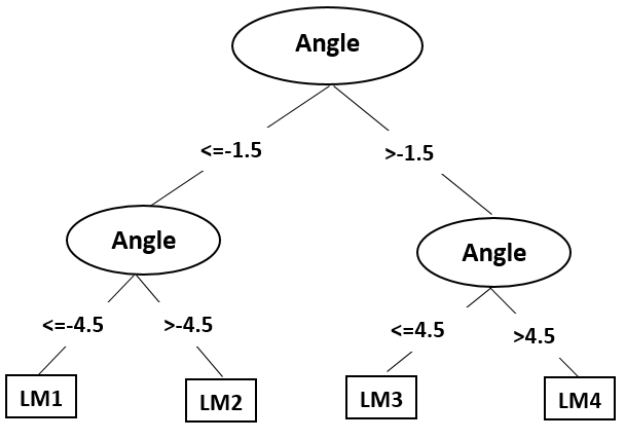

Angle <= -1.5:

| Angle <= -4.5: LM1

| Angle > -4.5: LM2

Angle > -1.5:

| Angle <=4.5: LM3

(a) (b)

Figure 9-19 (a) Decision tree for the output variable (F_{max}) (b) Model descriptions based on decision rule

In this case, if the rib angles equal to or lower than -1.5, then go to the left path. As such, the second decision is taken at the next sub-leaf. In this decision, if the angle equals to or less than -4.5, then go to the left path and a relationship LM1 is reached. Otherwise, go to the right path after the second decision. At that step, when the angle is greater than -4.5, a relationship LM2 is reached.

Back to the main leaf decision, if the angle equals to or greater than -1.5, then go to the right path and the next decision is taken in the next sub-leaf. In this decision, if the angle equals to or less than 4.5, then go to the left path and a relationship LM3 is reached. Otherwise, go to the right path. At that step, when the angle is greater than 4.5, a relationship LM4 is reached. All these relationships LM1, LM2, LM3 and LM4 are described in Eqs. [9-1a to 9-1d] based on each decision rule.

$$\text{LM1: } F_{max} = 4.9959 + 0.0216 \times \text{Angle} + 0.0003 \times \text{Mat} - 0.0002 \times \text{Thickness} + 0.0021 \times \text{Stiffness} \quad \text{Eq. [9-1a]}$$

$$\text{LM2: } F_{max} = 5.2044 + 0.0016 \times \text{Angle} + 0.0016 \times \text{Mat} - 0.0002 \times \text{Thickness} + 0.004 \times \text{Stiffness} \quad \text{Eq. [9-1b]}$$

$$\text{LM3: } F_{max} = 4.64 - 0.0498 \times \text{Angle} + 0.0042 \times \text{Stiffness} \quad \text{Eq. [9-1c]}$$

$$\text{LM4: } F_{max} = 4.7715 + 0.0055 \times \text{Angle} + 0.0016 \times \text{Mat} + 0.0013 \times \text{Thickness} + 0.0018 \times \text{Stiffness} \quad \text{Eq. [9-1d]}$$

where F_{max} = Maximum force (kN), Angle = Rib angle (degree), Mat = Rib cortical material properties (%), Thickness = Rib cortical thickness (%), and Stiffness = Thoracic viscera stiffness (%).

For analyzing the output variable peak deflection (d_{peak}), again the rib angle was found to be the factor that has the greatest impact and served as the top node in the decision tree analysis as shown in Figure 9-20(a). The associated linear regression models based on the decision rule is illustrated in Figure 9-20 (b). Two relationships LM1 and LM2 for the peak deflection are described in Eq. [9-20a-b] based on the decision rule.

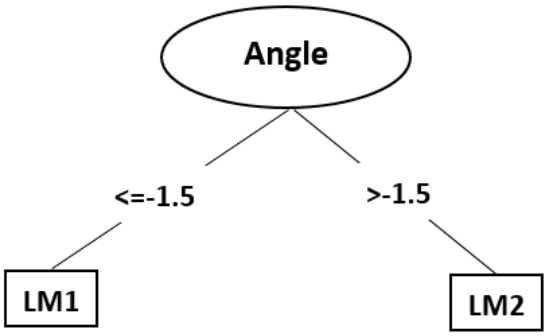

Angle <= -1.5: LM1

| Angle > -1.5: LM2

(a) (b)

Figure 9-20 (a) Decision tree for the output variable (d_{peak}) (b) Model descriptions based on decision rule

LM1: d_{peak} = 57.9947 - 5.3851× Angle - 0.0114 × Mat - 0.0222 × Thickness - 0.0754 × Stiffness

Eq. [9-2a]

LM2: d_{peak} = 88.1963 + 0.2313 × Angle - 0.0242 × Thickness - 0.0706 × Stiffness

Eq. [9-2b]

where d_{peak} = Peak deflection (mm), Angle = Rib angle (degree), Mat = Rib cortical material properties (%), Thickness = Rib cortical thickness (%), and Stiffness = Thoracic viscera stiffness (%).

For the analysis of output variable-peak energy (E_{peak}), again the rib angle was found to be the factor that has the greatest impact and served as top node in the decision tree analysis as shown in Figure 9-21(a). The linear regression models based on each decision rule is illustrated

in Figure 9-21 (b). The relationships LM1, LM2, LM3, LM4, LM5, and LM6 for the peak energy are described in Eq. [9-3a-e] based on the decision rule.

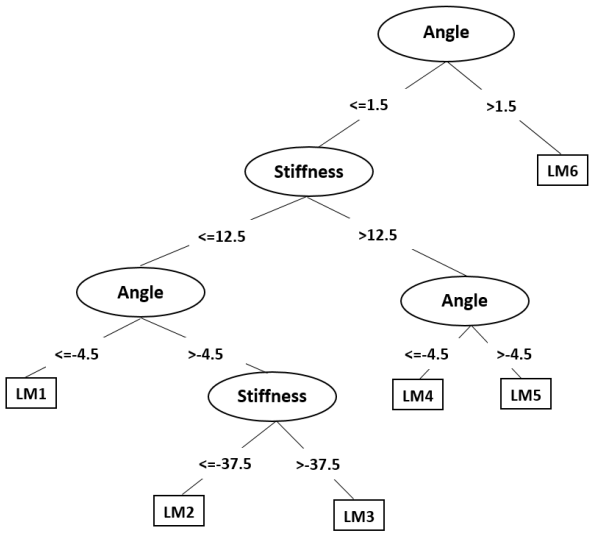


```
Angle <=1.5:
|  Stiffness <=12.5:
|  |  Angle <= -4.5: LM1
|  |  Angle > -4.5:
|  |  |  Stiffness <= -37.5: LM2
|  |  |  Stiffness > -37.5: LM3
|  Stiffness > 12.5:
|  |  Angle <= -4.5: LM4
|  |  Angle > -4.5: LM5
Angle > 1.5: LM6 (78/39.454%
```

(a) (b)

Figure 9-21 (a) Decision tree for output variable (E_{peak}) (b) Model descriptions based on decision rule

LM1: $E_{peak} = 283.67 + 0.356 \times Angle + 0.0806 \times Mat + 0.02 \times Thickness - 0.1374 \times Stiffness$

Eq. [9-3a]

LM2: $E_{peak} = 288.9 + 0.0991 \times Angle + 0.061 \times Mat + 0.029 \times Thickness - 0.0997 \times Stiffness$

Eq. [9-3b]

LM3: $E_{peak} = 286.87 + 0.154 \times Angle + 0.0814 \times Mat + 0.0508 \times Thickness - 0.104 \times Stiffness$

Eq. [9-3c]

LM4: $E_{peak} = 282.44 + 0.4398 \times Angle + 0.132 \times Mat + 0.0277 \times Thickness - 0.0401 \times Stiffness$

Eq. [9-3d]

LM5: $E_{peak} = 285.17 + 0.036 \times Angle + 0.1046 \times Mat + 0.0522 \times Thickness - 0.075 \times Stiffness$

Eq. [9-3e]

LM6: E_{peak} = 295.56 – 3.906 × Angle + 0.088 × Mat + 0.0317 × Thickness - 0.1132 × Stiffness

Eq. [9-3f]

where E_{peak} = Peak energy (Nm or J), Angle = Rib angle (degree), Mat = Rib cortical material properties (%), Thickness = Rib cortical thickness (%), and Stiffness = Thoracic viscera stiffness (%).

For the analysis of output variable-number of fracture (N), all factors have direct impact and decision tree showed just single leaf with model LM1 or in other words change in either of independent variable affected the number of rib fractures. The interactions between the independent variables could not be found, therefore no further leaves were generated by the algorithm. The relationship LM1 for number of rib fracture is described in Eq. [9-4]. A similar relationship could be achieved with the help of multi-variable regression model showing higher significance for all factors. In such a regression model, the corresponding equation is shown in Eq. [9-5] with a p value of 0.000* and an R^2 value of 0.796.

LM1: N = 10.3703 + 0.2179 × Angle - 0.1207 × Mat - 0.1233 × Thickness - 0.0112×Stiffness

Eq. [9-4]

where N = Number of rib fractures, Angle = Rib angle (degree), Mat = Rib cortical material properties (%), Thickness = Rib cortical thickness (%), and Stiffness = Thoracic viscera stiffness (%).

N (Multi-variable regression analysis) = 10.37 + 0.218 × Angle - 0.121 × Mat - 0.122 × Thickness - 0.011×Stiffness

Eq. [9-5]

The results of regression analysis showed that all independent variables had statistical significance value of 0.000* which shows that the number of rib fractures can be affected significantly by change in any of independent variables.

9.2.4. Discussion

The effect of each individual independent variable (rib cortical thickness, rib angle, rib cortical material properties, and thoracic viscera stiffness) on output parameters (maximum force, peak energy, peak deflection, and number of rib fractures) were studied through main effects analysis and were summarized in Table 9-5. Further, the effects of interactions between independent variables were studied with the help of data mining approach using the decision tree method. These interactions are equally important to understand the effects of changing the rib morphology and hard/soft tissue stiffness.

For example, Kent *et al.* (2005 b) showed that elderly people tends to have straighter rib angle than younger one. From the main effect analysis due to changing the rib angle (Figure 9-14), it can be judged that a larger rib angle (or straighter ribs) would have a higher peak thoracic deflection (d_{peak}), but the peak energy and maximum force will be lower. Aside from age associated changes in the rib angle, the cortical thickness and material properties of ribs also change with age (Chapter 5). Therefore, all attributes (the rib angle, cortical thickness, rib cortical mechanical properties, and thoracic viscera stiffness) are needed to predict d_{peak} in elderly. Hence, to correctly predict d_{peak} due to hub loading, the decision tree shown in Figure 9-19 and Eq. [9-2a and 9-2b] should be followed.

Further, from the decision tree studies for each dependent variable, the rib angle was found to be the main leaf in all interactions. These results suggest that the rib angle is the prime influencing factor in determining the impact responses of thorax. Also, the number of rib

fractures was affected by all independent variables. A single model (LM1: N) Eq. [9-4a] for predicting the number of rib fractures suggests that the interactions between the four independent variables cannot be characterized based on decision making algorithms. The effect of each independent variable should be considered to model the number of rib fractures using the decision tree method.

The study also showed that the changes in soft tissue stiffness (thoracic blood filled vessels and other soft tissue fillings) affected the model responses. Therefore, it is important to include age and gender dependent property of these soft tissues in the representative FE models. In the current study, thoracic properties were taken directly from GHBMC model as age and gender dependent properties of these soft tissues were not available in literature. Further, the outer flesh and fat properties were adjusted to match the overall response of the model against cadaveric experimental results. This can be considered as one of the limitations of the current study. Further research should be conducted to characterize the behavior of soft tissues (fat, aortic veins, other blood filled vessels, *etc*.) for different age and gender. This will further help in determining the stiffness values of these tissues which can be further incorporated in the next generation of FE model representing different segment of population, especially elderly and obese occupants.

To check the performance of models developed through the decision trees approach, scattered cross plots were made for the decision tree model predicted and FE model simulated response output variable values for each dependent variable as shown in Figures 9-22 (a-d). Assuming that the FE model-predicted responses are accurate results, a decision tree model-based response located on the diagonal (45°) line indicates an accurate prediction. It can be seen from Figure 9-22 (a) and (b) that the maximum force and peak deflection were well predicted by

the decision tree models as there are no outliars and most of the data is scattered closely around the diagonal line. For peak energy (Figure 9-22(c)), there were some predictions (hightlighted with circles in the figure) which were away from the diagonal line.

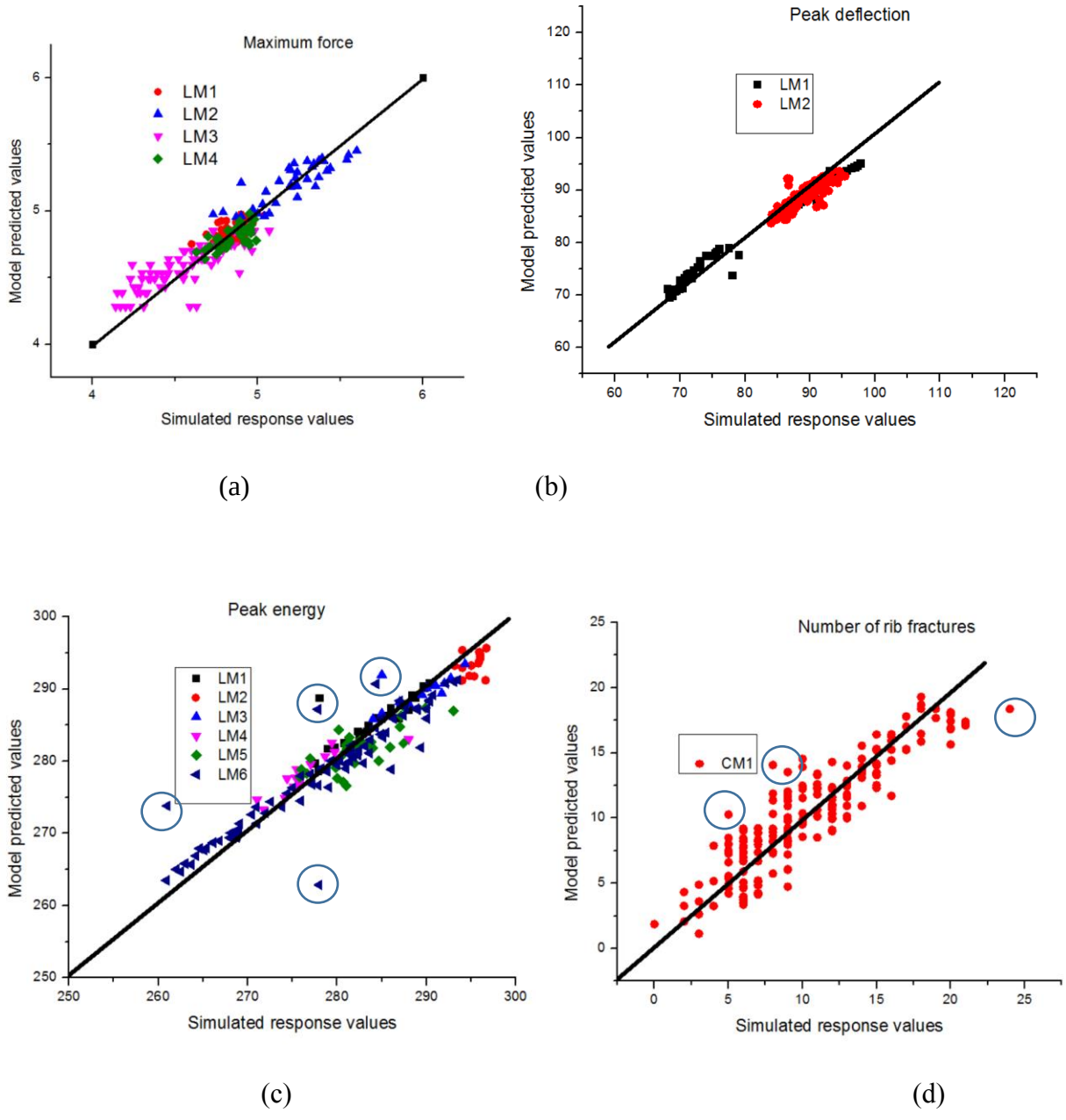

Figure 9-22 Comparison of the FE model-predicted and decision tree modelpredicted ouput response variables. Data poitns in circles were cases could be considered outliers.

The numbers of data point with such reponses are minimal and can be considered as outliars of the decision tree model. Also, the number of rib fractures were marginally predicted by the decision tree model. Since the interactions between the independent variables could not be found through decision tree approach, therefore a single model similar to linear regression analysis was predicted. Due to lack of decision making approach, the decision tree model-predicted responses were not very close to the diagonal line.

9.3. CHAPTER CONCLUSION

The developed 70 years old FE female model was used as a numerical surrogate to simulate frontal and side sled loading conditions and the model correlated well with the experimental results. The developed FE model has the capabilities of simulating rib fractures as well as soft tissue injuries sustained by that vulnerable segment of population in car crash loading conditions. A series of parametric studies was done with the help of 200 DOCEs selected by Latin Hypercube algorithm to determine the effect of changing the rib angle, rib cortical thickness values, rib cortical mechanical properties, and thoracic viscera stiffness on the maximum force, peak deflection, energy to peak deflection, and number of rib fractures for hub loading conditions. DOCE main effects analyses were conducted to identify the effect of each independent variable on the output responses. Further, decision tree analyses using data mining approach were conducted to model each output response to determine the interactions between independent variables based on conditional logics. Information provided with single parameter can be misleading until the interactions of other parameters are considered. The model developed through the decision tree approach can be used to predict the output response variables for the known independent variables. This will provide a direct information rather than running the FE simulation which takes a very long time. The parametric study also suggests that a change in

thoracic viscera stiffness also affects the model response and should be considered as an important attribute to develop a population specific FE model.

The current study has several limitations. The results are interpreted for a hub loading condition which mimics mainly steering wheel loading condition experienced by occupants in frontal car crash scenarios. The peak biomechanical responses as well as their interactions might be different for other loading conditions, such as belt loading and airbag loading. Further, the study limited the number of simulations to 200, from a complete factorial design of 1,575 simulations. Although a validated Latin hypercube algorithm was used to sample the dataset for 200 simulations to represent the complete factorial design, still some information might have been lost due to insufficient sampling. Further, the conclusion made for elderly female population may not be accurate, because the breast tissues and outer soft tissue layers covering the bony structure were treated as homogenous structure.

CHAPTER 10. CONCLUSIONS

The injury incidents and patterns encountered in real-world crashes led us to conclude that there was a strong need for the development of an elderly female FE model as the geometric and anthropomorphic details, the seating posture while driving, the structural and the mechanical changes in the properties of bone, and different injury response curves in the same type of crashes for the elderly female are far different from that of younger females or males. Current study fulfilled that need by developing a partially validated FE model of a 70 years old female. Since thoracic injuries were found to be the prime concern in automobile crashes involving elderly people, special attention was given during the development of this detailed torso model in the current dissertation.

The upper body model of a 70 years old female model was developed with the average anthropomorphic details for that sector of population. Ribs, the prime load bearing element of the ribcage, were modeled with the average morphological details like rib angle, width, and depth of the ribcage. As seen in Section 5-3, the age, gender, height, and weight related differences in biomechanical characteristics of rib bones were analyzed with isolated rib bending tests done on 278 samples taken from 82 cadavers. Significant differences were found based on age and gender for the maximum bending moment, the slope of the moment-angle curve, and the average cortical thickness of the ribs based on statistical analysis. The generalized estimated equations (GEEs) were derived for predicting biomechanical responses due to bending and cortical thicknesses of ribs in humans with known age, gender, height, and weight.

These biomechanical responses and thickness related differences were incorporated into the developed upper torso FE model of the 70 years old female FE model. The reverse engineering method was used to calibrate the rib cortical bone material model parameters to fit

the biomechanical responses predicted through GEE statistical model for 70 years old female with the help of FE simulations. The rib cortical thickness was assigned for different sections of ribs along the length based on statistical predictions identified in this study as well as based on another supporting study (Direct communication from Dr. Weaver, Virginia Tech University). Further, the biomechanical responses of isolated whole rib were validated against data available in literature (see Section 7-3) for this segment of population.

The developed torso model was validated against various loading conditions (frontal hub impact loading, lateral pendulum impact loading, seatbelt loadings of different configurations, *etc*.) that mimic physical insults as experienced by occupants in car crashes (Figure 10-1). Figure 10-1 shows the injury prediction capabilities of the model for rib fractures and soft tissue injury. The model was found to be suitable for predicting reasonably accurate number of rib fractures in frontal and side sled loading conditions during numerical simulation when compared with experiments done on elderly female cadavers. The injury mechanism and rib impact responses of the elderly female thorax can be identified using the detailed FE model developed in this dissertation. It is believed that this FE model can be used to help automobile safety engineers in the development of safer cars for this vulnerable group of the population.

Further, a series of parametric studies was conducted with the help of 200 DOCEs to determine the effect of changing the rib cortical thickness, rib angle, rib cortical material properties, and thoracic viscera stiffness on FE model-predicted biomechanical responses. DOCE main effects analyses as well as decision tree analyses based on data mining approach were conducted to study the effect of changes in each independent parameter and their interactions on output variables. It was found that it is important to model the interactions between independent variables to characterize the responses of thoracic stiffness of different set of populations. The

models obtained through decision tree approach can be used to predict the output biomechanical responses and number of rib fractures much quicker than an FF model due to changing values of the four independent parameters. For examples, the decision tree model can predict the risk of rib fractures due to change in bone condition, such as bone loss due to osteoporosis or other conditions.

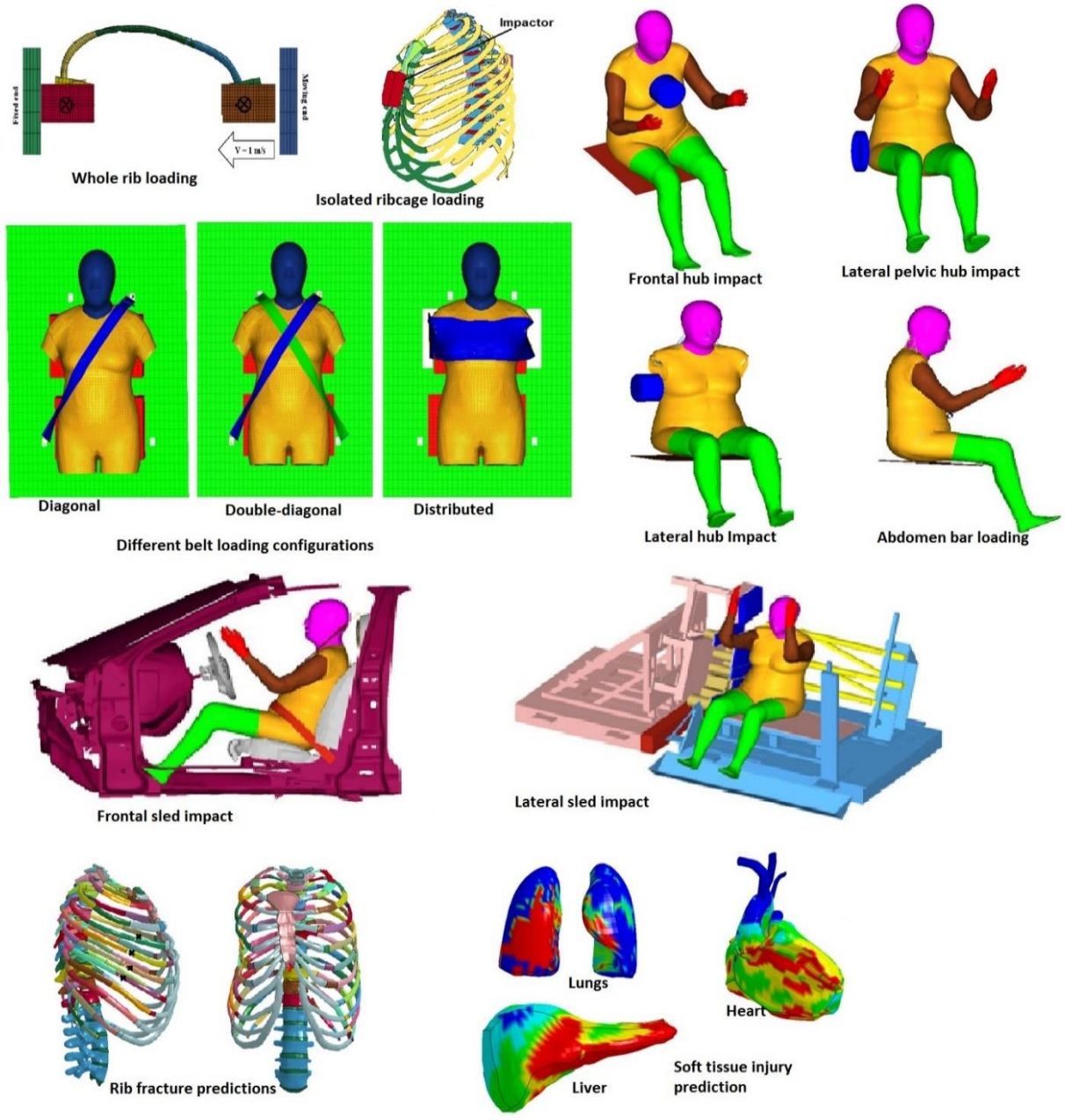

Figure 10-1 Different validated loading conditions and injury predictions

There are other potential applications of the developed FE model. It can be used to help engineer who designs subject-specific protection devices and implants. Also, the model can be used to study the ergonomics of the elderly subjects in different working conditions, such as changing the spine angle. One of the biggest injury sustained by elderly females is hip fracture, which frequently happens during fall. The model can be used to study the mechanism of such injury, since it has been validated against pelvic loading conditions and has the capability of predicting bony fractures as well.

Thus, the developed model can potentially be used to study impact responses and risks of injury for elderly females in different car crash scenarios, to benefit people designing subject-specific protection devices, to study ergonomics aspects for aging, to predict the probability of fractures due to different bone loss percentage, to guide surgical procedures, and to study the mechanism of fall related hip injuries. Apart from these possible contributions due to availability of developed elderly female model, the study also insights different findings that may be used as a guide for future work in human body modeling area. The study suggests that accurate modeling of the costovertebral joints and inclusion of age- and gender-dependent properties of soft and fat tissues can enhance the model bio-fidelity. Therefore, it is suggested that additional experiments should be conducted to characterize the behavior of soft and fat tissues so that more accurate stiffness of these tissues can be better modeled in HBMs. Further suggestions are to include testing of ribs at higher strain rates to better optimize the strain-rate dependent coefficients in the material models so that the model can be simultaneously validated for different loading rates.

APPENDIX A. RIB SECTION 3-POINT BENDING TEST DATA (WSU DATA)

Cadaver ID	Age (years)	Sex	Height (cm)	Weight (kg)	BMI (kg/m2)	Average Cortical Thickness (mm)			
						AvgR7	AvgL7	Avg R6	AvgL6
8	52	F	157.00	53.07	21.53	1.16	0.75	0.83	0.76
47	62	M	176.50	83.91	26.94	1.37	1.27	1.07	1.19
63	64	M	173.00	48.53	16.22	1.01	0.88	1.02	1.00
64	62	M	NA	NA	NA	NA	NA	0.60	0.68
99	47	M	NA	NA	NA	NA	NA	0.90	1.12
115	57	M	179.00	57.61	17.98	1.25	0.83	1.17	1.12
131	67	M	NA	69.00	NA	NA	NA	0.82	0.73
156	67	M	175.00	92.08	30.07	0.68	0.64	0.92	0.67
164	60	M	175.20	79.38	25.86	1.05	0.83	1.26	1.00
170	21	M	169.50	59.87	20.84	1.34	2.12	1.57	1.17
187	64	F	163.00	49.44	18.61	0.85	0.72	0.89	0.78
188	37	M	175.00	69.85	22.81	1.20	1.24	1.30	1.12
194	65	M	167.00	56.25	20.17	0.96	0.78	0.51	0.99
200	57	M	170.50	63.96	22.00	0.79	0.88	1.14	0.93
238	59	M	163.50	48.99	18.33	0.90	0.99	0.93	1.01
259	29	M	174.50	96.16	31.58	0.98	0.83	0.86	1.05
280	61	F	165.00	54.88	20.16	0.64	0.60	0.71	0.69
286	56	F	151.50	50.35	21.94	1.19	1.18	0.87	1.20
312	50	M	179.00	90.72	28.31	1.95	2.13	2.04	1.58
353	59	M	143.00	54.43	26.62	1.61	0.53	0.93	0.96
359	67	M	NA	NA	NA	NA	NA	0.96	1.28
360	72	M	169.00	63.50	22.23	1.32	0.92	1.29	1.13
362	63	M	173.00	68.95	23.04	1.66	1.52	1.41	1.45
371	58	F	NA	NA	NA	NA	NA	1.01	1.19
383	39	M	175.00	77.11	25.18	1.24	1.40	1.35	1.13
385	63	M	NA	NA	NA	NA	NA	1.13	1.93
386	43	F	154.00	68.95	29.07	0.75	0.71	0.69	0.74
395	57	M	NA	NA	NA	NA	NA	1.00	1.15
402	51	M	NA	NA	NA	NA	NA	0.54	0.82
440	50	F	168.00	58.97	20.89	0.90	0.81	0.96	0.91
458	54	M	NA	NA	NA	NA	NA	1.12	1.81
462	58	M	170.00	56.70	19.62	1.09	1.40	1.85	1.47
469	62	M	NA	NA	NA	NA	NA	0.84	1.01
473	43	F	NA	NA	NA	NA	NA	1.12	1.10
525	57	M	NA	NA	NA	NA	NA	0.72	1.04
558	81	F	158.10	41.05	16.42	1.19	0.70	0.88	0.65

563	61	M	170.00	73.03	25.27	1.70	1.87	2.52	2.21
578	57	F	163.00	75.30	28.34	1.13	1.25	1.26	1.36
646	37	M	181.00	48.99	14.95	0.55	0.92	0.91	0.91
682	77	F	160.00	51.26	20.02	0.56	0.65	0.53	0.80
684	50	M	168.50	87.54	30.83	0.94	0.70	1.13	1.14
690	71	M	169.00	49.44	17.31	1.28	1.05	1.32	1.26
698	59	M	172.50	63.50	21.34	0.57	1.11	0.86	1.04
712	51	F	159.00	54.88	21.71	1.34	1.43	1.37	1.37
721	66	M	170.40	70.31	24.21	1.09	1.12	1.00	1.25
731	87	M	175.50	92.08	29.90	1.35	0.77	1.73	1.43
736	67	M	166.50	65.32	23.56	0.69	0.97	0.95	0.80
739	43	M	171.50	62.60	21.28	0.86	1.13	0.93	0.94
741	54	M	186.50	65.32	18.78	0.96	0.63	0.83	0.60
781	59	F	151.10	60.78	26.62	1.02	0.81	0.81	0.83
791	59	F	NA	NA	NA	NA	NA	0.66	1.11
806	60	F	155.00	55.34	23.03	1.55	1.57	1.16	0.92
807	38	F	168.00	65.32	23.14	1.21	0.96	1.16	1.04
828	67	M	170.00	78.02	27.00	0.90	0.59	0.64	0.78
846	59	F	169.00	75.75	26.52	1.65	0.97	1.19	1.38
865	68	M	151.00	55.79	24.47	1.12	1.58	1.59	1.29
877	67	M	173.00	86.64	28.95	1.34	1.61	1.50	1.64
914	62	M	139.50	53.07	27.27	0.88	0.84	0.83	0.81
935	63	M	174.00	69.85	23.07	0.68	0.87	0.81	0.92
947	38	M	166.50	56.25	20.29	1.46	1.36	1.19	1.83
954	82	F	159.00	56.25	22.25	0.87	0.60	0.84	1.00
956	40	F	175.00	76.20	24.88	0.82	0.94	1.01	0.99
986	67	M	178.00	97.52	30.78	0.77	0.71	1.03	0.82
993	49	M	173.00	70.76	23.64	0.79	0.69	0.55	0.74
5144	51	F	NA	NA	NA	NA	NA	1.15	0.68
5145	60	F	NA	NA	NA	NA	NA	0.89	0.71
5146	58	F	NA	NA	NA	NA	NA	0.88	1.33
5155	58	F	NA	NA	NA	NA	NA	1.07	1.21
5211	66	F	NA	NA	NA	NA	NA	0.67	0.50
5213	61	F	NA	NA	NA	NA	NA	0.62	0.76
5236	66	M	NA	NA	NA	NA	NA	0.66	1.16
5246	68	M	NA	NA	NA	NA	NA	1.22	1.36
5288	56	F	NA	NA	NA	NA	NA	0.82	0.81
5302	61	F	NA	NA	NA	NA	NA	1.15	1.15
5337	67	M	NA	NA	NA	NA	NA	1.11	0.75
5350	57	M	NA	NA	NA	NA	NA	1.04	1.10

UM1	37	M	186.50	67.59	19.43	0.95	0.99	0.69	0.84
UM11	58	F	164.00	55.34	20.57	0.90	0.91	0.93	0.89
UM7	61	M	176.50	70.31	22.57	0.87	0.98	0.95	0.75
UM8	62	M	176.00	71.67	23.14	0.84	1.03	0.93	0.89
WI-1	87	F	145.00	34.02	16.18	0.73	0.54	0.87	0.68
WI-2	61	M	166.00	45.81	16.63	0.96	1.17	0.98	0.96

ID	Maximum Force (N)				Maximum Displacement (mm)				SFD (N/mm)			
	R7	L7	R6	L6	R7	L7	R6	L6	R7	L7	R6	L6
8	133.40	130.00	200.20	189.00	4.06	4.06	5.21	5.08	32.81	32.81	38.28	43.75
47	188.40	52.40	272.20	303.60	1.77	6.20	4.20	3.98	106.54	6.72	64.80	76.29
63	193.60	172.60	287.80	208.60	5.78	3.95	5.30	3.09	33.69	44.63	54.25	65.97
64	NA	NA	142.40	106.80	2.54	2.79	3.05	3.81	151.67	58.33	87.50	61.25
99	NA	NA	161.40	160.20	2.54	2.29	2.79	2.54	87.50	54.83	148.75	87.50
115	314.80	213.40	253.00	253.00	4.32	3.05	2.79	2.29	72.86	87.50	90.52	91.97
131	NA	NA	154.60	108.80	1.27	1.78	1.91	1.27	131.25	138.25	122.50	136.50
156	198.80	255.60	117.60	198.80	2.03	3.05	1.78	2.16	127.75	105.00	126.00	140.00
164	258.00	284.60	258.00	302.40	3.81	4.06	4.32	3.30	87.50	110.83	77.00	102.08
170	507.00	507.00	482.60	524.80	4.06	3.56	4.06	4.57	87.50	82.35	87.50	67.31
187	109.20	78.40	61.00	130.20	3.30	4.06	3.04	3.04	33.08	19.27	20.04	42.71
188	383.60	412.20	418.40	433.00	1.52	2.29	1.78	2.79	251.75	180.31	235.39	155.00
194	299.00	322.40	218.00	264.20	4.89	4.90	4.80	4.90	78.80	70.05	52.54	61.29
200	195.80	275.80	106.80	178.00	4.06	4.57	4.06	4.32	52.50	70.00	35.00	43.75
238	151.20	115.60	169.00	195.80	3.05	3.05	3.56	4.57	61.25	52.50	70.00	70.00
259	169.00	151.20	213.60	142.40	4.32	3.56	5.33	4.32	66.67	52.50	52.50	52.50
280	70.80	86.20	51.80	96.00	3.55	2.79	1.77	4.06	19.93	30.88	29.13	23.64
286	186.80	186.80	204.60	178.00	4.45	4.45	4.83	5.33	35.00	35.00	43.75	40.00
312	347.00	373.60	307.00	342.40	8.13	9.40	5.59	5.59	33.65	29.17	38.04	43.75
353	276.60	269.20	275.80	327.00	4.45	4.19	6.99	7.37	89.83	87.50	38.89	47.30

359	NA	NA	133.40	133.40	4.70	3.94	3.81	3.81	52.50	40.83	37.69	37.69
360	226.80	155.60	97.80	169.00	4.06	4.57	3.30	4.32	62.50	56.00	37.92	49.00
362	155.60	142.40	144.60	115.60	3.81	4.19	4.13	4.83	58.33	43.75	43.75	31.82
371	NA	NA	111.20	44.40	7.11	6.60	3.30	3.05	20.42	16.41	32.08	15.56
383	480.60	782.40	441.20	788.80	2.54	2.54	3.11	6.35	189.21	307.99	141.77	124.23
385	NA	NA	204.60	169.00	4.45	3.81	4.57	4.06	98.00	77.78	49.00	58.33
386	214.40	285.00	222.60	285.60	2.79	2.79	2.54	2.54	76.76	102.02	87.60	112.47
395	NA	NA	244.60	169.00	5.72	5.72	5.08	5.72	51.04	30.63	63.64	43.75
402	NA	NA	198.00	171.20	7.37	4.06	5.72	4.83	53.47	87.50	38.50	52.50
440	129.40	136.60	151.20	110.60	2.79	2.28	3.11	2.03	46.34	59.74	48.61	54.42
458	NA	NA	300.20	270.00	2.92	2.92	3.18	2.16	93.33	87.50	92.11	95.45
462	43.00	71.60	75.80	43.60	2.16	2.34	3.03	2.10	19.84	30.54	25.04	20.76
469	NA	NA	129.00	178.00	6.10	4.57	2.41	1.74	35.00	32.81	130.57	83.61
473	NA	NA	136.60	150.40	6.86	6.35	6.10	6.10	50.00	35.00	40.00	43.75
525	NA	NA	231.20	307.00	4.32	4.83	4.32	4.57	77.78	61.40	58.33	70.00
558	186.80	129.00	151.20	106.80	4.32	3.30	4.06	3.56	64.17	46.67	50.00	41.18
563	142.40	142.40	187.80	200.20	3.56	3.56	8.38	6.10	38.89	38.89	43.75	30.88
578	200.20	186.80	151.20	183.20	3.81	5.59	4.57	4.06	70.00	52.50	87.50	58.33
646	247.40	247.40	148.60	247.40	4.57	4.57	8.89	5.84	82.60	82.60	20.42	58.33
682	222.40	222.40	160.20	275.80	12.70	11.68	9.40	8.13	28.00	26.25	25.00	45.50
684	331.80	233.60	160.20	269.20	4.83	3.81	6.10	3.56	122.50	80.50	52.50	116.67
690	148.60	255.80	255.80	197.00	6.60	6.10	4.57	5.59	46.67	70.00	83.13	46.67
698	89.00	113.40	91.20	91.20	4.57	3.30	5.08	5.08	35.00	52.50	35.00	35.00
712	214.00	211.20	228.20	224.60	8.13	7.87	5.08	6.10	42.50	43.75	61.25	61.25
721	114.80	121.80	113.40	113.40	3.56	4.83	3.56	3.56	43.75	58.33	43.75	43.75
731	400.40	287.40	324.80	324.80	7.62	7.11	3.81	3.81	87.50	61.25	58.33	58.33
736	178.00	120.40	123.00	104.60	4.64	5.52	5.30	4.42	38.33	25.33	23.19	23.68

739	124.60	142.40	149.40	141.80	3.56	4.06	3.56	3.30	48.13	65.63	54.69	56.88
741	142.40	155.60	123.60	153.40	2.54	3.81	2.54	3.56	83.13	52.50	72.19	49.58
781	169.00	169.00	266.80	266.80	7.11	7.11	4.31	4.31	29.17	29.17	87.17	87.17
791	NA	NA	178.00	178.00	6.10	6.10	2.54	2.54	52.50	52.50	70.00	70.00
806	238.00	238.00	307.00	229.00	4.06	4.06	3.81	5.08	67.50	67.50	105.00	87.50
807	256.80	233.60	196.80	224.60	NA	NA	6.86	5.33			40.73	58.33
828	103.60	77.80	111.20	104.60	6.10	5.33	5.08	6.10	21.39	16.86	26.51	22.88
846	89.00	84.60	130.00	131.20	3.56	3.81	3.81	3.81	24.87	25.52	41.87	41.25
865	55.60	86.80	84.60	84.60	4.06	4.06	4.06	4.06	19.34	24.50	32.55	32.55
877	225.20	314.20	216.80	257.20	4.57	5.33	5.08	7.11	54.33	85.31	51.04	65.63
914	204.60	204.60	178.00	178.00	4.32	4.32	4.83	4.83	60.67	60.67	56.00	56.00
935	195.80	305.60	215.80	260.20	5.08	4.32	7.37	4.06	98.00	87.50	35.55	79.72
947	298.00	320.20	355.80	355.80	2.67	2.79	3.68	3.68	120.31	113.75	116.67	116.67
954	79.20	79.20	103.20	109.00	4.19	4.19	4.45	3.05	24.50	24.50	29.17	47.51
956	189.00	189.00	113.40	113.40	5.08	5.08	4.06	4.06	53.85	53.85	31.11	31.11
986	278.00	244.60	229.00	206.80	4.32	5.33	3.56	4.57	70.00	56.00	70.00	52.50
993	169.00	160.20	146.80	84.60	4.32	3.56	4.06	3.30	42.39	56.88	37.59	40.25
5144	NA	NA	342.40	173.40	NA	NA	NA	NA	NA	NA	NA	NA
5145	NA	NA	136.60	95.60	NA	NA	NA	NA	NA	NA	NA	NA
5146	NA	NA	129.00	133.40	NA	NA	NA	NA	NA	NA	NA	NA
5155	NA	NA	151.20	146.80	NA	NA	NA	NA	NA	NA	NA	NA
5211	NA	NA	112.60	112.60	NA	NA	NA	NA	NA	NA	NA	NA
5213	NA	NA	193.40	193.40	NA	NA	NA	NA	NA	NA	NA	NA
5236	NA	NA	71.20	71.20	NA	NA	NA	NA	NA	NA	NA	NA
5246	NA	NA	186.80	186.80	NA	NA	NA	NA	NA	NA	NA	NA
5288	NA	NA	182.40	227.80	NA	NA	NA	NA	NA	NA	NA	NA
5302	NA	NA	160.20	151.20	NA	NA	NA	NA	NA	NA	NA	NA
5337	NA	NA	160.2	169.0	NA	NA	NA	NA	NA	NA	NA	NA

			0	0								
5350	NA	NA	185.00	151.20	NA	NA	NA	NA	NA	NA	NA	NA
UM1	298.20	392.40	246.00	222.40	4.20	6.35	4.30	3.05	65.88	53.00	54.31	57.50
UM11	66.40	60.60	80.40	34.60	3.55	2.03	2.03	2.03	18.65	29.81	39.52	17.01
UM7	131.40	208.40	244.60	162.80	1.78	1.78	1.78	2.03	72.92	117.13	137.50	78.75
UM8	108.60	69.60	147.20	84.20	2.03	2.03	1.78	1.52	32.81	32.81	82.50	52.50
WI-1	212.60	151.40	255.80	155.60	4.83	4.32	6.60	5.84	49.58	49.58	47.73	29.17
WI-2	228.00	120.80	222.40	111.20	3.30	6.10	4.32	5.59	58.33	35.00	73.50	21.88

Where SFD- Slope of force-deflection curve, avg –Average values

APPENDIX B. RESULTS OF PARAMETRIC STUDIES

Mat	Angle	Thickness	Stiffness	F_{max}	d_{peak}	E_{peak}	Fracture
0	-6	40	-50	4.826	94.71	288.35	9
-20	-6	-40	-50	4.87	97.7	286.64	17
0	-6	20	-50	4.8	93	278	9
10	-6	-20	-50	4.82	96.79	288.74	12
30	-6	0	-50	4.82	95.52	290.31	9
-20	-6	-20	-50	4.73	97.29	285.95	14
30	-6	-30	-50	4.8	96.95	289.71	10
-10	-6	20	-50	4.8	95.612	287	9
30	-6	-20	-50	4.88	96.33	289.66	11
-30	-6	0	-50	4.6	96.95	286.91	11
30	-6	0	-25	4.86	92.68	285.96	8
-10	-6	-10	-25	4.84	93.13	282.85	11
20	-6	-30	-25	4.8	94.4	284.4	12
10	-6	-40	-25	4.69	94.81	283.47	14
-30	-6	-40	-25	4.75	95	278.87	20
20	-6	-10	-25	4.79	92.616	285.7	8
-20	-6	0	-25	4.81	93.9	282.47	9
0	-6	-40	-25	4.69	94.76	282.31	12
20	-6	30	-25	4.92	91.79	288	4
-30	-6	30	0	4.82	90.646	277.52	12
20	-6	-30	0	4.94	91.88	280.76	12
0	-6	40	0	4.83	90.02	281.4	7
30	-6	10	0	4.81	90.28	283.33	5
10	-6	-20	0	4.88	91.377	279.65	8
-30	-6	-10	0	4.78	91.67	278.06	10
0	-6	30	25	4.89	88.56	277.85	6
10	-6	20	25	4.87	88.59	278.65	7
10	-6	-20	25	4.9	90.017	277.04	12
-20	-6	10	25	4.87	89.51	275.2	12
0	-6	-40	25	4.81	90.63	275.38	14
-30	-6	0	25	4.97	89.9	274.16	12
30	-6	10	25	4.78	91	288	6
10	-6	40	25	4.76	87.7	279.72	3
-10	-6	-20	25	4.91	90.06	275.76	13
30	-6	30	50	4.9	86.43	279.42	3
-10	-6	40	50	4.94	86.9	274.4	6
0	-6	40	50	4.94	86.69	275.46	6
-30	-6	30	50	4.97	87.39	271.04	9
-30	-6	-20	50	5.04	88.13	271.79	10

-20	-3	20	-50	4.9	79	294	5
-20	-3	-40	-50	4.73	77.47	296.6	19
-10	-3	0	-50	5.07	75.49	294	9
-20	-3	30	-50	5.04	75	295	6
-30	-3	0	-50	4.97	75.57	295.32	14
-10	-3	-40	-50	4.79	76	294.8	18
30	-3	-20	-50	5.03	75.37	296	6
-10	-3	20	-50	5	75	295.79	6
0	-3	20	-50	4.97	74.9	296	6
-30	-3	-20	-50	4.87	76	294	15
10	-3	10	-50	4.97	74	296	4
30	-3	10	-25	5.05	73	285	4
-20	-3	40	-25	5.11	72.7	291.7	5
0	-3	-20	-25	5.24	73	288	10
0	-3	10	0	5.2	71	289	5
-10	-3	-20	0	5.24	72	286	11
-10	-3	0	0	5.35	71.49	286	9
-10	-3	20	0	5.2	71	288	6
20	-3	-40	0	5.3	72	288	10
20	-3	30	0	5.13	70.6	291	3
30	-3	-30	0	5.37	72	289	9
10	-3	10	0	4.9	78	292	5
30	-3	-10	0	5.23	71.25	289.4	6
10	-3	40	25	5.2	68	287.15	2
20	-3	-10	25	5.33	70.2	287	6
-10	-3	-40	25	5.24	71.7	284.66	14
20	-3	40	25	5.19	69.72	289.87	2
10	-3	-30	25	5.44	69.88	283.78	9
0	-3	-20	25	5.42	70.2	282.3	8
-20	-3	-30	50	5.3	69.84	280	15
-30	-3	-20	50	5.34	69.24	280.7	15
-10	-3	-10	50	5.54	68.7	281.95	10
10	-3	-30	50	5.55	69.38	280.56	9
0	-3	10	50	5.39	68.69	283.66	4
-10	-3	20	50	5.37	68.46	281.79	6
-30	-3	-30	50	5.22	70.38	281	16
30	-3	-30	50	5.6	69.2	282.53	9
-10	-3	30	50	5.4	68.8	284	5
-10	-3	40	50	5.3	68.28	283	5
10	0	30	-50	4.44	91.91	294	9
-20	0	20	-50	4.28	92.46	293.13	14
10	0	40	-50	4.25	91	296.7	7
20	0	0	-50	4.41	92.92	295.9	10

-10	0	30	-25	4.52	89.28	289.99	8
-10	0	10	-25	4.35	89.68	289.51	11
-30	0	20	-25	4.54	89.73	287.17	13
30	0	30	-25	4.46	88.28	294.31	6
10	0	-40	-25	4.89	86.7	287	16
-20	0	-40	-25	4.39	91.2	284	20
0	0	40	-25	4.45	88.92	292.7	8
0	0	20	-25	4.56	89.3	291	8
-10	0	-40	-25	4.3	91	285	20
10	0	10	-25	4.42	89.7	292	9
20	0	-10	0	4.61	88.21	289	8
0	0	0	0	4.67	87.88	287.17	10
20	0	30	0	4.52	86.6	289.82	7
-30	0	-10	0	4.76	88.02	286.16	17
20	0	0	0	4.46	87.75	293.7	9
0	0	-40	0	4.64	88	282	17
-30	0	30	0	4.66	87.5	283	12
-20	0	-20	0	4.74	87.89	283.65	16
-10	0	-10	0	4.69	87.9	284.48	13
0	0	-10	0	4.69	88	285.76	12
-20	0	0	25	4.84	86.14	280.87	13
-20	0	-40	25	4.65	87.5	279.85	21
20	0	-20	25	4.86	84.96	280.15	11
-30	0	30	25	4.7	85.72	281.11	13
30	0	20	25	4.7	84.9	287.51	6
30	0	10	25	4.72	85.47	293.02	7
0	0	-20	25	4.76	88	281	15
-20	0	20	25	4.74	85.7	281.58	12
20	0	-40	25	4.92	86.7	281.34	13
-20	0	-30	50	4.86	85.5	275.82	18
0	0	20	50	4.73	84.31	282.26	8
10	0	-40	50	5.07	85	277	14
-10	0	40	50	4.87	83.99	287.41	9
20	0	-30	50	4.96	85.08	285.9	12
-20	0	-10	50	4.96	84.5	276	11
-30	0	0	50	4.98	84.5	276.6	14
-20	3	-10	-50	4.17	95.4	287.7	17
20	3	0	-50	4.23	94.5	293.52	7
10	3	20	-50	4.23	93.85	293.06	7
0	3	-10	-50	4.2	95.05	290.74	13
-10	3	-10	-50	4.14	94.7	290.35	8
-30	3	10	-50	4.59	86.79	277.85	13
10	3	10	-50	4.63	86.5	284.36	6

0	3	40	-50	4.31	93.5	292.15	7
30	3	-30	-25	4.33	92.66	287	12
10	3	-10	-25	4.32	92.25	290	8
0	3	-10	-25	4.18	92.39	287.4	11
0	3	20	-25	4.27	91.5	288.87	7
-20	3	-30	-25	4.15	94.26	285.5	20
20	3	0	-25	4.29	92.059	290.33	9
20	3	10	0	4.44	89.45	290	7
10	3	40	0	4.55	88.24	285.04	3
-10	3	0	0	4.34	90.335	283.72	12
-30	3	-20	0	4.3	92.01	281.8	21
-20	3	-40	0	4.23	92.86	282.33	24
20	3	-30	0	4.377	90.85	284.25	15
30	3	-20	0	4.43	90.273	286.34	9
30	3	20	0	4.62	88.81	289	5
-30	3	30	0	4.35	89.74	281.6	13
0	3	-30	25	4.46	89.57	279.33	16
20	3	30	25	4.72	86.73	284.88	5
-10	3	30	25	4.47	87.67	281.15	7
-10	3	40	25	4.605	87.5	281.62	6
0	3	-40	25	4.35	91.43	282.96	20
30	3	-10	25	4.55	88.23	285.12	7
10	3	0	25	4.24	92.1	289.35	10
20	3	0	50	4.6	86.54	281.43	5
30	3	10	50	4.67	86.15	283.6	5
-30	3	0	50	4.56	87.27	274.43	15
20	3	-10	50	4.56	87.025	280.94	9
-10	3	40	50	4.66	86.04	278.92	6
20	3	-30	50	4.62	87.4	278.2	16
30	3	20	50	4.79	85.42	282.42	2
30	3	40	50	4.965	84.86	283.11	0
-30	3	40	50	4.55	86.39	277.17	12
10	6	10	-50	4.95	93	281	10
-20	6	30	-50	4.81	92.46	277	12
30	6	-30	-50	4.76	93.67	280	11
-20	6	20	-50	4.78	92.7	277.88	11
-30	6	-20	-50	4.68	94.55	275.92	19
20	6	20	-50	4.94	91.99	280.32	8
0	6	-40	-25	4.68	92.14	273.8	20
-10	6	-40	-25	4.63	92.53	272	20
-30	6	-30	-25	4.75	92.3	271	18
-10	6	10	-25	4.83	90.04	272.57	9
30	6	40	-25	4.96	91.56	286.05	6

20	6	-10	-25	4.99	91.824	279.08	12
30	6	-40	-25	4.76	91.65	275.02	15
30	6	20	-25	4.96	89.48	277.01	6
20	6	40	-25	4.94	88.9	275.97	6
20	6	-20	-25	4.92	90.75	270	9
10	6	20	0	4.955	87.56	270.97	5
30	6	-30	0	4.9	88.95	261	9
20	6	-40	0	4.83	89.7	270.45	15
-30	6	0	0	4.82	89.2	268.72	15
-30	6	30	0	4.76	88.11	269	13
-20	6	-30	0	4.71	89.89	268	17
-20	6	-20	25	4.75	87.5	264.2	16
-30	6	-30	25	4.81	88.21	263.67	18
20	6	10	25	4.96	86.24	269.12	6
0	6	-10	25	4.89	86.96	266.85	11
-30	6	40	25	4.82	86.06	264.61	9
-10	6	10	25	4.88	86.36	266.11	9
10	6	10	25	4.95	86.49	268.9	8
10	6	0	25	4.91	86.79	268.42	11
0	6	10	25	4.95	86.88	268.8	13
-20	6	10	50	4.9	85.85	262	12
-20	6	0	50	4.88	85.59	262.5	15
10	6	20	50	4.98	84.5	265.37	6
10	6	10	50	4.89	84.89	265.17	8
-30	6	-30	50	4.7	91	278	18
-30	6	-10	50	4.91	86.05	260.9	16
0	6	-20	50	4.87	85.94	263	9
30	6	30	50	4.95	84.13	268.13	6

Where F_{max}= Maximum force, d_{peak} = Peak deflection and E_{peak} = Peak energy

REFERENCES

Abrams, E., Mohr, M., Engel, C., & Bottlang, M. (2003). “Cross-sectional geometry of human ribs.” Cortex, 80, 2

Ashley, G. T. (1956).” The human sternum: the influence of sex and age on its measurements. Journal of Forensic Medicine 3:27-43.

Bai, Z., Jiang, B., Zhu, F., Cao, L., (2013). “Optimizing the Passenger Airbag of an Adaptive Restraint System for Multiple Size Occupants.” Traffic injury prevention.

Baker, T. K., T. Falb, R. Voas and J. Lacey (2003). "Older women drivers: Fatal crashes in good conditions." Journal of Safety Research 34(4): 399-405.

Bansal, V., Conroy, C., Chang, D., Tominaga, G.T., and Coimbra, R. (2011). "Rib and sternum fractures occupants." Technical report by NHTSA, No. HS-811 101. Accession number: 01123448.

Behiri, J., Bonfield, W., (1984). "Fracture mechanics of bone—the effects of density, specimen thickness and crack velocity on longitudinal fracture." Journal of biomechanics 17, 25-34.

Bellemare, F., A. Jeanneret and J. Couture (2003). "Sex Differences in Thoracic Dimensions and Configuration." American Journal of Respiratory and Critical Care Medicine 168(3): 305-312.

Bendjellal F., Walfisch G., Steyer C., (1997). "The programmed restraint system - a lesson from accidentology.” Proceedings of 41st Stapp Car Crash Conference, SAE 973333, pp 249-264.

Bose, D., Segui-Gomez M. and Crandall J. R. (2011). "Vulnerability of female drivers involved in motor vehicle crashes: an analysis of US population at risk." American journal of public health 101(12): 2368-2373.

Bulger, E. M., Arneson M. A., Mock C. N. and Jurkovich G. J. (2000). "Rib fractures in the elderly." The Journal of trauma 48(6): 1040-1046; discussion 1046-1047.

Cavanaugh, J. M., Nyquist, G. W., Goldberg, S. J., & King, A. I. (1986). “Lower abdominal tolerance and response.” SAE Technical Paper No 861878.

Cavanaugh, J., Zhu Y., Huang Y. and King A. (1993). "Injury and response of the thorax in side impact cadaveric tests." Proceedings of the 37th Stapp Car Crash Conference, SAE 933127.

Cerroni, A.M., Tomlinson, G.A., Turnquist, J.E., & Grynpas, M.D. (2000). "Bone mineral density, osteopenia, and osteoporosis in the rhesus macaques of Cayo Santiago." American journal of physical anthropology, 113(3), 389-410.

Cesari, D., Ramet, M., & Clair, P. Y. (1980). "Evaluation of pelvic fracture tolerance in side impact." SAE Technical Paper No. 801306.

Cesari, D., Bouquet, R., (1994) “Comparison of Hybrid III and human cadaver thoracic deformations.” SAE paper no. 942209.

Charpail, E., Trosseille, X., Petit, P., Laporte, S., Lavaste, F., & Vallancien, G. (2005) "Characterization of PMHS Ribs: A New Test Methodology." Stapp Car Crash Journal, 49, 183-198.

Chen, H., Zhou, X., Fujita, H., Onozuka, M., & Kubo, K. Y. (2013). "Age-related changes in trabecular and cortical bone microstructure." International journal of endocrinology, 2013

Choi H. Y. and Lee L.H. (1999). “Advanced finite element modeling of the human body for occupant safety simulation” Proceedings of 10th PUCA, Japan, pp. 469-478.

Cormier, J.M. (1998). "Microstructural and mechanical properties of human ribs." Virginia Tech University, MS Thesis.

Coughlin, J. F. and Reimer B. (2006). "New Demands from an Older Population: An Integrated Approach to Defining the Future of Older Driver Safety," In Proceedings of the Society of Automotive Engineers Convergence Conference.

Cummings, S. R., Kelsey J. L., Nevitt M. C. and O'Dowd K. J. (1985). "Epidemiology of osteoporosis and osteoporotic fractures." Epidemiologic reviews 7(1): 178-208.

Currey, J.D. (1969). "The relationship between the stiffness and the mineral content of bone." Journal of biomechanics, 2(4), 477-480.

Eppinger, R. H., Marcus J. H. and Morgan R. M. (1984). "Development of Dummy and Injury index for NHTSA's Thoracic Side Impact Protection Research Program." SAE International, Paper No. 840885.

Eppinger R.H., Marcus J.H., (1985)."Prediction of Injury in Blunt Frontal Impact.” 10th International Conference on Experimental Safety Vehicles, oxford, England, Page No. 90-104

Fon, G. T., Pitt, M. J., and Thies, A. C. Jr. (1980)."Thoracic kyphosis: range in normal subjects." American Journal of Roentgenology 134(5): 979-983.

Foret-Bruno J. Y., Trosseille X., Le Coz J. Y., (1998). "Thoracic injury risk in frontal car crashes with occupant restrained with belt load limiter.” SAE No. 983166, pp 331-352.

Granik, G. and Stein, I. (1973). "Human ribs: static testing as promising medical application." Journal of biomechanics 6(3): 237-240

Gayzik, F. S., Yu M. M., Danelson K. A., Slice D. E. and Stitzel J. D. (2008). "Quantification of age-related shape change of the human rib cage through geometric morphometrics." J Biomech 41(7): 1545-1554.

Guan, F., Han, X., Mao, H., Wagner, C., Yeni, Y.N., & Yang, K.H. (2011). "Application of optimization methodology and specimen-specific finite element models for investigating material properties of rat skull." Annals of biomedical engineering, 39(1), 85-95.

Hamilton, M. N., Hung-Hsu C., and Dennis G. A. (1986). "Adult to child scaling and normalizing of lateral thoracic impact data," In Proceedings of the Thirtieth Stapp Car Crash Conference P-189, Society of Automotive Engineers, Warrendale, PA.

Han J and Kamber M. (2006). "Mining: concepts and techniques." 2nd ed. San Francisco, CA: Morgan Kaufmann

Hanna, R. and Hershman, L. (2009). "Evaluation of thoracic injuries among older motor vehicle occupants." Technical report by NHTSA, No. HS-811 101. Accession number: 01123448.

Hardy, W. N., Shah, C. S., Kopacz, J. M., & Yang, K. H. (2006). "Study of potential mechanisms of traumatic rupture of the aorta using insitu experiments". Stapp car crash journal, 50, 247.

Herman, I. P. (2008). "Physics of the human body." Springer. ISBN:978-3-540-29603-4, page-246.

Hinman, M. R. (2004). "Comparison of thoracic kyphosis and postural stiffness in younger and older women." The Spine Journal 4(4): 413-417.

Holcomb, J. B., McMullin, N. R., Kozar, R.A., Lygas, M.H. and Moore, F.A (2003)."Morbidity from rib fractures increases after age 45." Journal of the American College of Surgeons 196(4): 549-555.

Imagama, S., Matsuyama Y., Hasegawa Y., Sakai Y., Ito Z., Ishiguro N. and Hamajima N. (2011). "Back muscle strength and spinal mobility are predictors of quality of life in middle-aged and elderly males." Eur Spine J 20(6): 954-961.

Indar J.,Jhingan V, and Kulkarni M.(1980). “Sexing in human sternum.” Am. J. Phys. Anthrop. 53:217-24.

Ito, O., Dokko, Y., Ohashi, K., (2009). "Development of adult and elderly FE thorax skeletal models." SAE Technical Paper, 2009-01-0381.

Iwamoto, M., Kisanuki, Y., Watanabe, I., Furusu, K., Miki, K., & Hasegawa, J. (2002). “Development of a finite element model of the total human model for safety (THUMS) and application to injury reconstruction”. In Proceedings of the International Research Council on the Biomechanics of Injury conference (Vol. 30, pp. 12-p).

Johnell, O. and Kanis J. (2006). "An estimate of the worldwide prevalence and disability associated with osteoporotic fractures." Osteoporosis International 17(12): 1726-1733.

Kahane, C. J. (May 2013). "Injury Vulnerability and Effectiveness of occupant protection technologies for older occupants and women." DOT HS 811 766. Washington, DC: National Highway Traffic Safety Administration.

Kallieris D., Rizzetti A., Mattern R.,(1995) “On the synergism of the driver air bag and the three-point belt in frontal collisions.” Proc. 39th Stapp Car Crash Conference, SAE 952700, pp 389-402.

Kalra, A., Saif, T., Shen, M., Jin, X., Zhu, F., Begeman, P., Millis, S. and Yang, K. (2015). "Characterization of Human Rib Biomechanical Responses due to Three-Point Bending." Stapp car crash journal, 59, 113-130.

Kemper, A.R., McNally C., Kennedy E.A., Manoogian S.J., Rath A.L., Ng T.P., Stitzel J.D., Smith E.P., Duma S.M., Matsuoka F., (2005). "Material properties of human rib cortical bone from dynamic tension coupon testing." Stapp Car Crash J 49: 199-230.

Kemper, A.R., McNally, C., Pullins, C.A., Freeman, L.J., Duma, S.M., & Rouhana, S.W. (2007) "The biomechanics of human ribs: material and structural properties from dynamic tension and bending tests." Stapp Car Crash Journal, 51, 235.

Kemper, A., Kennedy E., McNally C., Manoogian S. J., Stitzel, J. and Duma, S.M.(2011)."Reducing chest injuries in automobile collisions: rib fracture timing and implications for thoracic injury criteria." Annals of biomedical engineering 39(8): 2141-2151.

Kent, R., Lessley, D., Sherwood, C., (2004). "Thoracic response to dynamic, non-impact loading from a hub, distributed belt, diagonal belt, and double diagonal belts." Stapp Car Crash J 48: 495-519.

Kent, R. and Patrie, J., (2005). “Chest deflection tolerance to blunt anterior loading is sensitive to age but not load distribution.” Forensic science international 149, 121-128

Kent, R., Lee S. H., Darvish K., Wang S., Poster C. S., Lange A. W., Brede C., Lange D. and Matsuoka F. (2005b). "Structural and material changes in the aging thorax and their role in crash protection for older occupants." Stapp Car Crash J 49: 231-249.

Kent, R., Henary B. and Matsuoka F. (2005b). "On the fatal crash experience of older drivers." Annual Proceedings of Association of Advanced Automotive Medicine 49: 371-391.

Kent, R., Woods, W. and Bostrom, O. (2008). "Fatality risk and the presence of rib fractures." Annals of Advances in Automotive Medicine/Annual Scientific Conference, Association for the Advancement of Automotive Medicine

Kantardzic M. (2003). "Data mining: concepts, models, methods, and algorithms." Hoboken, (NJ): IEEE Press.123

Kimpara, H., Iwamoto M., Miki K., Lee J., Begeman P., Yang K. and King A. (2003). "Biomechanical properties of the male and female chest subjected to frontal and lateral impacts." In Proceedings of the International Research Council on the Biomechanics of Injury conference (Vol. 31, pp. 13p-13p). International Research Council on Biomechanics of Injury.

Kimpara, H., Lee J. B., Yang K. H., King A. I., Iwamoto M., Watanabe I. and Miki K. (2005). "Development of a Three-Dimensional Finite Element Chest Model for the 5(th) Percentile Female." Stapp Car Crash J 49: 251-269.

Kindig, M., Lau, A.G. and Kent, R.W. (2011). "Biomechanical response of ribs under quasi-static frontal loading." Traffic injury prevention 12(4): 377-387.

King, M.W., Kent, R.W., (2010). “Structural Response of Cadaveric Ribcages under a Localized Loading: Stiffness and Kinematic Trends”. Stapp Car Crash Journal 54

Koh S. W. (1998). “Effect of rib strength on injury tolerance in side impact”. Masters thesis in Wayne State University, Detroit, MI.

Kuppa S. M., and Eppinger R. H., (1998). “Development of an improved thoracic injury criterion.” Proc. 42nd Stapp Car Crash Conference, SAE 983153, pp 139-154.

Kroell, C. K., Schneider D. C. and Nahum A. M. (1971). "Impact Tolerance and Response of the Human Thorax,." SAE International.

Kroell, C. K., Schneider D. C. and Nahum A. M. (1974). "Impact Tolerance and Response of the Human Thorax II." SAE International, Paper No. 741187.

Krogman, W. M. (1962) “The Human Skeleton in Forensic Medicine.” Springfield III: Charles C Thomas.

Laituri, T. R., Prasad P., Sullivan K., Frankstein M. and Thomas R. S. (2005). "Derivation and Evaluation of a Provisional, Age-Dependent, AIS3+ Thoracic Risk Curve for Belted Adults in Frontal Impacts." SAE International Paer No. 2005-01-0297.

Lenard, J. and Welsh R. (2001). "A comparison of injury risk and pattern of injury for male and female occupants of modern European passenger cars." IN: Proceedings of the 2001 IRCOBI Conference on the Biomechanics of Impact, 10-12 October.

Li, Z., Kindig, M.W., Kerrigan, J.R., Untaroiu, C.D., Subit, D., Crandall, J.R. and Kent, R.W. (2010). "Rib fractures under anterior–posterior dynamic loads: experimental and finite-element study." Journal of biomechanics 43(2): 228-234.

Li Z., Kinding M.W., and Kent R. W. (2010) “Development of a Finite Element Ribcage Model of the 50th Percentile Male with Variable Rib Cortical Thickness”. Proceedings of the Thirty-Ninth International workshop on Injury Biomechanics research

Lin, C. H., Cheng, Y. P., Wang J.,(2014). “Evaluation of LS-DYNA® Corpuscular Particle Method for Side Impact Airbag Deployment Applications.” Proceedings of 13th International LS-DYNA Users conference.

Lyman, S., Ferguson S. A., Braver E. R. and Williams A. F. (2002). "Older driver involvements in police reported crashes and fatal crashes: trends and projections." Injury prevention : journal of the International Society for Child and Adolescent Injury Prevention 8(2): 116-120.

Lynch S., Weaver A, Schoell S., Stitzel J. (2015) “Characterization of Cortical Bone Thickness Changes in the Human Ribs with Age and Sex” available at http://ibrc.osu.edu/wp-content/uploads/2015/03/Abstract_Lynch_2015.pdf

Mayeur, O., Delattre, J., Kindig, M., Delille, R., Chaari, F., Lesueur, D., ... & Drazetic, P. (2011) "Numerical Anthropometry Comparison between the THOMO PMHS and GHBMC Model." Proceedings of the Thirty-Ninth International workshop on Injury Biomechanics research.

Mosekilde, L., Mosekilde, L., (1986). "Normal vertebral body size and compressive strength: relations to age and to vertebral and iliac trabecular bone compressive strength." Bone 7, 207-212

McCalden, R. W., McGeough J. A. and Court-Brown C. M. (1997). "Age-related changes in the compressive strength of cancellous bone. The relative importance of changes in density and trabecular architecture." The Journal of bone and joint surgery. American volume 79(3): 421-427.

Melvin, J. W., Stalnaker, R. L., Roberts, V. L., & Trollope, M. L. (1973). "Impact injury mechanisms in abdominal organs." SAE Technical Paper No. 730968.

Mika, A., Unnithan V. B. and Mika P. (2005). "Differences in Thoracic Kyphosis and in Back Muscle Strength in Women With Bone Loss due to Osteoporosis." Spine 30(2): 241-246 .

Mohr, M., Abrams, E., Engel, C., Long, W.B., & Bottlang, M. (2007). "Geometry of human ribs pertinent to orthopedic chest-wall reconstruction." Journal of biomechanics, 40(6), 1310-1317.

Moore K.L., Agur A. "Essential Clinical Anatomy" second edition

Morgan, R. M., Marcus J. H. and Eppinger R. H. (1986). "Side Impact - The Biofidelity of NHTSA's Proposed ATD and Efficacy of TTI". SAE International, Paer No. 861877

Morgan R.M., Eppinger R.H., Haffner M.P.,(1994).“Thoracic trauma assessment formulations for restrained drivers in simulated frontal impacts.” Proc. 38th Stapp Car Crash Conference, SAE 942206, pp 15-34.

NHTSA (Dec 2013). "Traffic safety for older people- 5-year plan." DOT HS 811 837.

Otte D., (1995) “Review of the air bag effectiveness in real life accidents demands for positioning and optimal deployment of air bag systems.” Proc. 39th Stapp Car Crash Conference, SAE 952701, pp 1-10.

Petitjean, A., Baudrit P. and Trosseille X. (2003). "Thoracic injury criterion for frontal crash applicable to all restraint systems." SAE Conference proceedings, Page No. 323-348, SAE; 1999-2003.

Petitjean, A., Trosseille, X., Yoganandan, N., & Pintar, F. A. (2015). "Normalization and scaling for human response corridors and development of injury risk curves." In Accidental Injury (pp. 769-792). Springer New York.

Polanco‐Loria, M., Daiyan, H., & Grytten, F. (2012). "Material parameters identification: An inverse modeling methodology applicable for thermoplastic materials." Polymer Engineering & science, 52(2), 438-448.

Ray, N. F., Chan J. K., Thamer M. and Melton L. J. (1997). "Medical expenditures for the treatment of osteoporotic fractures in the United States in 1995: report from the National Osteoporosis Foundation." Journal of Bone and Mineral Research 12(1): 24-35.

Reed, M. P., Manary M. A. and Schneider L. W. (1999). "Methods for Measuring and Representing Automobile Occupant Posture." SAE International, Paper No. 1999-01-0959.

Reed, M. P., Ebert, S. M., & Hallman, J. J. (2013). "Effects of driver characteristics on seat belt fit." Stapp car crash journal, 57, 43.

Report on CIREN cases by SC WANG (2008) on “Elderly occupants: Injury risks and Pattern” available online at http://crashedu.org/wiki/. named as ACN_Module_6_Elderly.

Roberts, V. L. and Compton C. (1993). "The relationship between Delta V and injury." SAE Technical Paper 933111.

Ruan, J., R. El-Jawahri, Chai L., Barbat S. and Prasad P. (2003). "Prediction and analysis of human thoracic impact responses and injuries in cadaver impacts using a full human body finite element model." Stapp Car Crash J 47: 299-321.

Sandoz, B., Laporte, S., Charpail, E., Trosseille, X., & Lavaste, F. (2007). "Influence of the velocity in human ribs response." Journal of Biomechanics, 40, S215.

Schaefer, K. E., McNulty, W. P., Carey, C., & Liebow, A. A. (1958). "Mechanisms in development of interstitial emphysema and air embolism on decompression from depth." Journal of Applied Physiology, 13(1), 15-29.

Schafman, M.A. (2015). "Dynamic Structural Properties of Human Ribs in Frontal Loading." The Ohio State University, MS Thesis.

Schultz, A.B., Benson, D.R., & Hirsch, C. (1974). "Force-deformation properties of human ribs." Journal of Biomechanics, 7(3), 303-309.

Shah, C. S., Yang, K. H., Hardy W., Wang H. K. and King A. I. (2001). "Development of a computer model to predict aortic rupture due to impact loading." Stapp car crash journal 45: 161.

Shi, X., Cao L., Reed M. P., Rupp J. D., Hoff C. N., & Hu J. (2014).” A statistical human rib cage geometry model accounting for variations by age, sex, stature and body mass index”. Journal of biomechanics 47(10):2277-85.

Shigeta, K., Kitagawa, Y., & Yasuki, T. (2009). "Development of next generation human FE model capable of organ injury prediction." In Enhanced Safety of Vehicle Conference, Stuttgart, Germany, June (pp. 15-18).

Slemenda, C. W., Hui, S. L. , Williams, C. J. , Christian, J. C., Meaney, F. J. and Johnston C. C. Jr., (1990). "Bone mass and anthropometric measurements in adult females." Bone and Mineral 11(1): 101-109.

Stawicki, S. P., Grossman, M. D., Hoey, B. A. , Miller D. L. and Reed, J. F. 3rd (2004). "Rib fractures in the elderly: a marker of injury severity." Journal of the American Geriatrics Society 52(5): 805-808.

Stewart, T. D. (1979). “Essentials of Forensic Anthropology especially as developed in the United States.” Springfield, III: Charles C. Thomas.

Steele D. G. and Bramblett C.A (2012). "The Anatomy and Biology of the Human Skeleton” edition Ninth in 2012, Texas A & M University Press, College Station.

Stitzel, J.D., Cormier, J.M., Barretta, J.T., Kennedy, E.A., Smith, E.P., Rath, A.L., & Matsuoka, F. (2002)."Defining regional variation in the material properties of human rib cortical bone and its effect on fracture prediction." Stapp Car Crash Journal, 47, 243-265

Stitzel, J. D., Kilgo, P. D., Weaver, A. A., Martin, R. S., Loftis, K. L. and Meredith, J. W. (2010). "Age thresholds for increased mortality of predominant crash induced thoracic injuries." Ann Adv Automot Med 54: 41-50.

Stitzel, J.D., Cormier, J.M., Barretta, J.T., Kennedy, E.A., Smith, E.P., Rath, A.L., & Matsuoka, F. (2002)."Defining regional variation in the material properties of human rib cortical bone and its effect on fracture prediction." Stapp Car Crash Journal, 47, 243-265.

Subit, D., de Dios, E. D. P., Valazquez-Ameijide, J., Arregui-Dalmases, C., & Crandall, J. (2011) "Tensile material properties of human rib cortical bone under quasi-static and dynamic failure loading and influence of the bone microstucture on failure characteristics." arXiv preprint arXiv:1108.0390.

Tamura, A., Watanabe, I. and Miki, K. (2005). "Elderly human thoracic FE model development and validation." Proceedings of the 19th ESV Conference, European Enhanced Safety of Vehicle.

Talantikite, Y., Bouguet, R., Rarnet, M., Guillernot, H., Robin, S., Voiglio, E., (1998). "Human thorax behaviour for side impact-Influence of impact mass and velocities." Proceedings of the Conference on the Enhanced Safety of Vehicles, pp. 98-S97-O-03.

Tille Y. (2006) "Sampling Algorithms." Springer Series in Statistics, Springer, Berlin, Germany

Tomasch, E., Kirschbichler, S., Sinz, W., Steffan, H., Darok, M., Dimai, H.P., & Patsch, J. (2010). "Methodology to predict thresholds for loading corridors of human ribs." In Proceedings of the International Research Council on the Biomechanics of Injury conference (Vol. 38, pp. 285-288).

Ural, A., Bruno, P., Zhou, B., Shi, X.T., Guo, X.E., (2013). “A new fracture assessment approach coupling HR-pQCT imaging and fracture mechanics-based finite element modeling.” Journal of biomechanics 46, 1305-1311.

Van Haaren, E.H., van der Zwaard, B.C., van der Veen, A.J., Heyligers, I.C., Wuisman, P.I. and Smit, T.H. "Effect of long-term preservation on the mechanical properties of cortical bone in goats" Acta Orthop. 2008 Oct; 79(5):708-16

Vezin, P., & Berthet, F. (2009). "Structural characterization of human rib cage behavior under dynamic loading." Stapp car crash journal, 53, 93.

Verriest, J.-P., (1985). "Validity of thoracic injury criteria based on the number of rib fractures." SAE Technical Paper 856027.

Viano, D.C., (1989). "Biomechanical responses and injuries in blunt lateral impact." SAE Technical Paper No. 892432.

Wang S.C. (2008) Report on CIREN cases on "Elderly occupants: Injury risks and pattern" available online at http://crashedu.org/wiki/ACN_Module_6_Elderly.

Wang, N. C., Holcombe, S., Kohoyda-inglis, C., & Wang, S. C. (2012). "Morphomic Analysis of Cervical Facet Angles." In Proceedings of the JSAE Annual Congress, Paper No. 20125158.

Weaver A., Schoell S., Urban J., Lynch S., Jones D., Lillie E., Stitzel J. (2015). “Development of an older occupant FE model incorporating geometry, material properties and cortical thickness variation.” available at http://www.nhtsa.gov/DOT/NHTSA/NVS/Public%20Meetings/SAE/2015/2015SAE-Rudd-OlderOccupant.pdf

Wierzbicki, T., Bao, Y., Lee, Y.-W., Bai, Y., (2005). “Calibration and evaluation of seven fracture models.” International Journal of Mechanical Sciences 47, 719-743

Witten I.H. and Frank E. (2011). "Data mining: practical machine learning tools and techniques." 3rd ed. Burlington, (MA): Morgan Kaufmann.

Wood, L. K., Miller, C. S., Madura, N. H., Reed, M. P., Schneider, L. W., Klinich, K. D., & Rupp, J. D. (2014). "Response and tolerance of female and/or elderly PMHS to lateral impact." Stapp car crash journal, 58, 423

Yamada, H., (1970). “Strength of Biological Materials," ed. Evans, F. G. The Williams and Wikins Company, Baltimore.

Yamagishi, M., Iyama, J., Araki, T., Natori, S., (2012). “Numerical Simulation of Out-of-Position Front Passenger Injuries in Frontal Crashes Using an Accurate Finite Element Model of the Cockpit Module.” SAE Technical Paper, 2012-01-0552

Yang, K. H., Hu, J., White, N. A., King, A. I., Chou, C. C., & Prasad, P. (2006). "Development of numerical models for injury biomechanics research: a review of 50 years of publications in the Stapp Car Crash Conference (No. 2006-22-0017)." SAE Technical Paper.

Yoganandan, N., Pintar, F.A., (2005). "Deflection, acceleration, and force corridors for small females in side impacts." Traffic injury prevention 6, 379-386.

Yoganandan, N. and Pintar, F. (1998)."Biomechanics of human thoracic ribs." Journal of biomechanical engineering 120(1): 100-104

Yoganandan, N, Pintar, F.A., Skrade, D., (1993). ”Thoracic biomechanics with air bag restraint.” Proc. 37th Stapp Car Crash Conference, SAE Paper No. 933121, pp 133-144.

Zhao, J. Z. and Narwani G. (2005). "Development of a human body finite element model for restraint system R&D applications". The 19th International Technical Conference on the Enhanced Safety of Vehicles (ESV), Paper No. 05-0399, Washington, DC; 2005.

Zhao, Z., Jin, X., Cao, Y., Wang, J., (2010). “Data mining application on crash simulation data of occupant restraint system.” Expert Systems with Applications 37, 5788-5794.

Zhou, Q., Rouhana, S.W., Melvin, J.W., (1996). “Age effects on thoracic injury tolerance.” SAE Technical Paper No. 962421.

Zhu, F., Chou, C. ., Yang, K.H., Chen, X., Wagner, D., Bilkhu, S., & Luo, A. (2012). "Calibrating material parameters to model the thin-walled components made of die cast AM60B magnesium alloy." International Journal of Crashworthiness, 17(5), 540-552

Zhu, F., Kalra, A., Saif, T., Yang, Z., Yang, K. H., & King, A. I. (2016). "Parametric analysis of the biomechanical response of head subjected to the primary blast loading–a data mining approach." Computer methods in biomechanics and biomedical engineering, 19(10), 1053-1059.

Zhu, F, Jiang, B., and Chou, C. “On the development of a new design methodology for vehicle characteristics based on data mining theory”, SAE Paper No. 2016-01-1524

ABSTRACT

DEVELOPMENT OF AN ELDERLY FEMALE TORSO FINITE ELEMENT MODEL FOR RESTRAINED SYSTEM R & D APPLICATIONS

by

ANIL KALRA

May 2017

Advisor: Dr. King Yang

Major: Mechanical Engineering

Degree: Doctor of Philosophy

Elderly females are found to be one of the most vulnerable segments of population during motor vehicle crashes and their population is increasing in the coming decades. Current designs of restraint systems as well as other passive safety measures are designed based on anthropomorphic details of younger population. Developing another dummy representing elderly female population is a costly effort, while a finite element (FE) model of elderly female with similar anthropomorphic details and age- and gender-specific material properties can be a better alternative solution. The current research focuses on the development of a FE model of an elderly female torso, because a thorough search through literature has identified thorax as the most severely injured body part for elderly females due to rib fractures in motor vehicle induced trauma.

Therefore, data from previously conducted rib bending experiments on 278 rib specimens taken from antero-lateral portion of 82 cadavers were analyzed to see the effect of age, gender, height, and weight on the rib bio-mechanical response parameters such as the maximum bending moment (MBM), maximum bending angle (Θ_{max}), slope of moment-angle curve (SMT), and on average cortical thickness value. It was found that, in comparison to males, females had

significantly lower values for the MBM ($p = 0.000$), SMT ($p = 0.000$), and average cortical-bone thickness ($p = 0.001$). Samples of ribs taken from elderly specimens failed at lower values of MBM than those from younger specimens, and had lower SMT, both in males and females ($p < 0.05$). The generalized estimating equations were developed for each biomechanical response parameter in terms of dependent variables, namely the age, gender, height, and weight.

Further, the material model parameters for elderly female rib specimen with constant cortical bone thickness were optimized, which in turn were used in developed whole body FE model. The cortical thickness variations in different sections (anterior, antero-lateral, lateral, posteo-lateral, and posterior) of whole rib were also assigned based on those reported in the literature. The model predicted peak responses as well as the fracture locations of the ribs were analyzed against whole rib bending tests with favorable result. Once the response of single whole rib was validated, further the response of elderly female whole rib cage was validated against data reported from frontal pendulum impacts at different speeds as well as data reported for belt loading. The validations results showed that the developed FE model can represent the overall behavior of elderly female during the type of loading as experienced in motor vehicle crashes.

AUTOBIOGRAPHICAL STATEMENT

ANIL KALRA

EDUCATION:

- Ph.D. Mechanical Engineering, Wayne State University, Detroit, Michigan, 2017.
- M.S., Mechanical Engineering, New Jersey Institute of Technology, Newark, New Jersey, 2009.
- B.Tech. Mechanical Engineering, Kurukshetra University, Kurukshetra, India, 2006.

EXPERIENCE:

- Graduate Research Assistant, Biomedical Engineering Department 08/12 - 08/16
  College of Engineering, Wayne State University, Detroit, MI
- Graduate Teaching Assistant, Mechanical Engineering Department 08/13 - 05/14
  College of Engineering, Wayne State University, Detroit, MI
- Project Associate, Mechanical Engineering Department 07/11 - 02/12
  Indian Institute of Technology, New Delhi, India